University of Windsor
Scholarship at UWindsor

Electronic Theses and Dissertations | Theses, Dissertations, and Major Papers

2017

Expanding the Oxidative Addition Route for the Rational Design of Multi-Metallic Dithiolene Complexes

Zeinab Sadiq Ahmed
University of Windsor

Follow this and additional works at: https://scholar.uwindsor.ca/etd

Recommended Citation

Ahmed, Zeinab Sadiq, "Expanding the Oxidative Addition Route for the Rational Design of Multi-Metallic Dithiolene Complexes" (2017). *Electronic Theses and Dissertations*. 7341.
https://scholar.uwindsor.ca/etd/7341

This online database contains the full-text of PhD dissertations and Masters' theses of University of Windsor students from 1954 forward. These documents are made available for personal study and research purposes only, in accordance with the Canadian Copyright Act and the Creative Commons license—CC BY-NC-ND (Attribution, Non-Commercial, No Derivative Works). Under this license, works must always be attributed to the copyright holder (original author), cannot be used for any commercial purposes, and may not be altered. Any other use would require the permission of the copyright holder. Students may inquire about withdrawing their dissertation and/or thesis from this database. For additional inquiries, please contact the repository administrator via email (scholarship@uwindsor.ca) or by telephone at 519-253-3000ext. 3208.

Expanding the Oxidative Addition Route for the Rational Design of Multi-Metallic Dithiolene Complexes

By

Zeinab S. Ahmed

A Thesis
Submitted to the Faculty of Graduate Studies
through the Department of Chemistry and Biochemistry
in Partial Fulfillment of the Requirements for
the Degree of Master of Sciences
at the University of Windsor

Windsor, Ontario, Canada

2017

© 2017 Zeinab S. Ahmed

Expanding the Oxidative Addition Route for the Rational Design of Multi-Metallic Dithiolene Complexes

by

Zeinab S. Ahmed

APPROVED BY:

_____

A. Fisk
Great Lakes Institute for Environmental Research

_____

C. Macdonald
Department of Chemistry & Biochemistry

_____

J. Rawson, Advisor
Department of Chemistry & Biochemistry

October 12, 2017

DECLARATION OF CO-AUTHORSHIP / PREVIOUS PUBLICATION

I. Co-Authorship Declaration

I hereby declare that this thesis incorporates some material that is the result of joint research, as follows:

For all the structures presented in Chapters 2 and 3 of this thesis, crystallographic data collection and refinement were performed by Dr. Jeremy Rawson, Dr. M. Usman Anwar, Dr. John Hayward, Dr. Elodie Heyer, or Konstantina Pringouri. All elemental analysis was performed by Dr. Janeen Auld or Konstantina Pringouri and high resolution mass spectrometry was performed by Dr. Janeen Auld.

Some samples of bis-(dimethoxybenzo)-1,2,5,6-tetrathiocin and bis-(15-crown-5-benzo)-1,2,5,6-tetrathiocin were prepared by Justin Wrixon and Adrian Debiasio. Crystals of $[CpCo(dmobdt)]_2$ and CpCo(b-15-c-5-dt) were grown by Dr. John Hayward.

I am aware of the University of Windsor Senate Policy on Authorship and I certify that I have properly acknowledged the contribution of other researchers to my thesis, and have obtained written permission from each of the co-author(s) to include the above material(s) in my thesis.

I certify that, with the above qualification, this thesis, and the research to which it refers, is the product of my own work.

II. Declaration of Previous Publication

At the time of submission of this thesis, some of the work originating from the studies described in this thesis have already been published as follows:

"Oxidative addition of bis-(dimethoxybenzo)-1,2,5,6-tetrathiocins to $Pt(PPh_3)_4$: Synthesis and Structures of mono- and di-metallic platinum dithiolate complexes, $(dmobdt)Pt(PPh_3)_2$ and $[(dmobdt)Pt(PPh_3)]_2$", Justin D. Wrixon, Zeinab S. Ahmed, M. Usman Anwar, Yassine Beldjoudi, Nabila Hamidouche, John J. Hayward and Jeremy M. Rawson, *Polyhedron*, 2016, **108**, 115–121.

Preparation of the manuscript was performed by Justin Wrixon, Dr. Hayward, and Dr. Rawson.

I certify that I have obtained written permission from the copyright owner(s) to include the above published material in my thesis. I certify that the above material describes work completed during my registration as a graduate student at the University of Windsor.

I declare that, to the best of my knowledge, my thesis does not infringe upon anyone's copyright nor violate any proprietary rights and that any ideas, techniques, quotations, or any other material from the work of other people included in my thesis, published or otherwise, are fully acknowledged in accordance with standard referencing practices. Furthermore, to the extent that I have included copyrighted material that surpasses the bounds of fair dealing within the meaning of the Canada Copyright Act, I certify that I have obtained a written permission from the copyright owner(s) to include such material(s) in my thesis.

I declare that this is a true copy of my thesis, including any final revisions, as approved by my thesis committee and the Graduate Studies office, and that this thesis has not been submitted for a higher degree to any other University or Institution.

ABSTRACT

This thesis describes studies on oxidative addition reactions of 1,2,5,6-tetrathiocins to low valent transition metals, yielding an array of multinuclear metal dithiolene complexes. Chapter 1 provides a literature review of metal dithiolene complexes, including their synthesis and applications.

Chapter 2 investigates the reaction of Pd_2dba_3 with tetramethoxydibenzotetrathiocin (**1**) and a range of monodentate phosphines with different Tolman cone angles. The isostructural series of homo-dimetallic complexes $[(dmobdt)Pd(P)]_2$ [P = $PPh_2{}^iPr$, $P(NMe_2)_3$, $P(^iPr)_3$, $P(m\text{-tol})_3$, PCy_3 and PBn_3] (**3** – **8**) were isolated as the major phosphine-containing metal complex. These were characterized by multinuclear ^1H and ^{31}P NMR spectroscopy and X-ray diffraction. The related reaction of $Pt(PPh_3)_4$ with tetrathiocin afforded a mixture of monometallic $(dmobdt)Pt(PPh_3)_2$ (**11**) and dimetallic $[(dmobdt)Pt(PPh_3)]_2$ (**10**). Experimental studies revealed that conversion of **11** to **10** appears to require the presence of oxygen and is characterized by formation of free phosphine oxide. Reaction of $Pt_{1.9}dba_3$ with **1** in the presence of the sterically demanding P^tBu_3 ligand led to the isolation of the homo bimetallic $[(dmobdt)Pt(PH^tBu_2)]_2$ (**13**) in which dealkylation of the phosphine occurs as well as characterization of the first hexanuclear homoleptic platinum complex, $[Pt(dmobdt)]_6$ (**12**).

Chapter 3 extends the oxidative addition of tetrathiocins to low valent metals by examining the reactivity of tetrathiocins to $CpCo(CO)_2$. Reaction of tetrathiocin **1** and its benzo-crown-5 analogue **16** with $CpCo(CO)_2$ under microwave conditions afforded the $16e^-$ Co^{III} organometallic complexes CpCo(dmobdt) (**17**) and CpCo(b-15-c-5-dt) (**18**). In the solid state **17** exists as the $18e^-$ dimer $[CpCo(dmobdt)]_2$ whereas **18** can exist in monomeric or dimeric forms depending upon crystallization conditions. Reactivity of **18** towards alkali metal cations afforded a series of 2:1 complexes in which the *s*-block metal is sandwiched between two benzo crowns. The structures of $[M\{CpCo(b15c5dt)\}_2][BPh_4]$ (M = Na, K, Rb, Cs) were determined by X-ray diffraction and ESI mass spectrometry. Reaction with $Cu(CF_3SO_3)_2$ led to a redox reaction and the isolation of a unique bimetallic complex exhibiting a disulfide S-S bond.

DEDICATION

I dedicate this work to my parents, Sadiq Ahmed Mohamed and Ines Da Costa, and to my brothers, Zeky, Adan, Dariq, and Omar. Without your unending love, understanding, and support, I would not have accomplished this. You're my rocks and my superheroes.

ACKNOWLEDGEMENTS

I would like to thank Dr Jeremy Rawson for everything he has done for me over the years. I first joined his group as a second year undergraduate student, brand new to the world of chemistry research, and throughout the years he has encouraged me, been patient and understanding with me, and has nurtured my growth and confidence as a student and a researcher. Dr. Rawson, you are an amazing teacher and mentor, and I can't thank you enough.

I would also like to thank Dr. John Hayward for all the guidance he has given me over the years. From teaching me the basics of research in undergrad, to working with me one-on-one to help me to get my Master's project completed, Dr. Hayward has continued to push me to understand my research and to do well in it. His door was always open if I had a question or needed a quick chat.

I would like to thank Dr. Elodie Heyer for always being available whenever I had questions or needed help understanding something in my research.

The Rawson group has been an invaluable support for me over the years. Thank you to all of you for all the conversations we've had, for your encouragement, and for the support you've all given me. It's been a pleasure getting to know each of you.

I would like to thank Dr. Janeen Auld for her help with elemental analysis and mass spectrometry, and Konstantina Pringouri for her help with elemental analysis and X-ray diffraction. I would also like to thank Dr. Elodie Heyer for all her help with X-ray diffraction, and Dr. Matt Revington for his help with NMR spectroscopy.

I would like to thank Dr. Charles Macdonald and Dr. Aaron Fisk for agreeing to be on my examination committee and for taking the time to read my work.

Last but most definitely not least, I would like to thank my family. My parents and brothers have always encouraged me, pushed me to be the best I can be, been patient with me, and given me room to grow. I would not have accomplished any of this without all of you.

TABLE OF CONTENTS

DECLARATION OF CO-AUTHORSHIP / PREVIOUS PUBLICATION iii

ABSTRACT v

DEDICATION vi

ACKNOWLEDGEMENTS vii

LIST OF TABLES xiii

LIST OF FIGURES xiv

LIST OF SCHEMES xviii

LIST OF ABBREVIATIONS, SYMBOLS AND NOMENCLATURE xx

LIST OF SELECTED COMPOUNDS AND COMPLEXES xxiii

CHAPTER 1. Introduction 1

1.1. An Introduction to Transition Metal Dithiolene Complexes 1

1.2. Preparation of Metal Dithiolene Complexes 2

1.2.1 From Benzenedithiols and Related Derivatives 2

1.2.2 From 1,2-Alkenedithiolates 4

1.2.3 From Thiophosphate Esters 5

1.2.4 From 1,2,-Dithietes and 1,2,5,6-Tetrathiocins 6

1.2.5 Addition of Alkynes to Metal Sulfides 7

1.2.6 From Metal Sulfides and α-Haloketones 8

1.2.7 By Dehydrogenation of Alkanedithiolates 8

1.2.8 From Dithiocarbonates 9

1.3. Properties and Applications of Metal Dithiolene Complexes 10

1.3.1 Conducting Materials 10

1.3.2 Magnetic Materials 14

1.3.3 Optical Properties and Non-Linear Optics 15
1.3.4 Biological Systems 18
1.3.5 Recent Advances 19
1.4. Overview of this Thesis 20
1.5. References 22
CHAPTER 2. Towards the rational design of homo-multimetallic dithiolene complexes: Phosphine control of group 10 dithiolates 31
2.1. Introduction 31
2.1.1 Structural Properties 33
2.1.2 Phosphine Ligands 36
2.1.2.a Tolman cone angles 37
2.1.2.b Phosphine control 39
2.1.3 Project Objectives 41
2.2. Results and Discussion 41
2.2.1 Synthesis of 2′,3′,8′,9′-tetramethoxy-dibenzo-1,2,5,6-tetrathiocin $[(MeO)_2C_6H_2S_2]_2$ (1) 41
2.2.2 Kinetics of Formation of the Palladium Dimer $[(dmobdt)Pd(PPh_3)]_2$ (2) .. 42
2.2.3 Synthesis and Studies of a Series of Dinuclear Palladium Complexes (3 – 8) 48
2.2.3.a Synthesis of dinuclear complexes 3 – 8 48
2.2.3.b Crystallographic studies of complexes 3 – 8 50
2.2.3.c Isolation of other products 53
2.2.4 Phosphine Requirement for the Palladium Hexamer $[Pd(dmobdt)]_6$ (9) 56
2.2.5 Kinetics of Formation of the Platinum Dimer $[(dmobdt)Pt(PPh_3)]_2$ (10) ... 58
2.2.6 Synthesis of a Platinum Hexamer $[Pt(dmobdt)]_6$ (12) 61
2.3. Conclusions 67

2.4. Experimental 68
2.4.1 Crystallographic Studies 68
2.4.2 General Experimental Procedures 68
2.4.3 Preparation of [(dmobdt)Pd(PPh_3)]$_2$, (2), through reaction with Pd(PPh_3)$_4$. 69
2.4.4 Preparation of [(dmobdt)Pd($PPh_2{}^iPr$)]$_2$, (3). 69
2.4.5 Preparation of [(dmobdt)Pd(P(NMe_2)$_3$)]$_2$, (4) 70
2.4.6 Preparation of [(dmobdt)Pd(P^iPr_3)]$_2$, (5). 70
2.4.7 Preparation of [(dmobdt)Pd(P(m-tol)$_3$)]$_2$, (6). 71
2.4.8 Preparation of [(dmobdt)Pd(PBn_3)]$_2$, (7). 72
2.4.9 Preparation of [(dmobdt)Pd(PCy_3)]$_2$, (8). 73
2.4.10 Preparation of [Pd(dmobdt)]$_6$, (9). 75
2.4.11 Preparation of [(dmobdt)Pt(PPh_3)]$_2$ (10) and (dmobdt)Pt(PPh_3)$_2$ (11). 75
2.4.12 Preparation of $Pt_{1.9}dba_3 \cdot CH_2Cl_2$. [27a] 76
2.4.13 Preparation of [Pt(dmobdt)]$_6$ (12) and [(dmobdt)Pt(PH^tBu_2)]$_2$ (13). 76
2.5. References 78

CHAPTER 3. Towards the rational design of hetero-multimetallic dithiolene complexes: Synthesis and reactivity of cobalt dithiolates 82

3.1. Introduction 82
3.1.1 Cobalt Dithiolene Complexes 82
3.1.2 Crown Ethers 84
3.1.3 Crown Ethers in Metal Dithiolene Complexes 88
3.1.4 Project Objectives 91
3.2. Results and Discussion 91
3.2.1 Synthesis of Bis-15-crown-5-dibenzo-1,2,5,6-tetrathiocin (16) 91
3.2.2 Synthesis of [CpCo(dmobdt)]$_2$ (17) and CpCo(b-15-c-5-dt) (18) 92

3.2.3 Crystal Structures of 17 and 18 94
3.2.4 Complexation of Alkali Metals into Complex 18 96
3.2.5 Crystallographic Studies of Complexes 19 – 22 96
3.2.6 Attempts to Incorporate Other Metals into 18 99
3.3. Conclusions 101
3.4. Experimental 103
3.4.1 Crystallographic Studies 103
3.4.2 General Experimental Procedures 103
3.4.3 Preparation of bis-15-crown-5-dibenzo-1,2,5,6-tetrathiocin, (16). 104
3.4.4 Preparation of $[CpCo(dmobdt)]_2$, (17). 104
3.4.5 Preparation of CpCo(b-15-c-5-dt), (18). 105
3.4.6 Preparation of $[Na\{CpCo(b\text{-}15\text{-}c\text{-}5\text{-}dt)\}_2][BPh_4]$, (19). 106
3.4.7 Preparation of $[K\{CpCo(b\text{-}15\text{-}c\text{-}5\text{-}dt)\}_2][BPh_4]$, (20). 106
3.4.8 Preparation of $[Rb\{CpCo(b\text{-}15\text{-}c\text{-}5\text{-}dt)\}_2][BPh_4]$, (21). 107
3.4.9 Preparation of $[Cs\{CpCo(b\text{-}15\text{-}c\text{-}5\text{-}dt)\}_2][BPh_4]$, (22). 108
3.4.10 Preparation of (b-15-c-5-dt)Pd(dppe), (14). 108
3.4.11 Preparation of $[Na\{(b\text{-}15\text{-}c\text{-}5\text{-}dt)Pd(dppe)\}][BPh_4]$. 109
3.4.12 Reaction of 18 and $Li[ClO_4]$. 110
3.4.13 Reaction of 18 and $Fe(BF_4)_2 \cdot 6H_2O$. 110
3.4.14 Reaction of 18 and $Cu(ClO_4)_2 \cdot 6H_2O$. 110
3.4.15 Preparation of $[CpCo(b\text{-}15\text{-}c\text{-}5\text{-}dt)]_2$, (23). 111
3.4.16 Preparation of $[CpCo(b\text{-}15\text{-}c\text{-}5\text{-}dt]_2[CF_3SO_3]_2$, (24). 111
3.4.17 Reaction of 17 and $Cu(CF_3SO_3)_2$. 111
3.4.18 Reaction of 18 and $Sm(NO_3)_3 \cdot 6H_2O$. 111
3.4.19 Reaction of 18 and $Yb(CF_3SO_3)_2 \cdot xH_2O$. 112

3.4.20 Reaction of 18 and $Dy(ClO_4)_3 \cdot 6H_2O$. 112

3.4.21 Reaction of 14 and $Dy(ClO_4)_3 \cdot 6H_2O$. 113

3.5. References 114

CHAPTER 4. Conclusions and Future Work 117

4.1. Conclusions 117

4.2. Future Work 118

4.3. References 121

APPENDIX 122

Crystallographic Information 122

VITA AUCTORIS 141

LIST OF TABLES

Table 1.1 Magnetic properties of [$Cp_2Mo(dmit)$][Y] salts.[63] 15
Table 1.2 Wavelengths of maximum absorption (nm) in various solvents (±0.5 nm).[67] . 17
Table 2.1 Some cone angles reported by Tolman.[19] 38
Table 2.2 Influence of cone angle on M-P bond length.[19] 38
Table 2.3 ^{31}P NMR chemical shift with increasing bulkiness. *Table reproduced from reference 4.* 39
Table 2.4 Phosphines used and their cone angles.[19,24] 48
Table 2.5 Selected bond lengths for complexes **3** to **8** (Å). 52
Table 2.6 Selected angles for complexes **3** to **8** (°). 53
Table 2.7 Observed peaks in ^{31}P NMR spectra of the crude reaction mixtures for complexes **4** to **8**. Percentages indicate what fraction of the mixture each product accounts for, and is based on integration of the NMR peaks. The major product is highlighted in blue for each reaction. 54
Table 3.1 Ratio of crown to cation for 15-crown-5 and 18-crown-6, with approximate size of the crowns and cations specified. *Table reproduced from data found in references 5 and 6.* 86
Table 3.2 Shift in wavelength of maximum absorption in UV/vis upon complexation of alkali metals into some of the crown ether metal dithiolene complexes reported by Lowe and Garner. *Table reproduced from reference 23.* 90
Table 3.3 Shift in redox potential (mV) according to cyclic voltammetry upon complexation of alkali metals into some of the crown ether metal dithiolene complexes reported by Lowe and Garner. *Table reproduced from reference 23.* 90
Table 3.4 Values of θ, Φ, and C_2S_2-CoS_2 angles for complexes **19** to **22** (°). C_2S_2-CoS_2 angle is the angle between the C_2S_2 and CoS_2 planes and indicates deviation from planarity at Co. 98
Table 3.5 Crystallographic data for the previously found polymorph of **14**[25] versus the new polymorph. 99

LIST OF FIGURES

Figure 1.1 Resonance forms of metal dithiolene complexes: **(a)** 1,2-enedithiolate and **(b)** 1,2-dithioketone. 1

Figure 1.2 Metal dithiolene complexes bearing tetrathiafulvalene groups. 5

Figure 1.3 Structure of the 1,2-dithiete $S_2C_2(CF_3)_2$. 6

Figure 1.4 Schematic band structures for insulators, semiconductors, and metals. 11

Figure 1.5 Formation of conducting states by doping of insulators/semiconductors. 11

Figure 1.6 Schematic band structures for the charge transfer salt TTF·TCNQ. 12

Figure 1.7 Structures of **(a)** $[Au(bdt)_2]^{\bullet}$, **(b)** $[Au(F_2pdt)_2]^{\bullet}$, and **(c)** $[Au(\alpha\text{-tpdt})_2]^{\bullet}$ 13

Figure 1.8 Structures of **(a)** $Ni(tmdt)_2$ and **(b)** $Ni(dmit)_2$ 14

Figure 1.9 DFT diagram showing the contribution of the dithiolene ligand (and some metal) to the HOMO and the diimine (and some metal) to the LUMO. Picture taken from reference 64. 16

Figure 1.10 Structure of the dithiolate molybdopterin found in the active site of many enzymes 18

Figure 1.11 Some monometallic, dimetallic, and hexametallic group 10 dithiolene complexes previously reported in this group.[28,29] 21

Figure 2.1 Structures of **(a)** mnt^{2-} and **(b)** $dmit^{2-}$ ligands. 31

Figure 2.2 Number of some substituted benzo-fused group 10 dithiolene complexes reported in the CSD. 32

Figure 2.3 General structure of a 1,2,5,6-tetrathiocin. 32

Figure 2.4 Range of tetrathiocins synthesized by this group. *Diagram reproduced from reference 4*. 33

Figure 2.5 Some examples of dimeric group 10 dithiolene complexes reported in literature. 34

Figure 2.6 Examples of trinuclear nickel dithiolene complexes reported in literature. Hydrogen atoms have been omitted for clarity. 35

Figure 2.7 Trinuclear palladium dithiolene complex reported by Shimizu and coworkers.[12] Hydrogen atoms have been omitted for clarity. 35

Figure 2.8 Structures of the **(a)** tetranuclear and **(b)** pentanuclear nickel dithiolene complexes. Hydrogen atoms have been omitted for clarity. 36
Figure 2.9 Structures of two hexanuclear palladium dithiolates reported in literature. Hydrogen atoms have been omitted for clarity. 37
Figure 2.10 Representation of the Tolman cone angle. *Diagram reproduced from reference 4.* 38
Figure 2.11 Products of the reaction of bis-(dimethoxybenzo)-1,2,5,6-tetrathiocin, Pd_2dba_3 and PR_3, giving: **(a)** mononuclear structures when PR_3 = dppm (R' = CH_2), dppe (R' = CH_2CH_2), dppf (R' = $(C_5H_5)_2Fe$), **(b)** a dinuclear structure when PR_3 = PPh_3, **(c)** a hexanuclear structure when PR_3 = P^tBu_3. Hydrogen atoms have been omitted for clarity. 40
Figure 2.12 Crystal structure of tetrathiocin **1** with thermal ellipsoids drawn at the 50% probability level. 42
Figure 2.13 Monomeric intermediate isolated from the reaction of $Pt(PPh_3)_4$ with tetrathiocin **1**.[3] Hydrogen atoms have been omitted for clarity. 43
Figure 2.14 ^{31}P NMR spectra in $CDCl_3$ for the reaction of Pd_2dba_3, tetrathiocin **1** and PPh_3 at: **(a)** 150 °C, microwave conditions, 1 min; **(b)** 60 °C, microwave conditions, 5 min; **(c)** 90 °C, thermal conditions, 1 h..... 44
Figure 2.15 ^1H NMR spectra in $CDCl_3$ for the reaction of Pd_2dba_3, tetrathiocin **1** and PPh_3 at: **(a)** 150 °C, microwave conditions, 1 min; **(b)** 60 °C, microwave conditions, 5 min; **(c)** 90 °C, thermal conditions, 1 h..... 45
Figure 2.16 NMR spectra in $CDCl_3$ for the reaction of $Pd(PPh_3)_4$ and tetrathiocin **1** at 1 min: **(a)** ^{31}P NMR (121 MHz), **(b)** ^1H NMR (300 MHz)..... 47
Figure 2.17 ^1H NMR spectrum of complex **7**. 50
Figure 2.18 Crystal structures of complexes **3** to **8** with thermal ellipsoids drawn at the 50% probability level. Hydrogen atoms have been omitted for clarity. 51
Figure 2.19 Crystal structure of **3** showing the bending between the S_3P1 and S_3P2 planes in these complexes (left) and atom labelling (right). 52
Figure 2.20 ^{31}P NMR spectra of the crude reaction mixture for the reaction of tetrathiocin **1**, Pd_2dba_3, and PBn_3 at: **(a)** 0.75 equiv., **(b)** 1 equiv., **(c)** 1.5 equiv., **(d)** 2 equiv., **(e)** 4 equiv., and **(f)** 5 equiv. of phosphine. 55

Figure 2.21 ^{31}P NMR spectra of the crude reaction mixture for the reaction of tetrathiocin **1**, Pd_2dba_3, and PCy_3 at: **(a)** 0.75 equiv., **(b)** 1 equiv., **(c)** 1.5 equiv., **(d)** 2 equiv., **(e)** 4 equiv., and **(f)** 5 equiv. of phosphine. 56
Figure 2.22 ^{1}H NMR spectrum of complex **9** in $CDCl_3$, showing six resonances for the benzo protons and six for the methoxy protons. 57
Figure 2.23 ^{31}P NMR spectrum after **11** was heated in dry toluene at 150 °C for 60 min. 59
Figure 2.24 ^{31}P NMR after heating **11** at 150 °C in the microwave for 60 min in: **(a)** wet THF, **(b)** dry THF, and **(c)** degassed (wet) THF..... 61
Figure 2.25 ^{1}H NMR spectrum of complex **12** with an inset showing six resonances for the methoxy protons..... 63
Figure 2.26 Crystal structure of complex **12** (left), and platinum atom labelling (right). Hydrogen atoms have been omitted for clarity. 63
Figure 2.27 ^{31}P{^{1}H} NMR spectrum of the orange band showing a possible mixture of dimeric (red) and monomeric (blue) products. 64
Figure 2.28 ^{1}H NMR spectra of the orange band showing a possible mixture of products, including possible monomer (blue) and dimer (red) formation shown in the methoxy and ^{t}Bu regions (above). 65
Figure 2.29 Crystal structure of complex **13** with thermal ellipsoids drawn at the 50% probability level. Hydrogen atoms have been omitted for clarity. 66
Figure 3.1 (a) The first crown ether discovered by Pedersen[5] and **(b)** some examples of crown ethers: (i) benzo-15-crown-5, (ii) perhydrodibenzo-18-crown-6, (iii) dibenzo-21-crown-7, and (iv) perhydrodibenzo-24-crown-8. 85
Figure 3.2 An example of a crown ether used as a dye reported by Gokel.[6] 87
Figure 3.3 Crown ether complexes exhibiting magnetic properties reported by Pilkington and coworkers.[11,12] 88
Figure 3.4 The range of transition metal dithiolene complexes produced by Lowe and Garner[22] which incorporated crown ethers into their structures. 89
Figure 3.5 Structures of complexes **14** (left) and **15** (right)..... 91
Figure 3.6 ^{1}H NMR spectrum of complex **17**. 93
Figure 3.7 ^{1}H NMR spectrum of complex **18**. 94

Figure 3.8 Crystal structure of **17** with thermal ellipsoids drawn at the 50% probability level. Hydrogen atoms have been omitted for clarity. 95
Figure 3.9 Crystal structure of **18** with thermal ellipsoids drawn at the 50% probability level (left) and structure showing planarity at Co (right). Hydrogen atoms have been omitted for clarity. 95
Figure 3.10 Crystal structures of **19** to **22** with thermal ellipsoids drawn at the 50% probability level. Hydrogen atoms, solvent molecules, and BPh_4^- counterions have been omitted for clarity. 97
Figure 3.11 Crystal structure of complex **22** showing the **(a)** angle of opening in the sandwich (θ) and **(b)** angle of offset of the dithiolene complexes (Φ). 98
Figure 3.12 Crystal structures of the **(a)** previously reported[25] and **(b)** new polymorph of **14**, with thermal ellipsoids drawn at the 50% probability level. Hydrogen atoms have been omitted for clarity. 99
Figure 3.13 Preliminary crystal structure of complex **23** with thermal ellipsoids drawn at the 50% probability level. Hydrogen atoms have been omitted for clarity. 100
Figure 3.14 Crystal structure of the product of the reaction of **18** and $Cu(CF_3SO_3)_2$ showing possible formation of a new S-S bond. Hydrogen atoms and $CF_3SO_3^-$ counterions have been omitted for clarity. 100

LIST OF SCHEMES

Scheme 1.1 Preparation of 1,2-benzenedithiol. 2

Scheme 1.2 Synthesis of **(a)** $M(bdt)_3$, (M = Mo, W, Re; bdt = 1,2-benzenedithiolate) and **(b)** $[PPh_4][W(Cl_2bdt)_3]$ (Cl_2bdt = 3,6-dichloro-1,2-benzenedithiolate) *via* condensation of the dithiol with metal chlorides. 3

Scheme 1.3 Thiol exchange of $(NEt_4)_2[OMo(p\text{-}S\text{-}C_6H_4Cl)_4]$ with a Ph_3Si-substituted benzenedithiol. 3

Scheme 1.4 Reaction of 1,2-benzenedithiol with $CpV(CO)_4$. 4

Scheme 1.5 Synthesis of alkenedithiolates from 1,3-dithiol-2-ones. 4

Scheme 1.6 Synthesis of $Cp_2Ti(S_2C_3S_3)$ through ligand exchange. 5

Scheme 1.7 Synthesis of metal dithiolene complexes from α-hydroxyketones *via* thiophosphate esters. 6

Scheme 1.8 Oxidative addition of 1,2,5,6-tetrathiocins to zero-valent metals, where M^0 = $Ni(COD)_2$, Pd_2dba_3, $Pt(dppe)_2$. 7

Scheme 1.9 Synthesis of a titanium dithiolate from DMAD and Cp_2TiS_5 7

Scheme 1.10 Catalytic cycle for the reduction of acetylene to ethene. 8

Scheme 1.11 Synthesis of metal dithiolates from metal sulfides and α-bromoketones, where M = Ni, Pd, or Pt. 8

Scheme 1.12 Preparation of zinc dithiolene complexes from zinc polysulfides and an alkene. 9

Scheme 1.13 Synthesis of molybdenum dithiolene complexes from dithiocarbonates and metal sulfides. 10

Scheme 2.1 Synthesis of tetrathiocin **1** 42

Scheme 2.2 Previously reported synthesis of palladium dimer **2**.[15] 43

Scheme 2.3 General reaction scheme for the synthesis of complexes **3** to **8**. 49

Scheme 2.4 Synthesis of **9** without addition of phosphine. 57

Scheme 2.5 Proposed mechanism for the formation of platinum dimer **10**.[3] 58

Scheme 2.6 Reaction equilibrium shifted by oxidation of PPh_3. 60

Scheme 2.7 Synthesis of platinum hexamer **12**. 62

Scheme 3.1 Synthesis of a cobalt dithiolene complex from oxidative addition of the dithiete $S_2C_2(CF_3)_2$. 83
Scheme 3.2 Reaction equilibrium between the monomer CoCp(bdt) and the dimer $[CoCp(bdt)]_2$. 84
Scheme 3.3 Synthesis of tetrathiocin **16**. 91
Scheme 3.4 General synthetic procedure for complexes **17** and **18**. 92
Scheme 3.5 General synthesis of complexes **19** to **22**. 96
Scheme 3.6 The reaction of complex **14** and $Dy(ClO_4)_3 \cdot 6H_2O$. 101

LIST OF ABBREVIATIONS, SYMBOLS AND NOMENCLATURE

μwave	microwave
AC	alternating current
ASAP	atmospheric solids analysis probe (mass spectrometry)
b-15-c-5-dt^{2-}	benzo-15-crown-5-dithiolate dianion, $[(C_2H_4O)_4O(C_6H_2)S_2]^{2-}$
benzo-15-crown-5	1,4,7,10,13-pentaoxa[13]orthocyclophane
bddt^{2-}	4a,5,6,7,8,8a-hexahydro-1,4-benzodithiin-2,3-dithiolate dianion, $[C_6H_{10}S_2C_2S_2]^{2-}$
bdt^{2-}	1,2-benzenedithiolate dianion, $[C_6H_4S_2]^{2-}$
bdtH_2	1,2-benzenedithiol, $C_6H_4(SH)_2$
Bu	butyl group, $[CH_2CH_2CH_2CH_3]^-$
^{n}Bu	*neo*-butyl group, $[(CH_2)_3CH_3]^-$
^{t}Bu	*tert*-butyl group, $[C(CH_3)_3]^-$
Bn	benzyl group, $[CH_2(C_6H_5)]^-$
Bz$_2$pipdt^{2-}	1,4-dibenzylpiperazine-3,2-dithiolate dianion, $[C_2H_4N_2(C_6H_5CH_2)C_2S_2]^{2-}$
Cl$_2$bdt^{2-}	3,6-dichloro-1,2-benzenedithiolate dianion, $[C_6H_2Cl_2S_2]^{2-}$
COD	1,5-cyclooctadiene
Cp	cyclopentadienyl group, $[C_5H_5]^-$
15-crown-5	1,4,7,10,13-pentaoxacyclopentadecane
18-crown-6	1,4,7,10,13,16-hexaoxacyclooctadecane
CSD	Cambridge Structural Database
Cy	cyclohexyl group, $[C_6H_{11}]^-$
cyclam	1,4,8,11-tetraazacyclotetradecane, $(NHCH_2CH_2NHCH_2CH_2CH_2)_2$
d	doublet
D	deuterium
dba	dibenzylideneacetone
DC	direct current
dddt^{2-}	5,6-dihydro-1,4-dithiine-2,3-dithiolate dianion, $[C_2H_4S_2C_2S_2]^{2-}$
DFT	density functional theory
dibenzo-18-crown-6	6,7,9,10,17,18,20,21-octahydrodibenzo[b,k] [1,4,7,10,13,16]hexaoxacyclooctadecine
dibenzo-21-crown-7	6,7,9,10,12,13,20,21,23,24-decahydrodibenzo[b,k] [1,4,7,10,13,16,19]heptaoxacyclohenicosine
DMAD	dimethyl acetylenedicarboxylate
dmbpy	4,4′-dimethyl-2,2′-bipyridine, $[(CH_3)C_5H_3N]_2$
DMF	dimethylformamide
dmit^{2-}	1,3-dithiole-2-thione-4,5-dithiolate dianion, $[SCS_2C_2S_2]^{2-}$
dmobdt^{2-}	4,5-dimethoxy-benzo-1,2-dithiolate dianion, $[(MeO)_2C_6H_4S_2]^{2-}$

DMS	dimethyl sulfide
DMSO	dimethyl sulfoxide
DNA	deoxyribonucleic acid
dppe	diphenylphosphinoethane, $Ph_2PCH_2CH_2PPh_2$
dppf	diphenylphosphinoferrocene, $Ph_2PC_5H_4FeC_5H_4PPh_2$
dppm	diphenylphosphinomethane, $Ph_2PCH_2PPh_2$
dpphen	4,7-diphenyl-1,10-phenanthroline, $(C_{11}H_9N)C_2H_2(C_{11}H_9N)$
ΔE	energy difference
e^-	electron
edt^{2-}	ethane-1,2-dithiolate dianion, $[H_4C_2S_2]^{2-}$
EDT-TTF	ethylenedithiotetrathiafulvalene, $H_4(C_2S_2)_3C_2H_2$
E_F	Fermi energy level
EPR	electron paramagnetic resonance
equiv.	equivalent
ESI-TOF	electrospray ionisation time-of-flight (mass spectrometry)
Et	ethyl group, $[CH_2CH_3]^-$
EtO	ethoxy
Et_2O	diethyl ether
EtOH	ethanol
F_2pdt^{2-}	6,6-difluoro-6,7-dihydro-5*H*-[1,4]dithiepine-2,3-dithiolate dianion, $[F_2C_3H_4S_2C_2S_2]^{2-}$
FT-IR	Fourier-transform infra-red
GPC	gas phase chromatography
HOMO	highest occupied molecular orbital
HRMS	high resolution mass spectrometry
IR	infra-red
LUMO	lowest unoccupied molecular orbital
m (in NMR)	multiplet
m (in IR)	medium
Me	methyl group, $[CH_3]^-$
Me_2bpy	5,5'-dimethyl-2,2'-bipyridine
MeCN	acetonitrile
MeO	methoxy
MeOH	methanol
mesityl	1,3,5-trimethylbenzyl group, $[(CH_3)_3C_6H_2]^-$
MMLLCT	mixed-metal ligand-to-ligand charge transfer
mnt^{2-}	maleonitriledithiolate dianion, $[(CN)_2C_2S_2]^{2-}$
m-tol	*meta*-tolyl group, $[(CH_3)C_6H_4]^-$
m/z	mass to charge ratio
NIR	near infra-red
NLO	nonlinear optics
NMR	nuclear magnetic resonance
o-tol	*ortho*-tolyl group, $[(CH_3)C_6H_4]^-$

p-anisyl	1-methyl-4-methoxybenzyl group, $[CH_2(C_6H_4)OCH_3]^-$
pdt^{2-}	propane-1,2-dithiolate dianion, $[CH_3C_2H_3S_2]^{2-}$
perhydrodibenzo-18-crown-6	icosahydrodibenzo[b,k][1,4,7,10,13,16] hexaoxacyclooctadecine
perhydrodibenzo-24-crown-8	tetracosahydrodibenzo[b,n][1,4,7,10,13,16,19,22] octaoxacyclotetracosine
Ph	phenyl group, $[C_6H_5]^-$
phen	phenanthroline, $C_{12}H_8N_2$
PhMe	toluene
PMDETA	*N*,*N*,*N*′,*N*″,*N*″-pentamethyldiethylenetriamine, $[(CH_3)_2NCH_2CH_2]_2NCH_3$
ppb	parts per billion
ppm	parts per million
^{i}Pr	*iso*-propyl group, $[CH(CH_3)_2]^-$
p-tol/*p*-tolyl	*para*-tolyl group, $[(CH_3)C_6H_4]^-$
PXRD	powder x-ray diffraction
R	alkyl group
R_f	retention factor
s (in NMR)	singlet
s (in IR)	strong
SMM	single molecule magnet
TCNQ	tetracyanoquinodimethane, $(NC)_2C(C_6H_4)C(CN)_2$
tdt^{2-}	4-methyl-benzene-1,2-dithiolate (toluenedithiolate) dianion, $[(CH_3)C_6H_3S_2]^{2-}$
$tfadt^{2-}$	3-trifluoromethylacrylonitrile-2,3-dithiolate dianion, $[(CF_3)(CN)C_2S_2]^{2-}$
tfd^{2-}	1,2-bis(trifluoromethyl)ethene-1,2-dithiolate dianion, $[(CF_3)_2C_2S_2]^{2-}$
THF	tetrahydrofuran
TLC	thin layer chromatography
$tmdt^{2-}$	trimethylenetetrathiafulvalenedithiolate dianion, $[C_5S_2C_2S_2C_2S_2]^{2-}$
tmeda	tetramethylethylenediamine, $(H_3C)_2NCH_2CH_2N(CH_3)_2$
TMS	trimethylsilyl group, $Si(CH_3)_3$
TOF	time-of-flight
TPD	tetrathiapentalenedione, $OCS_2C_2S_2CO$
α-$tpdt^{2-}$	2,3-thiophenedithiolate dianion, $[SC_4S_2]^{2-}$
TTF	tetrathiafulvalene, $H_2C_2S_2C_2S_2C_2H_2$
UV/vis	Ultraviolet-visible (spectroscopy)
vs (in IR)	very strong
w	weak
X	halide group
XRD	x-ray diffraction

LIST OF SELECTED COMPOUNDS AND COMPLEXES

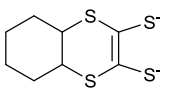

bbdt^{2-}

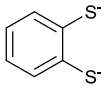

bdt^{2-}

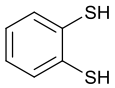

bdtH$_2$

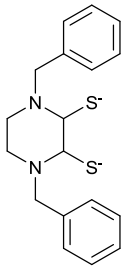

Bz$_2$pipdt^{2-}

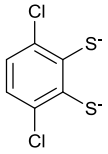

Cl$_2$bdt^{2-}

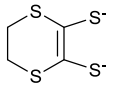

dddt^{2-}

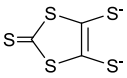

dmit^{2-}

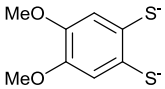

dmobdt^{2-}

edt^{2-}

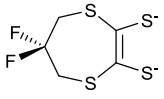

F$_2$pdt^{2-}

mnt^{2-}

pdt^{2-}

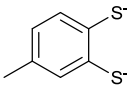

tdt^{2-}

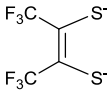

tfd^{2-}

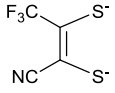

tfadt^{2-}

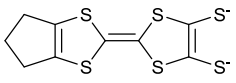

tmdt^{2-}

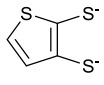

a-tpdt^{2-}

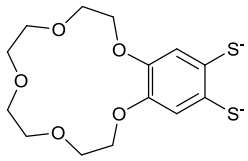

b-15-c-5-dt^{2-}

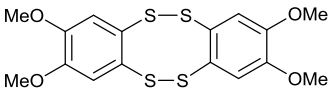

1

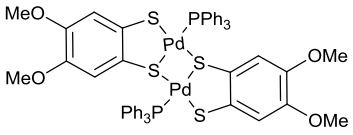

2

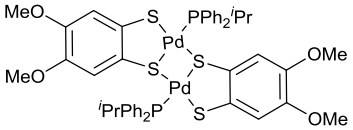

3

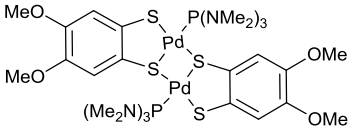

4

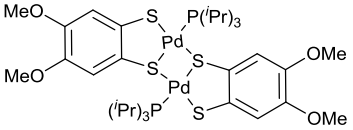

5

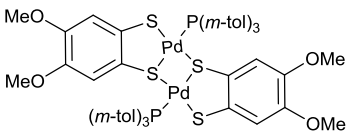

6

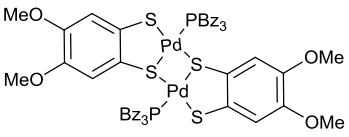

7

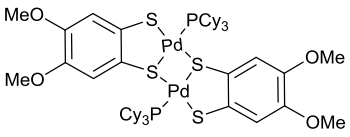

8

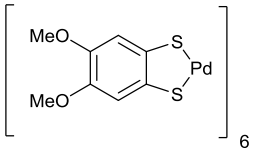

9

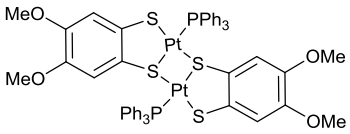

10

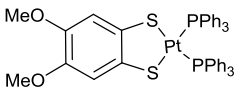

11

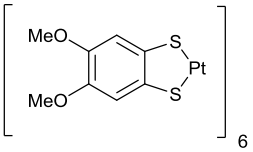

12

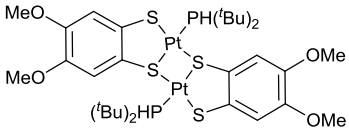

13

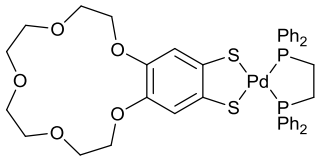

14

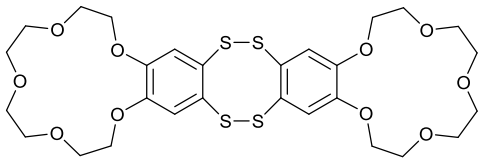

16

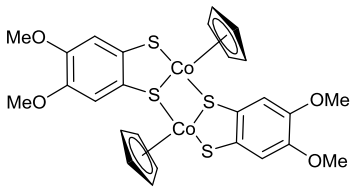

17

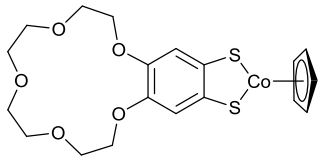

18

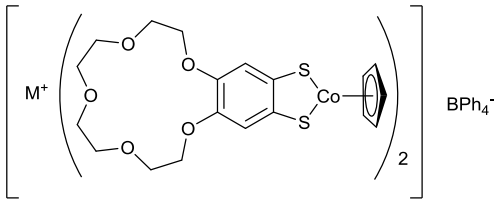

19 $M^+ = Na^+$
20 $M^+ = K^+$
21 $M^+ = Rb^+$
22 $M^+ = Cs^+$

CHAPTER 1. Introduction

1.1. An Introduction to Transition Metal Dithiolene Complexes

Transition metal dithiolene complexes are complexes that consist of at least one unsaturated bidentate sulfur donor ligand bound to a central transition metal. 1,2-dithiolenes contain an unsaturated ethene or benzo bridging group between the two sulfur donors and typically exist in the dianionic 1,2-ene-dithiolate or neutral 1,2-dithioketone forms (**Figure 1.1**).[1] The ligand's non-innocent nature makes the determination of its oxidation state, and therefore the oxidation state of the metal, difficult. This led McCleverty[2] to coin the term 'dithiolene' to encompass both forms. The oxidation state of specific complexes can be clarified by crystallographic studies, where the length of the carbon-carbon and carbon-sulfur bonds can be examined. Lengths matching the reported[3a] shorter carbon-sulfur double bond of 1.671(24) – 1.681(20) Å may indicate a dithioketone structure, while bond lengths matching the longer carbon-sulfur single bond of 1.712(13) – 1.751(17) Å would point to a dithiolate structure. Assignments can be further supported by IR spectroscopy, wherein a weak band in the 700 – 600 cm^{-1} region belongs to a C-S stretch and a strong band in the 1225 – 1025 cm^{-1} region belongs to a C=S stretch.[3b]

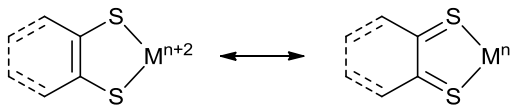

Figure 1.1 Resonance forms of metal dithiolene complexes: **(a)** 1,2-enedithiolate and **(b)** 1,2-dithioketone.

Many metal complexes of dithiolenes have been explored with the most common examples being complexes of the softer metals Ni, Pd, Pt, Cu, Au, Zn, Fe, Co, V, Mo, and W.[1] These complexes can take on a variety of structures, including mono-, bis-, or tris-dithiolenes as well as polynuclear metal complexes in which one or more additional S lone pairs become involved in bonding to form bridging dithiolenes with the S atoms adopting μ_2- or even μ_3-bridging modes. Transition metal dithiolene complexes comprising square planar, tetrahedral, trigonal prismatic, octahedral, and square

pyramidal geometries have been reported. The structures and geometries can have a marked effect on the complexes' properties and potential applications. In this context the 'non-innocent' redox-active nature of the dithiolene is often central to reactivity and materials applications.

1.2. Preparation of Metal Dithiolene Complexes

Several methods exist to synthesize transition metal dithiolene complexes; sections **1.2.1** and **1.2.2** cover reactions where the dithiolene ligand is pre-formed and coordinated to the metal, while sections **1.2.3** to **1.2.8** describe transition metal-assisted routes in which the dithiolate is prepared *in situ* during the chemical reaction.

1.2.1 From Benzenedithiols and Related Derivatives

Benzenedithiols and their derivatives are valuable stable precursors to metal dithiolene complexes. They are traditionally produced by the reductive dealkylation of 1,2-$C_6R_4(SR')_2$[1] but can also be made by reacting benzenethiol with 2 equivalents of BuLi and elemental sulfur, followed by an acidic work up (**Scheme 1.1**).[4]

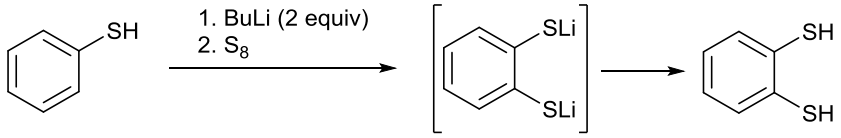

Scheme 1.1 Preparation of 1,2-benzenedithiol.

Metal dithiolene complexes derived from benzenedithiol precursors are typically made in one of three ways: by a condensation reaction (elimination of HCl) during the reaction of the benzenedithiol with metal halides; by thiol exchange; or by condensation of the benzenedithiol with oxo, alkoxo, or amido precursors.[1] Stiefel *et al*. in the 1960s reported the synthesis of a series of tris(benzene-1,2-dithiolate) and tris(toluene-3,4-dithiolate) complexes in moderate yields by the condensation of the dithiols with $MoCl_5$, WCl_6, and $ReCl_5$ in CCl_4 (**Scheme 1.2a**).[5] Similarly, Sugimoto and coworkers produced a series of tungsten(IV) and (V) benzenedithiolate complexes by reacting 3,6-dichloro-1,2-benzenedithiols with tungsten halides (**Scheme 1.2b**).[6] It is notable that in both these

studies that the elimination reaction is often coupled with a redox reaction at the metal center to afford the most thermodynamically favorable product.

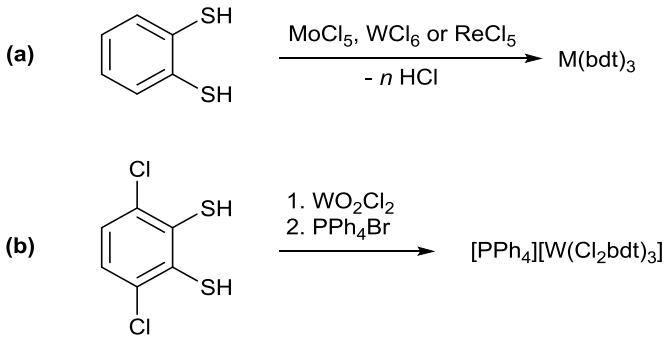

Scheme 1.2 Synthesis of **(a)** $M(bdt)_3$, (M = Mo, W, Re; bdt = 1,2-benzenedithiolate) and **(b)** $[PPh_4][W(Cl_2bdt)_3]$ (Cl_2bdt = 3,6-dichloro-1,2-benzenedithiolate) *via* condensation of the dithiol with metal chlorides.

Huynh *et al*. improved this synthesis using $W(CH_3)_6$ in diethyl ether instead of the metal chlorides, eliminating methane gas as the by-product.[7]

Thiol ligand exchange has also been employed as a method to produce metal dithiolene complexes. Here monodentate (and often sterically demanding) thiolates are displaced by chelating dithiolate ligands. For example, exchange of the monodentate PhS^- anion ligands in $[PPh_4][OMo(SPh)_4]$ with benzenedithiol ($bdtH_2$) in a 2:1 ratio gave $[PPh_4][OMo(bdt)_2]$ which was examined as a model for the active site of oxomolybdo-enzymes found in *E. coli* and other bacteria.[8] Similar studies were conducted on benzenedithiols containing bulkier functional groups; $[NEt_4]_2[OMo(bdt\text{-}SiPh_3)_2]$ was produced from $[NEt_4]_2[OMo(p\text{-}S\text{-}C_6H_4Cl)_4]$ and a Ph_3Si-substituted benzenedithiol (**Scheme 1.3**).

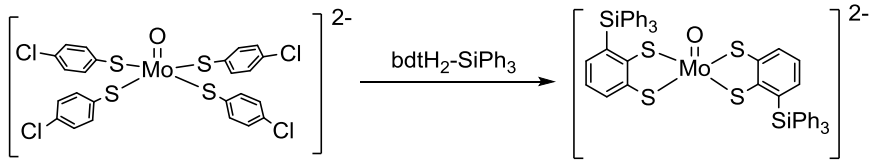

Scheme 1.3 Thiol exchange of $(NEt_4)_2[OMo(p\text{-}S\text{-}C_6H_4Cl)_4]$ with a Ph_3Si-substituted benzenedithiol.

Stephan *et al*.[10] reported the synthesis of a dinuclear vanadium dithiolene complex from $CpV(CO)_4$, with the evolution of H_2 gas (**Scheme 1.4**). The reaction includes a redox reaction in which the V(I) centre is oxidized to V(III) and the dithiol is reduced to dithiolate and H_2. The intermediate CpV(bdt) dimerizes with each dithiolate S atom adopting a μ_2-bridging mode.

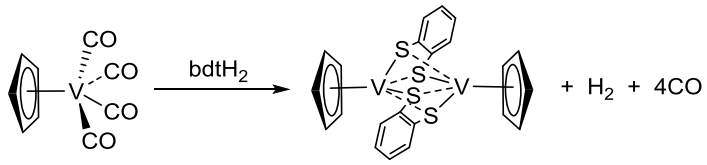

Scheme 1.4 Reaction of 1,2-benzenedithiol with $CpV(CO)_4$.

1.2.2 From 1,2-Alkenedithiolates

While 1,2-alkenedithiols are relatively unstable with respect to reduction, the corresponding alkenedithiolates are useful precursors to transition metal dithiolene complexes. These anions can be prepared by the reductive dealkylation of cis-1,2-bis(benzylthio)ethene derivatives with sodium[11] or *via* the base hydrolysis of 1,3-dithiol-2-ones.[12,13] Falaras *et al*. produced a series of dithiolates from various 1,3-dithiol-2-ones in refluxing ethanol, to which sodium was added (**Scheme 1.5**).[14] In a similar manner, 1,3-dithiol-2-thiones can be used to make alkenedithiolates.[15]

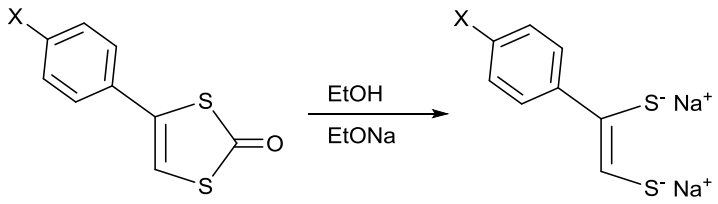

Scheme 1.5 Synthesis of alkenedithiolates from 1,3-dithiol-2-ones.

Once the alkenedithiolates have been made, ditholene complexes can be produced by salt metathesis with metal halides[11-14] or *via* ligand exchange, as in the synthesis of the titanium dithiolene complex shown in **Scheme 1.6** from $[NEt_4]_2[Zn(S_2C_3S_3)_2]$ and Cp_2TiCl_2.[16] The precursor $[Zn(S_2C_3S_3)_2]^{2-}$ complex was made from reacting $Na_2[S_2C_3S_3]$ with $ZnCl_2$.[17]

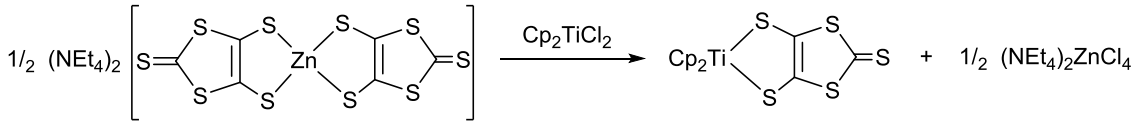

Scheme 1.6 Synthesis of $Cp_2Ti(S_2C_3S_3)$ through ligand exchange.

Schrauzer *et al.*[18] reported the formation of the iron dithiolate $Fe_2(CO)_6(S_2C_2R_2)$ from $M(S_2C_2R_2)_2$ (M = Fe, Ni and R = H, Ph, CH_3, *p*-tolyl, *p*-anisyl) and excess $Fe(CO)_5$ in benzene. In a similar way, $Ni(S_2C_2Ph_2)_2$ could be produced from the reaction of $Fe(S_2C_2Ph_2)_2$ and $Ni(CO)_4$ upon addition of acid. This method was extended to include the hexacarbonyls of Cr, Mo, and W which, when reacted with $Ni(S_2C_2R_2)_2$, could produce the corresponding (tris)dithiolene complexes.[19] Matsubayashi and coworkers[20] reported the synthesis of the vanadium (tris)dithiolate $[N^nBu_4]_2[V(dmit)_3]$ from $[N^nBu_4]_2[Zn(dmit)_2]$ and VCl_3 under ambient conditions. Similarly reaction of *cis*-$PtCl_2(PPh_3)_2$ with $(C_5H_4R)_2Ti\{S_2C_2(CO_2Me)_2\}$ formed $(PPh_3)_2Pt\{S_2C_2(CO_2Me)_2\}$.[21] These methods could be used to prepare more complex metal dithiolene complexes with tetrathiafulvalene groups (Figure 1.2).[22]

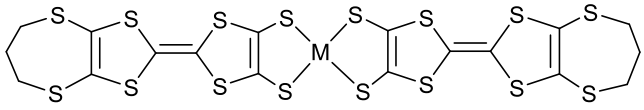

Figure 1.2 Metal dithiolene complexes bearing tetrathiafulvalene groups.

1.2.3 From Thiophosphate Esters

An alternate source of dithiolene complexes is from thiophosphate esters. Thiophosphate esters can be prepared from heating α-hydroxyketones, such as benzoin and acyloin, in an inert organic solvent with P_4S_{10}. Metal halides can then be added to allow for the formation of the metal dithiolene complexes (**Scheme 1.7**). Schrauzer and Mayweg[23] used this method to synthesize a series of group 10 dithiolates, with various metal centres and various functional groups on the dithiolene ligand. α-haloketones can be used instead of the hydroxyketones; Schrauzer *et al.*[24] reported the synthesis of a thiophosphate ester from α-bromoacetophenone and P_4S_{10}. More complex starting materials have been used as well. Reaction of 4,4'-dibromobenzil with P_4S_{10}, followed by addition of $NiCl_2{\cdot}6H_2O$, gave the nickel dithiolate, bis[*cis*-1,2-(4-bromobenzene)-1,2-ethenedithiolene]nickel.[25]

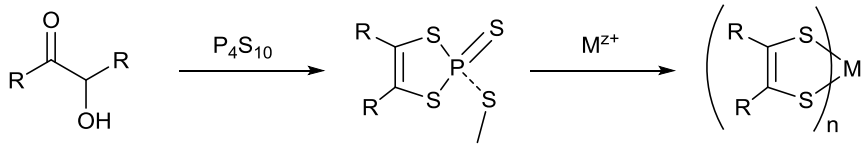

Scheme 1.7 Synthesis of metal dithiolene complexes from α-hydroxyketones *via* thiophosphate esters.

1.2.4 From 1,2,-Dithietes and 1,2,5,6-Tetrathiocins

Another method of synthesizing metal dithiolene complexes that has been reported is the oxidative addition of 1,2-dithietes to low valent transition metals. Oxidative addition of the dithiete $(F_3C)_2C_2S_2$ (**Figure 1.3**) to $[CpMo(CO)_3]_2$ afforded the purple dinuclear molybdenum dithiolate $Cp(CO)_2Mo[S_2C_2(CF_3)_2]_2MoCp$ which was isolated in *ca*. 50% yield by column chromatography.[26] Here, the two dithiolene ligands bridge between the molybdenum centres. When THF solutions of this complex are exposed to ultraviolet light, the colour becomes yellow, and the $[CpMo(S_2C_2(CF_3)_2)_2]_2$ complex is obtained in 90% yield, with evolution of CO gas.

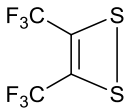

Figure 1.3 Structure of the 1,2-dithiete $S_2C_2(CF_3)_2$.

Following this, the Rawson group extended this method to 1,2,5,6-tetrathiocins. These tetrathiocins can be viewed as dimers of 1,2-dithietes and would be expected to exhibit similar chemistry. A range of benzo-fused tetrathiocins can be made in multi-gram quantities in a simple one-pot synthesis developed by Stender[27] from the reaction of S_2Cl_2 with functionalized benzenes. Subsequent oxidative addition of bis-(dimethoxybenzo)-1,2,5,6-tetrathiocin to zero-valent group 10 metals led to a series of metal dithiolene complexes, obtained in good yields (77 – 89%) (**Scheme 1.8**).[28] Further studies showed that this method could be extended to include other tetrathiocins and that the phosphine co-ligand used can have marked effects on the structures of these complexes.[29] These studies will be expanded upon in more detail in later chapters of this thesis.

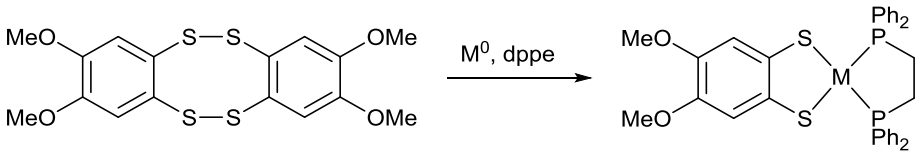

Scheme 1.8 Oxidative addition of 1,2,5,6-tetrathiocins to zero-valent metals, where M^0 = $Ni(COD)_2$, Pd_2dba_3, $Pt(dppe)_2$.

1.2.5 Addition of Alkynes to Metal Sulfides

Multiple studies have been conducted on the formation of metal dithiolene complexes from the reaction of metal sulfides and alkynes. A common activated alkyne in the literature is dimethyl acetylenedicarboxylate (DMAD). Coucouvanis *et al*.[30] reported the reactions of DMAD with molybdenum sulfides, such as $[OMo(S_4)_2]^{2-}$, $[O_2Mo_2S_9]^{2-}$, and $[OMo_2S_7]^{2-}$, in acetonitrile or dimethyl formamide to give a series of molybdenum dithiolates. Rauchfuss and Bolinger[31] studied titanium dithiolates prepared from DMAD and Cp_2TiS_5 (**Scheme 1.9**). The dark green crystalline solids recovered from these reactions were purified using GPC in moderate yields (*ca.* 40%). The resultant complexes could then be used to make nickel, platinum and rhodium dithiolates. Similar studies were undertaken using selenium-based precursors.

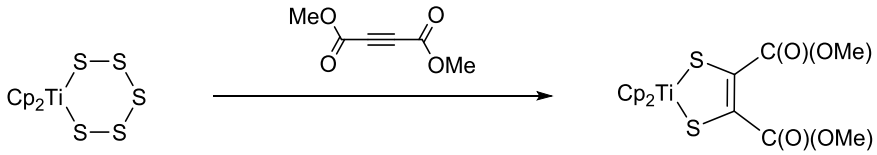

Scheme 1.9 Synthesis of a titanium dithiolate from DMAD and Cp_2TiS_5.

Unactivated alkynes can also be used to form these complexes. DuBois *et al*.[32] found that adding acetylene to a $CHCl_3$ solution of $[CpMo(S_2C_2H_4)]_2$ or $[CpMo(S_2C_3H_6)]_2$ led to exchange of the hydrocarbon bridge of the dithiolate ligands, giving the product $[CpMo(S_2C_2H_2)]_2$ in good yields (54 – 62%) along with free ethene. This new metal dithiolene complex can be converted back to its original form with the addition of H_2, which reduces the ethene bridge to ethane. In this way, a catalytic cycle can be developed for the reduction of acetylene to ethene (**Scheme 1.10**). Further studies showed similar reactions could be undertaken using $[(Me_nCp)Mo(S)SH]_2$ as a starting material, replacing the bridging S and SH with dithiolenes.[33]

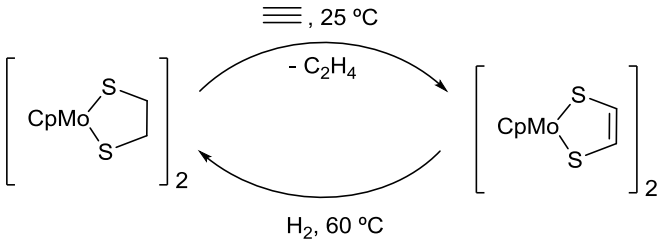

Scheme 1.10 Catalytic cycle for the reduction of acetylene to ethene.

Studies into the production of metal dithiolene complexes from $[ReS_4]^-$ showed that these reactions were dependent on the ratio of reactants. Mononuclear complexes such as $[ReS_2(S_2C_2(TMS)_2)]^-$ can be formed from $[ReS_4]^-$ and excess TMSC≡CTMS, which then dimerize to the dinuclear $[Re_2S_4(S_2C_2(TMS)_2)_2]^{2-}$, while stoichiometric deficiency of the alkyne led to formation of a tetranuclear $[Re_4S_{12}(S_2C_2(TMS)_2)_2]^{4-}$ complex.[34]

1.2.6 From Metal Sulfides and α-Haloketones

Related to the thiophosphate method is the reaction of α-haloketones with metal sulfides. A series of nickel, palladium, and platinum dithiolates were obtained by the condensation of $(dppe)M(SH)_2$ with heterocycle-substituted α-bromoketones in DMF (one example is shown in **Scheme 1.11**).[35] These complexes were positively charged and could be reduced with the addition of base, thereby removing a proton from the heterocycle, giving neutral complexes in moderate yields (30 – 54%). This method can be extended to include other related compounds, including α-tosyl and α-phosphorylated ketones.[36]

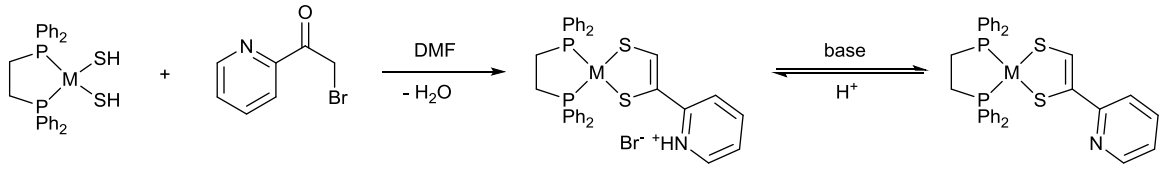

Scheme 1.11 Synthesis of metal dithiolates from metal sulfides and α-bromoketones, where M = Ni, Pd, or Pt.

1.2.7 By Dehydrogenation of Alkanedithiolates

An alternative strategy to these complexes is the dehydrogenation of alkanedithiolates to alkenedithiolates. Similar to the studies with alkynes such as DMAD to give alkenedithiolates, these alkanedithiolates can be made from alkenes. Zinc dithiolene

complexes were synthesized from zinc polysulfides and alkenes such as dimethyl maleate and dimethyl fumarate in refluxing acetonitrile *via* an alkanedithiolate intermediate.[37] The zinc alkanedithiolate undergoes dehydrogenation to form the alkenedithiolate (**Scheme 1.12**). In the cyano-substituted dithiolene complex, the dithiolene ligand could be removed by reaction with Cp_2TiCl_2, giving the titanium dithiolene complex.

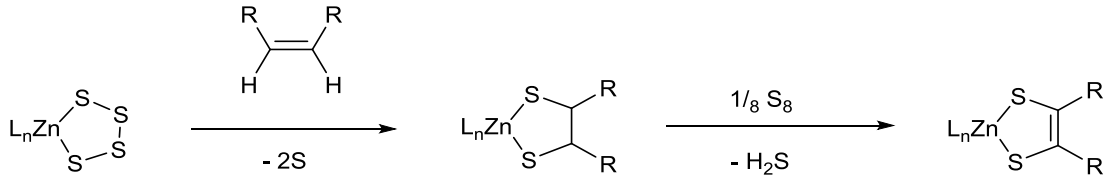

Scheme 1.12 Preparation of zinc dithiolene complexes from zinc polysulfides and an alkene.

DuBois *et al*.[38] studied the thermal dehydrogenation of the ethanedithiolate complex $Re(EtMe_4C_5)Cl_2(S_2C_2H_4)$ to form the dithiolene complex $Re(EtMe_4C_5)Cl_2(S_2C_2H_2)$ in yields of 30 – 50%. They also found that the ethenedithiolate could be obtained under milder temperatures by reacting the ethanedithiolate with dry oxygen gas.

1.2.8 From Dithiocarbonates

Previously, 1,3-dithiol-2-ones were mentioned as a source for alkenedithiolates (section **1.2.2**). These dithiocarbonates can also be reacted with metal sulfides to produce metal dithiolene complexes directly. Yang *et al*.[39] reported the synthesis of complexes from MS_4^{2-} (M = Mo, W) and tetrathiapentalenedione (TPD). These reactions gave bright green and dark blue crystals of the corresponding molybdenum and tungsten dithiolates, with COS gas as the major side product. The negatively charged dithiolate $[Mo(S_2C_2S_2CO)_3]^{2-}$ could be oxidized by addition of iodine, nitrosonium salts, or ferrocenium salts to give the neutral $Mo(S_2C_2S_2CO)_3$, which is then used to produce dithiolates with various sulfur-based functional groups, by reaction with sodium methoxide and alkyl iodides (**Scheme 1.13**).

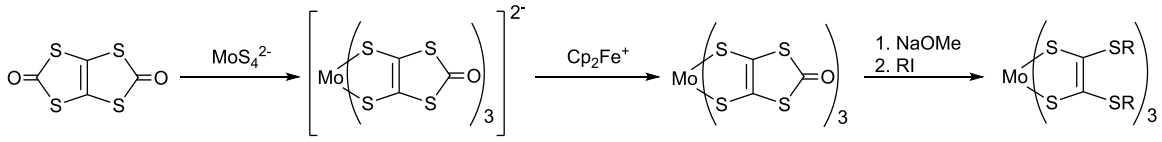

Scheme 1.13 Synthesis of molybdenum dithiolene complexes from dithiocarbonates and metal sulfides.

Pafford *et al.*[40] studied the synthesis of zinc dithiolates from the polysulfide ZnS_4(PMDETA) and TPD in a similar manner. These studies were extended to include complexes from sulfur-based thiones and CpCo(COD).[41]

1.3. Properties and Applications of Metal Dithiolene Complexes

Due to their redox and spectroscopic properties, metal dithiolene complexes may be used in many different applications, including the preparation of conducting and magnetic materials, dyes, nonlinear optics, and as models of biological systems, which allow them to serve as building blocks for various materials applications. This section highlights some of these possible applications.

1.3.1 Conducting Materials

For compounds to exhibit metallic conductivity, certain basic criteria should be met. These typically include: (i) the formation of π-stacked structures which affords efficient π–π orbital overlap along the stacking direction required to develop a band structure (i.e. a set of delocalized 'crystal orbitals') and (ii) the band needs to be partially occupied. The band structure for a typical diamagnetic insulator is shown in **Figure 1.4a** and shows a large band gap (ΔE) between the full 'valence' and empty 'conduction' band. Increasing the band width through better orbital overlap or reducing the HOMO-LUMO gap can lead to a semiconductor (**Figure 1.4b**) in which the low-lying nature of the conduction band (small ΔE) means there is some thermal population of the valence band ($e^{-\Delta E/kT}$). Semiconductors therefore exhibit an increase in conductivity with increasing temperature. Metallic systems exhibit a gapless state (ΔE = 0) and are formed when the HOMO-LUMO gap is small (or zero) and the band width large, leading to a touching or complete overlap of the valence and conduction bands (**Figure 1.4c**).

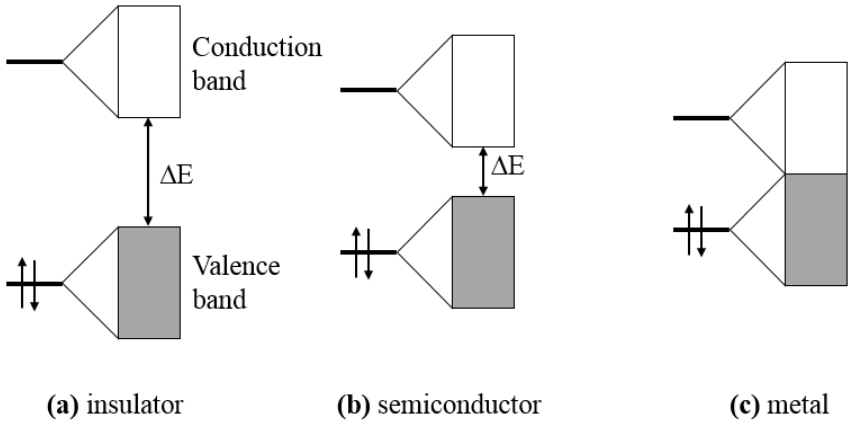

Figure 1.4 Schematic band structures for insulators, semiconductors, and metals.

Doping is an efficient way of improving conductivity. In an insulator, the Fermi level lies between bands, well away from states which are able to carry current. In *n*-type doping, a negative charge (electron) is added to the system and the extra electron is accommodated in the previously empty 'LUMO' band which becomes partially occupied (**Figure 1.5a**). Now the Fermi level (E_F) is raised and lies within a band giving rise to an increase in conductivity. For extended solids this might be done by doping a small amount of phosphorus (group V) into silicon (group IV) for example. In *p*-type doping a positive charge is added to the system (**Figure 1.5c**), leading to removal of electrons from the fully occupied band, lowering the Fermi level into the valence band. This is often done by adding iodine, for example, which acts as an acceptor (forming I^-).

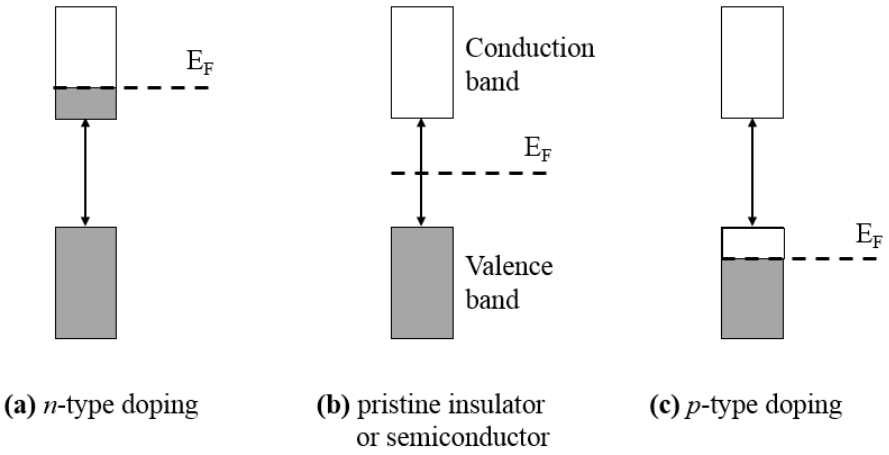

Figure 1.5 Formation of conducting states by doping of insulators/semiconductors.

Charge transfer salts are a family of organic or inorganic/organic hybrids in which the cation, the anion or both cation and anion typically adopt π-stacked structures. A textbook example is TTF·TCNQ in which TTF (tetrathiafulvalene) has a relatively high-lying HOMO whereas TCNQ (tetracyanoquinodimethane) has a low-lying LUMO (**Figure 1.6a**). In the solid, state the top of the HOMO band of TTF is higher than the bottom of the LUMO band of TCNQ and some electrons (charge) are transferred from TTF (a 'donor') to TCNQ (an 'acceptor'). The amount of charge transfer from donor to acceptor stack can be adjusted at the molecular level by tuning the donor HOMO and acceptor LUMO energies. Both TTF and TCNQ bands are partially occupied and can contribute to conduction (**Figure 1.6b**). In this context, square-planar metal dithiolene complexes have attracted particular attention since they can adopt efficient π-stacked structures and the HOMO and LUMO orbital energies can be tuned through the oxidation state of the metal and the electron-withdrawing/releasing properties of the dithiolate substituents.

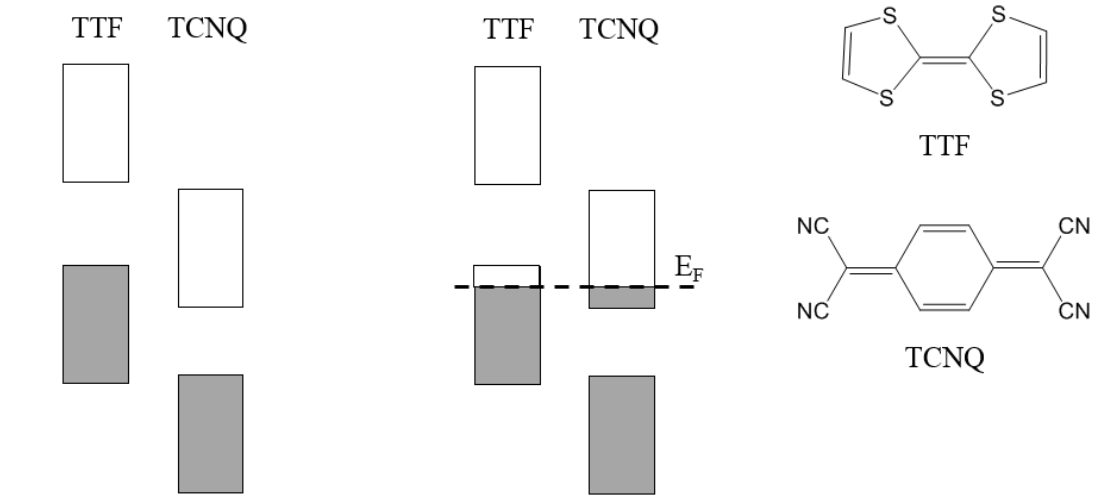

Figure 1.6 Schematic band structures for the charge transfer salt TTF·TCNQ.

The development of conducting charge transfer materials therefore requires appropriate symmetry matching and close packing to afford good orbital overlap (band width), as well as partial filling of the conduction band either through partial oxidation or through partial electron transfer.[1,42] This often leads to complexes which have formally fractional

oxidation states with partially filled conduction bands.[43] Many conducting metal dithiolene complexes have been reported in literature, including ones based on nickel,[44] palladium,[45] platinum,[46] gold,[47] cobalt,[48] copper,[49] iron,[48a] and even a conducting dithiolene-based metal-organic framework.[50]

The conductivity of metal dithiolene complexes can be affected by the nature of the metal centre, dithiolene ligand, oxidation state, and even counterion. In comparing the group 10 dithiolates TTF[Ni(dmit)$_2$]$_2$, TTF[Pd(dmit)$_2$]$_2$, and TTF[Pt(dmit)$_2$]$_3$, room temperature conductivities were measured as 300 S/cm, 750 S/cm, and 20 S/cm, with the nickel complex exhibiting high conductivity at temperatures even as low as 4 K with the conductivity increasing as temperature decreases, the palladium complex displayed a maximum in its conductivity at 220 K, and the platinum complex acted as a semiconductor throughout the temperature range studied (300 – 100 K).[51] Comparing (EDT-TTF)$_2$[Pd(dmit)$_2$]$_2$ to γ-(EDT-TTF)[Ni(dmit)$_2$] shows a room temperature conductivity of 55 S/cm and metallic behaviour down to 0.5 K for the former and 100 S/cm and 100 K for the latter.[52] By changing the dithiolene ligand, conductivity can be changed. Dautel *et al*.[53] reported that going from [Au(bdt)$_2$]$^{\bullet}$ to [Au(F$_2$pdt)$_2$]$^{\bullet}$ to [Au(α-tpdt)$_2$]$^{\bullet}$ gives room temperature conductivities of 10^{-3} S/cm, 0.05 S/cm, and 5 S/cm (**Figure 1.7**).

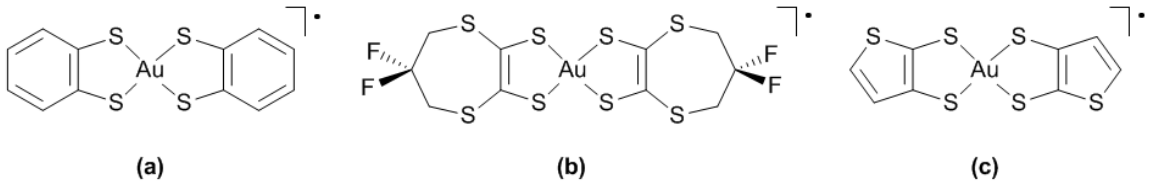

Figure 1.7 Structures of **(a)** [Au(bdt)$_2$]$^{\bullet}$, **(b)** [Au(F$_2$pdt)$_2$]$^{\bullet}$, and **(c)** [Au(α-tpdt)$_2$]$^{\bullet}$.

Studies by Kobayashi *et al*.[54] showed that by extending the π-conjugated system on the dithiolene ligand structure, conductivity can be increased. For example, Ni(tmdt)$_2$ (**Figure 1.8**) exhibited a room temperature conductivity of 400 S/cm and was metallic down to 0.6 K whereas Ni(dmit)$_2$ shows a room temperature conductivity of 3.5×10^{-3} S/cm.[55]

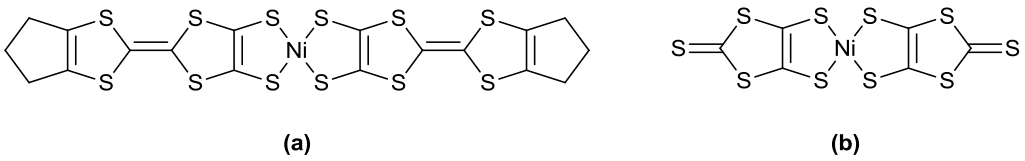

Figure 1.8 Structures of **(a)** Ni(tmdt)$_2$ and **(b)** Ni(dmit)$_2$.

As we saw earlier, doping affects the oxidation state and resultant conductivity by adjusting the position of the Fermi level. This is exemplified by Ni(dmit)$_2$ which exhibits a conductivity of 3.5×10^{-3} S/cm[55] whereas TTF[Ni(dmit)$_2$]$_2$ shows conductivity up to 300 S/cm.[51] Similarly, (N^nBu_4)$_{0.5}$[Pd(dmit)$_2$] has a value of 12 S/cm with a transition temperature of 120 K, compared to 150 S/cm with a transition temperature of 240 K for (N^nBu_4)$_{0.33}$[Pd(dmit)$_2$].[56] Small changes in counterion can have large effects on the conductivity as well, as shown by the observation that room temperature conductivity increases significantly upon changing one of the methyl groups on the counterion of [NMe$_4$]$_{0.5}$[Ni(dmit)$_2$] for a hydrogen, from 60 S/cm to 140 S/cm, although the lowest temperature at which the complex remains metallic increases from 100 K to 220 K.[57] By changing any one of these factors, conductivity can be tuned, and properties can be optimized for desired applications. Conducting metal dithiolene complexes have found applications in electrical sensors to detect gases,[58] films for memory switching,[59] and powders for fingerprint development.[60]

1.3.2 Magnetic Materials

The electronic structure of paramagnetic metal dithiolene complexes allows them to exhibit magnetic properties. The non-innocent nature of the dithiolate ligand typically leads to π-delocalization of spin density from the metal to the ligand. In many cases, dithiolate complexes display antiferromagnetic behavior arising from direct π-π overlap between radicals.[1,61] Studies comparing the isostructural [Cp$_2$Mo(dddt)][TCNQ] and [Cp$_2$W(dddt)][TCNQ] salts showed antiferromagnetic behaviour coming from the [Cp$_2$M(dddt)]$^{\bullet+}$ unit.[62] [Cp$_2$Mo(dddt)]$^{\bullet+}$ displayed Curie-Weiss behaviour in the high temperature regime, with a maximum in the χ vs T graph of T(χ_{max}) = 32 K, and a value for the Weiss constant of θ = –42 K and for the exchange interaction of J/k = –26 K. [Cp$_2$W(dddt)]$^{\bullet+}$ displayed similar behaviour, with T(χ_{max}) = 18 K and J/k = –16 K (θ was not reported). The smaller magnitude for J/k in the tungsten complex was attributed

to increased metal localization in this complex. The effect of the counterion on the magnetic properties of $[Cp_2Mo(dmit)]^+$ cation salts is shown in **Table 1.1** and shows that the increasing size of the anion leads to longer intermolecular contacts and weaker interactions between S = ½ ions.[63] Recently Jeannin *et al.*[61] reported ferromagnetic coupling in the copper dithiolate salt $[Ni(cyclam)][Cu(tfadt)_2]$.

Table 1.1 Magnetic properties of $[Cp_2Mo(dmit)][Y]$ salts.[63]

Complex	$\theta_{Curie\text{-}Weiss}$ *(K)*	T_{Neel} *(K)*
$[Cp_2Mo(dmit)][PF_6]$	–37	11.5
$[Cp_2Mo(dmit)][AsF_6]$	–21	9.5
$[Cp_2Mo(dmit)][SbF_6]$	–14	7.5

1.3.3 Optical Properties and Non-Linear Optics

Many metal dithiolenes exhibit very intense absorptions in the near infrared (NIR) region allowing them to play important roles in the development of laser dyes as well as solar cell applications. Absorptions above 700 nm have been attributed to HOMO-LUMO π-π* transitions. In these complexes, the HOMO and LUMO are predominantly ligand-based, with some small contribution from the metal, leading to the formation of a mixed-metal ligand-to-ligand charge transfer (MMLLCT), in which one ligand acts as a charge donor that is easily oxidized and the other acts as a charge acceptor that is easily reduced.[64] In the (dithiolene)M(diimine) systems commonly used, the HOMO is primarily dithiolene-based while the LUMO comes from the diimine (**Figure 1.9**). The fact that the metal is involved in charge transfer means that the identity of the metal will affect the energy of the charge transfer.[65] The HOMO-LUMO energy gap can be tuned by changing the functional groups on the ligands, wherein electron-donating groups will increase the π orbital energy and electron-withdrawing groups will decrease the π orbital energy.[64] Strategies in which electron-donating groups are added to the ligand responsible for the HOMO and electron-withdrawing groups are added to the ligand containing the LUMO would lower the HOMO-LUMO gap, giving absorptions at higher wavelengths and increasing the first molecular hyperpolarizability, which is important for nonlinear optical (NLO) applications.

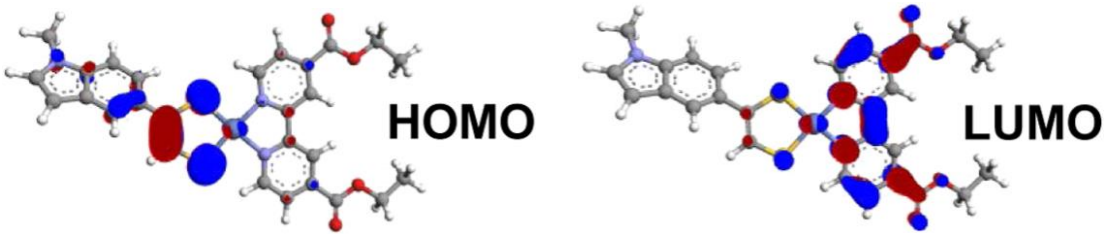

Figure 1.9 DFT diagram showing the contribution of the dithiolene ligand (and some metal) to the HOMO and the diimine (and some metal) to the LUMO. Picture taken from reference 64.

In addition to high absorptivities, these complexes provide high thermal and photochemical stability, and good solubility in nonpolar organic solvents, all useful qualities for device applications and processing. They also provide the opportunity to tune their absorption with changing the structures of the dithiolene ligands.[1]

Most of the complexes which have been examined to date are nickel-dithiolates which have a more electron-delocalized structure than the heavier group 10 palladium and platinum complexes. A number of research groups have examined complexes containing extended π systems, with bulky electron-donating functional groups as coplanar to the Ni(dithiolene) as possible.[1]

Studies into the effect that changing the functional groups of the dithiolene ligand has on the NIR absorption have been conducted. Madhu and Das[66] observed that the absorption band in $[NBu_4][Ni(XPhdt)_2]$ went from 970 nm to 1020 nm to 1030 nm when X = NO_2, F, and Cl, respectively. It was postulated that the absorption of the NO_2-substituted complex at lower wavelength was because this substituent was the most electron-withdrawing, decreasing the electron density on the dithiolene ligand, thereby lowering the HOMO and leading to a larger gap between the HOMO and LUMO. The effects of adding electron-withdrawing or electron-donating groups was further explored by Miao and coworkers.[67] Substituting the phenyl group on the nickel dithiolene complex $Ni[S_2C_2(C_6H_4R)_2]_2$ with a hydrogen, a methyl group, or a methoxycarbonyl gave absorption maxima at 857, 884, and 868 nm. The electron-donating methyl group increases electron density on the dithiolene, giving a smaller HOMO-LUMO gap, and therefore an absorption at higher wavelength. The electron-withdrawing methoxycarbonyl, on the other hand, lowers the electron density on the dithiolene in

comparison to the methyl group, giving a similar effect as the NO_2-substituted complex mentioned previously. The higher absorption maximum in the methoxycarbonyl complex compared to the hydrogen-substituted complex was attributed to the increased electron delocalization. The effects of solvent on these systems are shown in **Table 1.2** with more polar solvents leading to a red-shift.

Table 1.2 Wavelengths of maximum absorption (nm) in various solvents (±0.5 nm).[67]

Complex	*Solvents (increasing polarity from left to right)*						
	Et_2O	**CH_2Cl_2**	**THF**	**$CHCl_3$**	**Dioxane**	**DMF**	**DMSO**
$Ni[S_2C_2(C_6H_5)_2]_2$	844	857	856	858	856	871	871
$Ni[S_2C_2(C_6H_4CH_3)_2]_2$	869	884	880	883	880	895	896
$Ni[S_2C_2(C_6H_4CO_2CH_3)_2]_2$	861	868	867	871	869	944	957

Oxidation state can also influence the NIR absorption. The monoanion $[NBu_4][Ni(bddt)_2]$ displayed a strong absorption at 1180 nm, while the neutral complex $Ni(bddt)_2$, obtained from I_2 oxidation, showed a high intensity absorption maximum at 1035 nm.[68]

Metal dithiolene complexes have been found to display second and third order nonlinear optical properties. Most of the systems studied for these properties are those containing a diimine co-ligand.[1] In such cases, the HOMO-LUMO transition is associated with charge transfer from the dithiolate to the diimine. Cummings and coworkers[69] found that for a series of platinum dithiolene complexes, negative values for the first hyperpolarizability could be obtained, at -16×10^{-30} esu for Pt(phen)(tdt) and -15×10^{-30} esu for the similar Pt(dmbpy)(tdt) complex which contained a methyl-substituted diimine. Changing the metal centre from palladium to zinc in the M(dpphen)(tdt) complex gave similar hyperpolarizabilities of -4×10^{-30} esu. This second order nonlinearity can also be displayed by dithiolene complexes comprising two different dithiolenes, rather than a dithiolene/diimine combination;[70] Espa and coworkers reported the mixed-dithiolene complexes M(Bz_2pipdt)(dmit) (M = Ni, Pd, Pt) and found that they displayed first hyperpolarizabilities which were much higher than those exhibited by the complexes containing diimine ligands. Nickel complexes exhibiting third order nonlinear optical properties were studied by Underhill *et al.*,[71] who found that complexes which absorb at

wavelengths around 800 nm gave the best applications, with a large value for the second hyperpolarizability and a small value for the linear absorption coefficient.[1] Metal dithiolene complexes displaying these optical properties have been used in such material applications as Q-switch laser dyes,[72] dye-sensitized solar cells,[67,73] NIR absorbing filters,[67] optical limiters,[68] all-optical switching devices,[74] photocatalysts,[75] and photoelectrical conversion.[76]

1.3.4 Biological Systems

Dithiolene complexes can be found in nature in the active sites of most molybdenum and some tungsten-containing enzymes.[77] These enzymes are present in most living organisms, serving a variety of different functions, such as the oxidation of sulfite to sulfate and aldehydes to carboxylic acids, and the reduction of nitrate to nitrite and DMSO to DMS. These enzymes are also referred to as oxotransferases, given that the reactions they catalyze involve two-electron redox reactions with the transfer of an oxygen atom. Commonly, the dithiolene ligand found in the active site of these enzymes is molybdopterin (**Figure 1.10**). There are several classes of these complexes based on their structures, with all the known tungsten-based complexes falling in the DMSO reductase family with two molybdopterin ligands bound to the central tungsten. The exact role the dithiolene ligands play in these enzymes is unclear. Studies into analogues of the complexes found in the active sites have been conducted in order to learn more about the structural and spectroscopic characteristics of these complexes, the reactions catalyzed by them, and the role played by these complexes.[78]

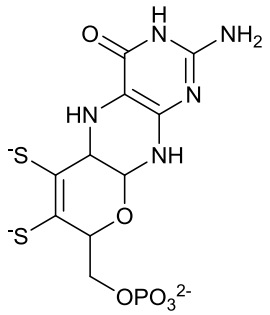

Figure 1.10 Structure of the dithiolate molybdopterin found in the active site of many enzymes.

1.3.5 Recent Advances

The field of metal dithiolene chemistry has been undergoing a growth of interest in recent years. Some of these studies touch upon applications already discussed thus far. For example, Cioncoloni and coworkers[79] synthesized $[Co_2(bdt)_2(Me_2bpy)_3](NO_3)_2$, which was the first example of a mixed diimine/dithiolene dicobalt complex. The metal centres in this complex were in different coordination environments, with one of the cobalt atoms bound to two bipyridine ligands and the other bound to only one bipydridine, and the two dithiolates bridging between the metal centres. As a result, these two centres have different redox properties that were rationalized by DFT calculations, in which it was shown that the cobalt atom bound to two bipyridines is easier to reduce, while reduction of the other cobalt led to irreversible decomposition of the complex. At the beginning of this year, Wang *et al.*[80] reported a zinc bis(dithiolene) complex synthesized from the reaction of 4,5-bis(2-methyl-5-phenylthiophen-3-yl)-1,3-dithiol-2-one with sodium methoxide and $ZnCl_2$. This dianionic complex exhibited reversible photochromism, in which a stepwise ring-closing took place in the dithiolene ligands upon UV light irradiation at 312 nm. This photocyclization could be reversed by irradiating the new complexes with light at wavelengths larger than 480 nm. Last year, Pilia *et al.*[81] reported the first example of a (diimine)M(dithiolate) complex incorporated into a NLO-active film, which showed a NLO response higher than those showed by similar push-pull chromophores.

However, other applications have been explored recently. In the field of catalysis, Zarkadoulas and coworkers[82] found that a series of nickel dithiolates $[Ni(bdt)_2](NBu_4)$, $[Ni(tdt)_2](NBu_4)$, and $[Ni(mnt)_2](NBu_4)$ could be used to catalyze a hydrogen evolution reaction from trifluoroacetic acid. Two pathways were proposed for this catalytic process; both began with reduction of the catalyst to the dianion and protonation at sulfur, followed by either: (i) a second protonation then reduction; or (ii) reduction then protonation. The final step in both these pathways was evolution of H_2 gas. In their studies, they found that electron-donating substituents on the dithiolene ligands helped improve catalytic activity, while catalytic activity was reduced in the $[Ni(mnt)_2](NBu_4)$ complex, which contained the strong electron-withdrawing CN groups.

In a biological application, two metal dithiolene complexes bearing bulky carborane groups were shown to have applications as anti-cancer therapeutics.[83] Both the ruthenium and osmium complexes were highly active towards human ovarian cancer cells, with only moderate toxicity towards normal cells. However, these complexes were hydrophobic, and encapsulation into micelles allowed these complexes to be soluble in water so that they could be administered in a manner suitable for cancer cell treatment, although it reduced the anti-cancer activity. However, these micelles proved more selective towards the cancer cells over normal cells.

1.4. Overview of this Thesis

Our previous studies into transition metal dithiolene complexes showed that the oxidative addition chemistry of 1,2,5,6-tetrathiocins to low oxidation state group 10 metals in the presence of a phosphine is a versatile method to synthesize a variety of group 10 dithiolate complexes. Reaction of bis-(dimethoxybenzo)-1,2,5,6-tetrathiocin with zero valent group 10 substrates ($Ni(COD)_2$, $Pt(PPh_3)_3$ or Pd_2dba_3) in the presence of the chelate phosphine dppe afforded a series of square planar complexes of formula (dmobdt)M(dppe) (M = Ni, Pd, Pt) in good yields.[28] This work has been extended to the synthesis of (dithiolate)Ni(NN') complexes where NN' can be a chelate diimine or bipyridine or phenanthroline ligand.[84] Following this, the effects of the phosphine co-ligand was explored with PPh_3 favoring formation of dimetallic complexes $[(dmobdt)M(PPh_3)]_2$ in which one of the two S atoms of each dithiolate ligand adopts a μ_2-bridging mode. In the presence of P^tBu_3, Pd_2dba_3 reacts with bis-(dimethoxybenzo)-1,2,5,6-tetrathiocin to form the hexanuclear complex $[Pd(dmobdt)]_6$ in which every S atom in the structure adopts a μ_2-coordination mode.[29]

The easy synthesis of the tetrathiocins and the potential to functionalize the benzo group has allowed a diverse array of complexes with different functional groups on the dithiolene ligand to be synthesized.[85] The ability to control the structure of the metal dithiolene complexes (metal, aggregation state, dithiolate, co-ligand) could lead to the production of complexes whose electronic and optical properties can be systematically tuned.

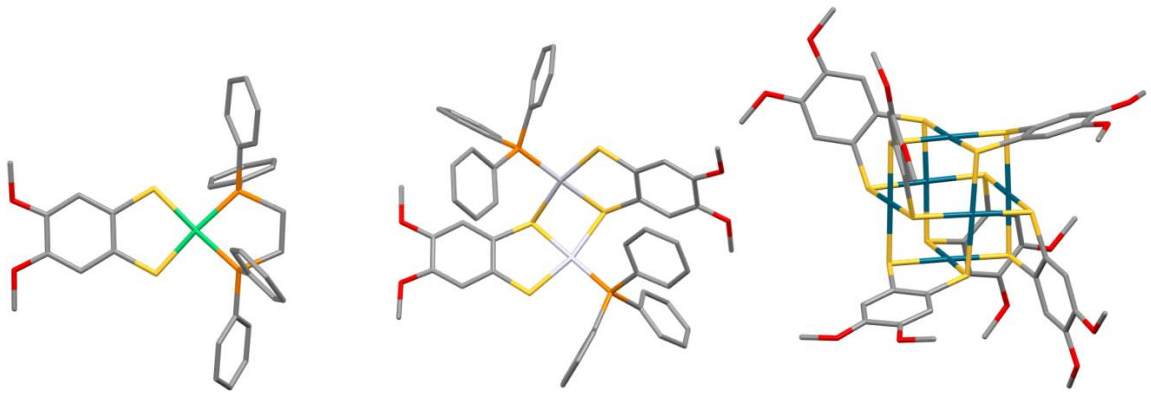

Figure 1.11 Some monometallic, dimetallic, and hexametallic group 10 dithiolene complexes previously reported in this group.[28,29]

This thesis expands upon previous studies in the Rawson group. Chapter 2 further explores the effect of the phosphine co-ligand on the structure of the complexes formed for the group 10 metals palladium and platinum, particularly focusing on the steric demands of the phosphine in directing the outcome of the oxidative addition reaction. Previous studies in the group have been limited to group 10 metals (Ni, Pd, Pt) and Chapter 3 extends this oxidative addition method to the formation of group 9 metal complexes focusing on the preparation and characterization of a series of CpCo(dithiolate) complexes, including an exploration of the crown-functionalized dithiolene complex to bind *s*-block metals to build heterometallic complexes.

1.5. References

1. *Dithiolene chemistry: Synthesis, properties, and applications,* ed. E. I. Stiefel, Interscience, Hoboken, New Jersey, 2003.

2. J. A. McCleverty, *Prog. Inorg. Chem.*, 1968, **10**, 49–221.

3. **(a)** F. H. Allen, O. Kennard, D. G. Watson, L. Brammer, A. G. Orpen and R. Taylor, *J. Chem. Soc., Perkin Trans. II*, 1987, S1; **(b)** C. N. R. Rao, R. Venkataraghavan and T. R. Kasturi, *Can. J. Chem.*, 1964, **42**, 36–42.

4. D. M. Giolando and K. Kirschbaum, *Synthesis*, 1992, 451–452.

5. E. I. Stiefel, R. Eisenberg, R. C. Rosenberg and H. B. Gray, *J. Am. Chem. Soc.*, 1966, **88**, 2956–2966.

6. H. Sugimoto, Y. Furukawa, M. Tarumizu, H. Miyake, K. Tanaka and H. Tsukube, *Eur. J. Inorg. Chem.*, 2005, 3088–3092.

7. H. V. Huynh, T. Lugger and F. E. Hahn, *Eur. J. Inorg. Chem.*, 2002, 3007–3009.

8. S. Boyde, S. R. Ellis, C. D. Garner and W. Clegg, *J. Chem. Soc., Chem. Commun.*, 1986, 1541–1543.

9. H. Oku, N. Ueyama, M. Kondo and A. Nakamura, *Inorg. Chem.*, 1994, **33**, 209–216.

10. D. W. Stephan, *Inorg. Chem.*, 1992, **31**, 4218–4223.

11. R. B. King and C. A. Eggers, *Inorg. Chem.*, 1968, **7**, 340–345.

12. J. L. Zuo, T. M. Yao, F. You, X. Z. You, H. K. Fun and B. C. Yip, *J. Mater. Chem.*, 1996, **6**, 1633–1637.

13. C. T. Vance, R. D. Bereman, J. Bordner, W. E. Hatfield and J. F. Helms, *Inorg. Chem.*, 1985, **24**, 2905–2910.

14. P. Falaras, C. Mitsopoulou, D. Argyropoulos, E. Lyris, N. Psaroudakis, E. Vrachnou and D. Katakis, *Inorg. Chem.*, 1995, **34**, 4536–4542.

15. **(a)** H. Tamura, S. Tanaka, G. Matsubayashi and W. Mori, *Inorg. Chim. Acta*, 1995, **232**, 51–55; **(b)** D. D. Doxsee, C. P. Galloway, T. B. Rauchfuss, S. R. Wilson and X. Yang, *Inorg. Chem.*, 1993, **32**, 5467–5471.

16. X. Yang, T. B. Rauchfuss and S. R. Wilson, *J. Am. Chem. Soc.*, 1989, **111**, 3465–3466.

17. L. Yu and D. Zhu, *Phos, Sulf., Sil and Rel. Elts*, 1996, **116**, 225–234.

18. G. N. Schrauzer, V. P. Mayweg, H. W. Finck and W. Heinrich, *J. Am. Chem. Soc.*, 1966, **88**, 4604–4609.

19. G. N. Schrauzer, V. P. Mayweg and W. Heinrich, *J. Am. Chem. Soc.*, 1966, **88**, 5174–5179.

20. G. Matsubayashi, K. Akiba, and T. Tanaka, *Inorg. Chem.*, 1988, **27**, 4744–4749.

21. C. M. Bolinger and T. B. Rauchfuss, *Inorg. Chem.*, 1982, **21**, 3947–3954.

22. M. Kumasaki, H. Tanaka and A. Kobayashi, *J. Mater. Chem.*, 1998, **8**, 301–307.

23. G. N. Schrauzer and V. P. Mayweg, *J. Am. Chem. Soc.*, 1965, **87**, 1483–1489.

24. G. N. Schrauzer, V. P. Mayweg and W. Heinrich, *Inorg. Chem.*, 1965, **4**, 1615–1617.

25. C. L. Kean, D. O. Miller and P. G. Pickup, *J. Mater. Chem.*, 2002, **12**, 2949–2956.

26. K. Roesselet, K. E. Doan, S. D. Johnson, P. Nicholls and G. L. Miessler, *Organomet.*, 1987, **6**, 480–485.

27. K. W. Stender, N. Wolki and G. Klar, *Phos, Sulf., Sil and Rel. Elts*, 1989, **42**, 111–114.

28. J. D. Wrixon, J. J. Hayward, O. Raza and J. M. Rawson, *Dalton Trans.*, 2014, **43**, 2134–2139.

29. **(a)** J. D. Wrixon, J. J. Hayward and J. M. Rawson, *Inorg. Chem.*, 2015, **54**, 9384–9386; **(b)** J. D. Wrixon, Z. S. Ahmed, M. U. Anwar, Y. Beldjoudi, N. Hamidouche, J. J. Hayward and J. M. Rawson, *Polyhedron*, 2016, **108**, 115–121.

30. D. Coucouvanis, A. Iladjikyriacou, A. Toupadakis, S. M. Koo, O. Ileperuma, M. Draganjac and A. Salifoglou, *Inorg. Chem.*, 1991, **30**, 154–161.

31. C. M. Bolinger and T. B. Rauchfuss, *Inorg. Chem.*, 1982, **21**, 3947–3954.

32. M. Rakowski, M. R. DuBois, R. C. Haltiwanger, D. J. Miller and G. Glatzmaier, *J. Am. Chem. Soc.*, 1979, **101**, 5245–5252.

33. M. R. DuBois, M. C. VanDerveer, D. L. DuBois, R. C. Haltiwanger and W. K. Miller, *J. Am. Chem. Soc.*, 1980, **102**, 7456–7461.

34. J. T. Goodman and T. B. Rauchfuss, *Inorg. Chem.*, 1998, **37**, 5040–5041.

35. S. P. Kaiwar, J. K. Hsu, L. M. Liable-Sands, A. L. Rheingold and R. S. Pilato, *Inorg. Chem.*, 1997, **36**, 4234–4240.

36. J. K. Hsu, C. J. Bonangelino, S. P. Kaiwar, C. M. Boggs, J. C. Fettinger and R. S. Pilato, *Inorg. Chem.*, 1996, **35**, 4743–4751.

37. R. J. Pafford, J. H. Chou and T. B. Rauchfuss, *Inorg. Chem.*, 1999, **38**, 3779–3786.

38. J. A. Kanney, B. C. Noll and M. R. DuBois, *J. Am. Chem. Soc.*, 2002, **124**, 9878–9886.

39. X. Yang, G. K. W. Freeman, T. B. Rauchfuss and S. R. Wilson, *Inorg. Chem.*, 1991, **30**, 3034–3038.

40. R. J. Pafford and T. B. Rauchfuss, *Inorg. Chem.*, 1998, **37**, 1974–1980.

41. A. Dinsmore, J. H. Birks, C. D. Garner and J. A. Joule, *J. Chem. Soc., Perkin Trans. I*, 1997, 801–807.

42. B. Garreau-de Bonneval, K. I. M. Ching, F. Alary, T. Bui, L. Valade, *Coord. Chem. Rev.*, 2010, **254**, 1457–1467.

43. N. Robertson and L. Cronin, *Coord. Chem. Rev.*, 2002, **227**, 93–127.

44. **(a)** A. Kobayashi, T. Naito, A. Sato and H. Kobayashi, *Synth. Met.*, 1997, **86**, 1841–1842; **(b)** Y. Kashimura, Y. Okano, J. I. Yamaura and R. Sato, *Synth. Met.*, 1999, **103**, 2123–2124; **(c)** E. B. Yagubskii, L. A. Kushch, V. V. Gritsenko, O. A. Dyachenko, L. I. Buravov and A. G. Khomenko, *Synth. Met.*, 1995, **70**, 1039–

1041; **(d)** L. A. Kushch, V. V. Gritsenko, L. I. Buravov, A. G. Khomenko, G. V. Shilov, O. A. Dyachenko, V. A. Merzhanov, E. B. Yagubskii, R. Rousseau and E. Canadell, *J. Mater. Chem.*, 1995, **5**, 1633–1638.

45. **(a)** C. Faulmann, A. Errami, B. Donnadieu, I. Malfant, J. P. Legros, P. Cassoux, C. Rovira and E. Canadell, *Inorg. Chem.*, 1996, **35**, 3856–3873; **(b)** A. Kobayashi, A. Sato, K. Kawano, T. Naito, H. Kobayashi and T. Watanabe, *J. Mater. Chem.*, 1995, **5**, 1671–1679; **(c)** R. T. Henriques, L. Alcacer, J. P. Pouget and D. Jerome, *J. Phys. C*, 1984, **17**, 5197–5208; **(d)** I. D. Parker, R. H. Friend, P. I. Clemenson and A. E. Underhill, *Nature (London)*, 1986, **324**, 547–549.

46. **(a)** B. Garreau, B. Pomarede, P. Cassoux and J. P. Legros, *J. Mater. Chem.*, 1993, **3**, 315–316; **(b)** L. Alcacer, H. Novais, F. Pedroso, S. Flandrois, C. Coulon, D. Chasseau and J. Gaultier, *Solid State Commun.*, 1980, **35**, 945–949.

47. **(a)** A. I. Kotov, L. A. Kushch, E. E. Laukhina, A. G. Khomenko, A. V.Zvarykina, R. P. Shibaeva, E. B. Yagubskii, S. S. Nagapetyan and Y. T. Struchkov, *Synth. Met.*, 1991, **42**, 2355–2358; **(b)** R. T. Henriques, M. Almeida, M. J. Matos, L. Alcacer and C. Bourbonnais, *Synth. Met.*, 1987, **19**, 379–384; **(c)** R. T. Henriques, V. Gama, G. Bonfait, I. C. Santos, M. J. Matos, M. Almeida, M. T. Duarte and L. Alcacer, *Synth. Met.*, 1993, **56**, 1846–1851; **(d)** G. Bonfait, E. B. Lopes, M. J. Matos, R. T. Henriques and M. Almeida, *Solid State Commun.*, 1991, **80**, 391–394.

48. **(a)** V. Gama, I. C. Santos, G. Bonfait, R. T. Henriques, M. T. Duarte, J. C. Waerenborgh, L. Pereira, J. M. P. Cabral and M. Almeida, *Inorg. Chem.*, 1992, **31**, 2598–2604; **(b)** V. Gama, R. T. Henriques, G. Bonfait, M. Almeida, A. Meetsma, S. van Smaalen and J. L. de Boer, *J. Am. Chem. Soc.*, 1992, **114**, 1986–1989.

49. **(a)** V. Gama, M. Almeida, R. T. Henriques, I. C. Santos, A. Domingos, S. Ravy and J. P. Pouget, *J. Phys. Chem.*, 1991, **95**, 4263–4267; **(b)** V. Gama, R. T. Henriques, M. Almeida and L. Alcacer, *J. Phys. Chem.*, 1994, **98**, 997–1001.

50. Y. Kobayashi, B. Jacobs, M. D. Allendorf and J. R. Long, *Chem. Mater.*, 2010, **22**, 4120–4122.

51. M. Bousseau, L. Valade, J. P. Legros, P. Cassoux, M. Garbauskas and L. V. Interrante, *J. Am. Chem. Soc*., 1986, **108**, 1908–1916.

52. **(a)** J. P. Legros, L. Valade, B. Garreau, B. Pomarede, P. Cassoux, L. Brossard, S. Dubois, A. Audouard and J. P. Ulmet, *Synth. Met.*, 1993, **56**, 2146–2153; **(b)** A. Kobayashi, A. Sato, K. Kawano, T. Naito, H. Kobayashi and T. Watanabe, *J. Mater. Chem.*, 1995, **5**, 1671–1679.

53. O. J. Dautel, M. Fourmigue, E. Canadell, P. Auban-Senzier, *Adv. Funct. Mater*., 2002, **12**, 693–698.

54. **(a)** A. Kobayashi, H. Tanaka and H. Kobayashi, *J. Mater. Chem*., 2001, **11**, 2078–2088; **(b)** H. Tanaka, Y. Okano, H. Kobayashi, W. Suzuki and A. Kobayashi, *Science*, 2001, **291**, 285–287.

55. L. Valade, J. P. Legros, M. Bousseau, P. Cassoux, M. Garbauskas and L.V. Interrante, *J. Chem. Soc., Dalton Trans.*, 1985, 783.

56. J. P. Legros, L. Valade and P. Cassoux, *Synth. Met.*, 1988, **27**, 347–352.

57. **(a)** H. Kim, A. Kobayashi, Y. Sasaki, R. Kato, H. Kobayashi, *Chem. Lett*., 1987, 1799–1802; **(b)** B. Pomarede, B. Garreau, I. Malfant, L. Valade, P. Cassoux, J. P. Legros, A. Audouard, L. Brossard, J. P. Ulmet, M. L. Doublet and E. Canadell, *Inorg. Chem.*, 1994, **33**, 3401–3414.

58. J. W. Grate. U. S. Patent 4,992,244, 1991.

59. S. G. Liu, P. J. Wu, Y. Q. Liu and D. B. Zhu, *Mol. Cryst. Liq. Cryst.*, 1996, **275**, 211–223.

60. C. Mahadevan, *J. Crystall. Spect. Research*, **16**, 1986, 347–416.

61. O. Jeannin, R. Clerac, T. Cauchy and M. Fourmigue, *Inorg. Chem.*, 2008, **47**, 10656–10661.

62. **(a)** M. Fourmigue, C. Lenoir, C. Coulon, F. Guyon and J. Amaudrut, *Inorg. Chem.*, 1995, **34**, 4979–4985; **(b)** I. V. Jourdain, M. Fourmigue, F. Guyon and J. Amaudrut, *J. Chem. Soc., Dalton Trans.*, 1998, 483–488.

63. M. Fourmigue, *Acc. Chem. Res.*, 2004, **37**, 179–186.

64. L. Pilia, M. Pizzotti, F. Tessore and N. Robertson, *Inorg. Chem.*, 2014, **53**, 4517−4526.

65. A. Acosta, J. I. Zink, J. Cheon, *Inorg. Chem.*, 2000, **39**, 427–432.

66. V. Madhu and S. K. Das, *Inorg. Chem.*, 2008, **47**, 5055–5070.

67. Q. Miao, J. Gao, Z. Wang, H. Yu, Y. Luo and T. Ma, *Inorg. Chim. Acta*, 2011, **376**, 619–627.

68. J. F. Bai, J. L. Zuo, W. L. Tan, W. Ji, Z. Shen, H. K. Fun, K. Chinnakali, I. Abdul Razak, X. Z. You and C. M. Che, *J. Mater. Chem.*, 1999, **9**, 2419–2423.

69. S. D. Cummings, L. T. Cheng and R. Eisenberg, *Chem. Mater.*, 1997, **9**, 440–450.

70. D. Espa, L. Pilia, L. Marchi, M. L. Mercuri, A. Serpe, A. Barsella, A. Fort, S. J. Dalgleish, N. Robertson and P. Deplano, *Inorg. Chem.*, 2011, **50**, 2058–2060.

71. C. S. Winter, S. N. Oliver, R. J. Manning, J. D. Rush, C. A. S. Hill and A. E. Underhill, *J. Mater. Chem.*, 1992, **2**, 443–447.

72. D. Qing, C. X. Feng, C. Hong, G. Xing, Z. X. Ping and C. Zhusheng, *Supramol. Sci.*, 1998, **5**, 531–536.

73. **(a)** C. L. Linfoot, P. Richardson, K. L. McCall, J. R. Durrant, A. Morandeira and N. Robertson, *Solar Energy*, 2011, **85**, 1195–1203; **(b)** E. A. M. Geary, K. L. McCall, A. Turner, P. R. Murray, E. J. L. McInnes, L. A. Jack, L. J. Yellowlees and N. Robertson, *Dalton Trans.*, 2008, 3701–3708.

74. S. Oliver and C. Winter, *Adv. Mater.*, 1992, **4**, 119–121.

75. A. Zarkadoulas, E. Koutsouri and C. A. Mitsopoulou, *Coord. Chem. Rev.*, 2012, **256**, 2424–2434.

76. **(a)** J. Zhai, C. Huang , T. X. Wei, L. Gan and H. Cao, *Polyhedron*, 1999, **18**, 1513–1518; **(b)** J. Zhai, T. X. Wei, C. H. Huang and H. Cao, *J. Mater. Chem.*, 2000, **10**, 625–630; **(c)** W. S. Xia, C. H. Huang and D. J. Zhou, *Langmuir*, 1997, **13**, 80–84.

77. F. J. Hine, A. J. Taylor and C. D. Garner, *Coord. Chem. Rev*., 2010, **254**, 1570–1579.

78. **(a)** H. Sugimoto and H. Tsukube, *Chem. Soc. Rev.*, 2008, **37**, 2609–2619; **(b)** J. H. Enemark and J. J. A. Cooney, *Chem. Rev.*, 2004, **104**, 1175−1200; **(c)** S. Groysman, J. J. Wang, R. Tagore, S. C. Lee and R. H. Holm, *J. Am. Chem. Soc*.,

2008, **130**, 12794–12807; **(d)** B. S. Lim, M. W. Willer, M. Miao and R. H. Holm, *J. Am. Chem. Soc.*, 2001, **123**, 8343–8349; **(e)** J. Jiang and R. H. Holm, *Inorg. Chem.*, 2005, **44**, 1068−1072; **(f)** B. S. Lim and R. H. Holm, *J. Am. Chem. Soc.*, 2001, **123**, 1920–1930; **(g)** K. M. Sung and R. H. Holm, *J. Am. Chem. Soc.*, 2002, **124**, 4312–4320.

79. G. Cioncoloni, S. Sproules, C. Wilson and M. D. Symes, *Eur. J. Inorg. Chem.*, 2017, 3707–3713.

80. J. Wang, L. X. Shi, J. Y. Wang, J. X. Chen, S. H. Liu and Z. N. Chen, *Dalton Trans.*, 2017, **46**, 2023–2029.

81. L. Pilia**,** D. Marinotto**,** M. Pizzotti**,** F. Tessore and Neil Robertson, *J. Phys. Chem. C*, 2016, **120**, 19286–19294.

82. A. Zarkadoulas, M. J. Field, V. Artero and C. A. Mitsopoulou, *Chem. Cat. Chem.*, 2017, **9**, 2308–2317.

83. N. P. E. Barry, A. Pitto-Barry, I. Romero-Canelon, J. Tran, J. J. Soldevila-Barreda, I. Hands-Portman, C. J. Smith, N. Kirby, A. P. Dove, R. K. O'Reilly and P. J. Sadler, *Faraday Discuss.*, 2014, **175**, 229–240.

84. **(a)** N. Fendi, N. Hamidouche, Y. Beldjoudi and J. M. Rawson, unpublished work, 2015; **(b)** N. Fendi, *Synthesis, structural and physical studies "Push-Pull" nickel complexes of dithiolene based ligand*, University of Windsor, 2015, unpublished results.

85. J. D. Wrixon, *Reactivity of 1,2,5,6-Tetrathiocines*, University of Windsor, 2015.

CHAPTER 2. Towards the rational design of homo-multimetallic dithiolene complexes: Phosphine control of group 10 dithiolates

2.1. Introduction

Almost 80% of homoleptic bis(dithiolene) metal complexes, in which both ligands attached to the central metal are the same dithiolene, are based on the group 10 nickel, palladium, and platinum metals.[1] Of these, the majority are nickel complexes, due to extensive studies into their materials applications. These complexes usually take on square planar geometries, with the S-M-S angles ranging from 89.6° to 94.5° and a dihedral angle between the two S-M-S planes near 0°. Many of the complexes studied consist of mnt^{2-} or $dmit^{2-}$ dithiolene ligands (**Figure 2.1**). Several heteroleptic complexes, in which two or more different types of ligands are present, have been reported as well, including those with phosphorus or nitrogen based co-ligands.[2]

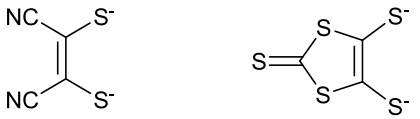

(a) **(b)**

Figure 2.1 Structures of **(a)** mnt^{2-} and **(b)** $dmit^{2-}$ ligands.

The substituents present on the dithiolenes will influence the electronics, molecular, and solid state structures and therefore the properties of metal dithiolene complexes. Extending π conjugation in the dithiolene ligand will lengthen the metal-sulfur bond, and electron-withdrawing groups will further extend this bond distance.[1] Despite the π conjugation and opportunity to add a range of substituents to modify the electronics, few benzo-fused group 10 complexes have been reported. Of the 197 structures reported in the CSD (2017), over half have been of either the unsubstituted benzene dithiolates (39%) or the toluene dithiolates (15%). Some examples of more commonly reported substituted complexes are shown in **Figure 2.2**.

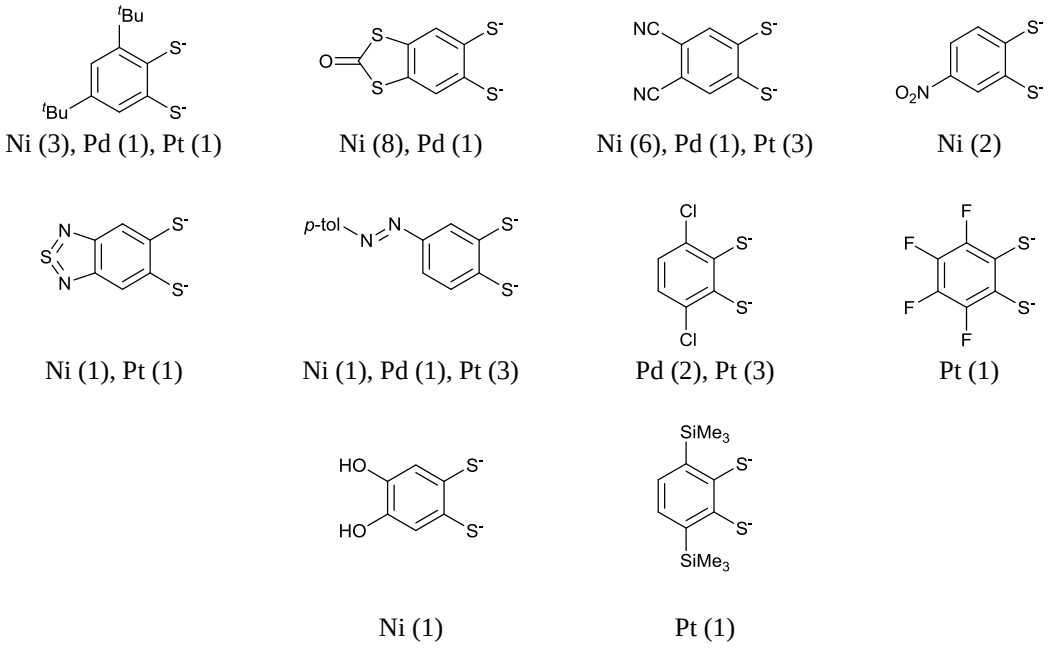

Figure 2.2 Number of some substituted benzo-fused group 10 dithiolene complexes reported in the CSD.

Tetrathiocins provide a facile route to accessing a diverse range of these functionalized ligands. Tetrathiocins are 8-membered heterocyclic rings, with four sulfur atoms. 1,2,5,6-tetrathiocins (**Figure 2.3**) contain two disulfide bonds, are 12π anti-aromatic,[3] and can be considered as dimers of 1,2-dithietes. There have been several methods reported to synthesize these compounds, most of which gave poor to moderate yields,[4] but the one-pot method employed by Stender[5] allowed several alkoxy-benzo tetrathiocins to be made in multi-gram quantities. Using this method, Wrixon prepared a range of electon-rich, π-donating alkoxy-substituted benzo-fused tetrathiocins in good yields (41 – 88%) and one nitrogen-based tetrathiocin (71% yield) (**Figure 2.4**).[4]

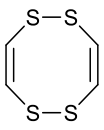

Figure 2.3 General structure of a 1,2,5,6-tetrathiocin.

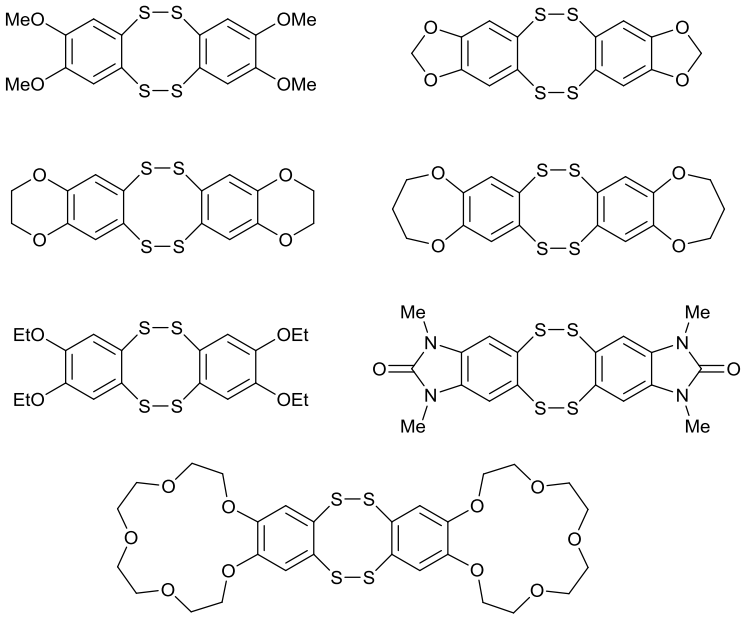

Figure 2.4 Range of tetrathiocins synthesized by this group. *Diagram reproduced from reference 4*.

Oxidative addition of bis-(dimethoxybenzo)-1,2,5,6-tetrathiocin to $Ni(COD)_2$, Pd_2dba_3, and $Pt(dppe)_2$ in the presence of the chelating phosphine dppe (see **Scheme 1.8**) gave square planar dithiolene complexes for palladium and platinum, and a pseudo square planar structure for the nickel complex, confirmed by X-ray crystallography, NMR studies and high resolution mass spectrometry.[6] Cyclic voltammetry studies of these complexes showed the effect of metal on redox properties, with the nickel complex displaying a quasi-reversible one-electron metal-based reduction at –1.61 V, while the palladium and platinum complexes both displayed two quasi-reversible one-electron ligand-based oxidations (+0.51 and +1.35 V for Pd, and +0.58 and +1.36 V for Pt).[4,6]

2.1.1 Structural Properties

The majority of group 10 dithiolate structures reported in the CSD are mononuclear (64% of all reported structures), most of which are homoleptic $M(dithiolene)_2$. Dimeric complexes have been reported for all three group 10 metals, some examples of which are shown in **Figure 2.5**.[2a,7] In these systems dimerization is supported by either just a M-M bond or a briging μ_2-S dithiolate for M^{II} species. M^{III} and M^{IV} system are also supported by a μ_2-S.

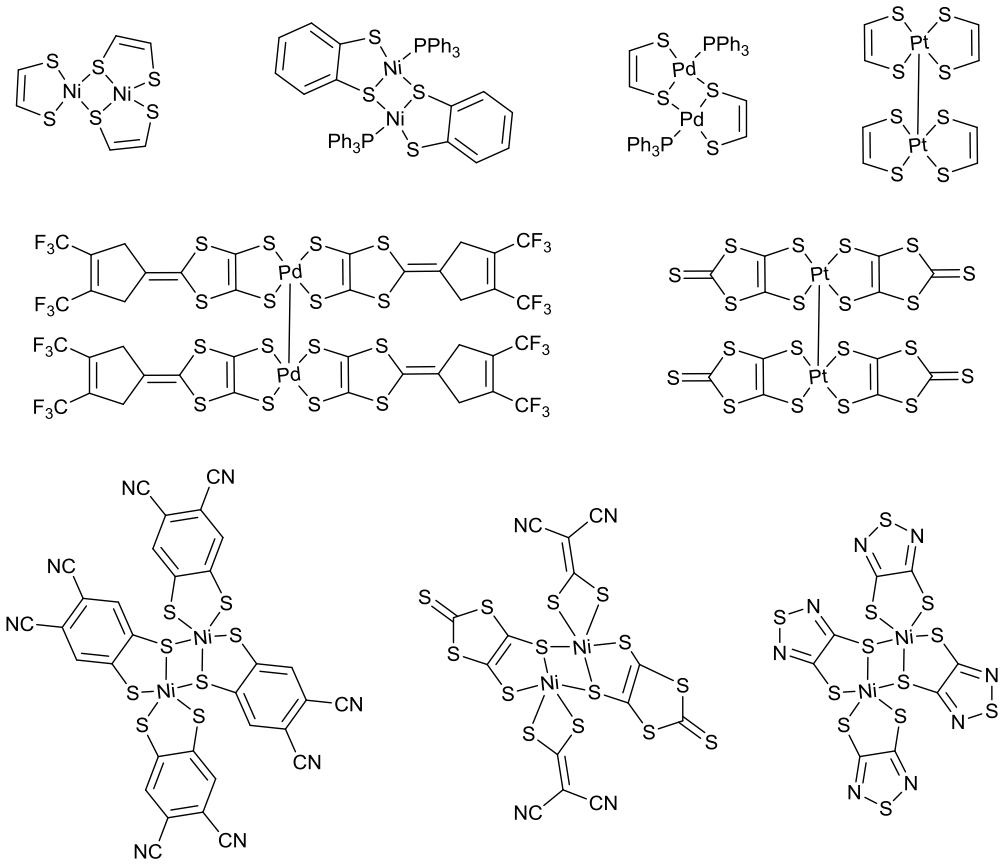

Figure 2.5 Some examples of dimeric group 10 dithiolene complexes reported in literature.

Nicholson *et al.*[8] reported the first trimeric nickel dithiolene complex, $[Ni_3(edt)_4]^{2-}$, in 1987 (**Figure 2.6a**). The structure of this complex could be described as two $[Ni(edt)_2]^{2-}$ units chelated to a central Ni(II) atom. The Ni_3S_8 core has C_{2h} symmetry and takes on a chair conformation, with each nickel atom exhibiting approximately square planar geometry, although the central nickel has some deviation (S-Ni-S angle is 99.59(9)°). Cha and coworkers[9] synthesized a trinuclear complex consisting of three bridging benzenedithiolate ligands, two of which form a distorted square planar base with one of the nickel atoms, and with an overall trigonal prismatic structure (**Figure 2.6b**). A similar structure was reported[10] with PPh_2Me instead of PPh_3 as a co-ligand on the two apical nickel atoms. These two five-coordinate metal centres take on distorted square pyramidal geometries. Sheng and coworkers[11] reported a complex containing two different types of dithiolenes, with pdt^{2-} ligands bridging between the metal atoms and $dmit^{2-}$ ligands coordinated to the terminal nickel atoms (**Figure 2.6c**).

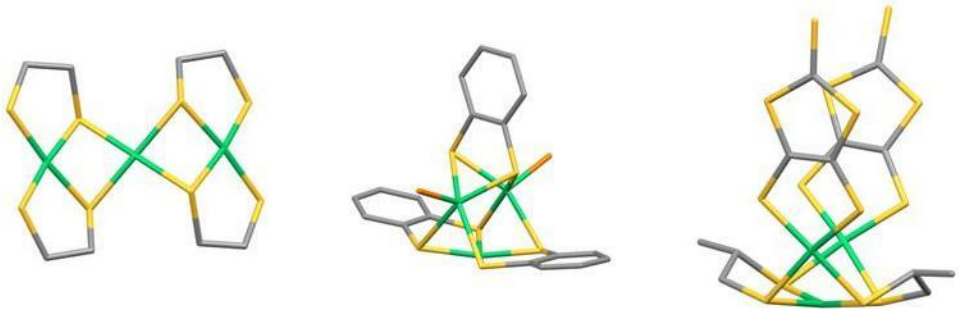

Figure 2.6 Examples of trinuclear nickel dithiolene complexes reported in literature. Hydrogen atoms have been omitted for clarity.

Reaction of $Pd(PPh_3)_4$ with a hexathioether containing bulky substituents produced the trinuclear palladium dithiolate shown in **Figure 2.7**.[12]

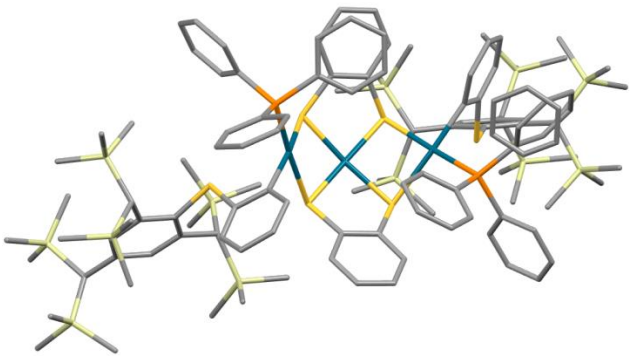

Figure 2.7 Trinuclear palladium dithiolene complex reported by Shimizu and coworkers.[12] Hydrogen atoms have been omitted for clarity.

A single tetrameric structure has been reported for the group 10 dithiolene complexes. Reaction of $[Ni(\alpha\text{-tpdt})_2]^-$ with $[K(15\text{-crown-}5)_2]^+$ gave the complex shown in **Figure 2.8a**.[13] The two terminal nickel atoms are four-coordinate with two dithiothiophene ligands of square planar geometry, while the internal nickel atoms are five-coordinate with {4+1} coordination. The differing lengths for internal and external Ni-S bonds (2.272(4) and 2.189(5) Å) indicates two different oxidation states for the nickel atoms, which was supported by DFT calculations. The internal Ni(III) and external Ni(II) centres are antiferromagnetically coupled, resulting in an EPR silent diamagnetic ground state. A mixed-dithiolene pentamer $[Ni_5(edt)_4(dmit)_2]^{2-}$ was reported, in which all metal centres are square planar (**Figure 2.8b**).[11]

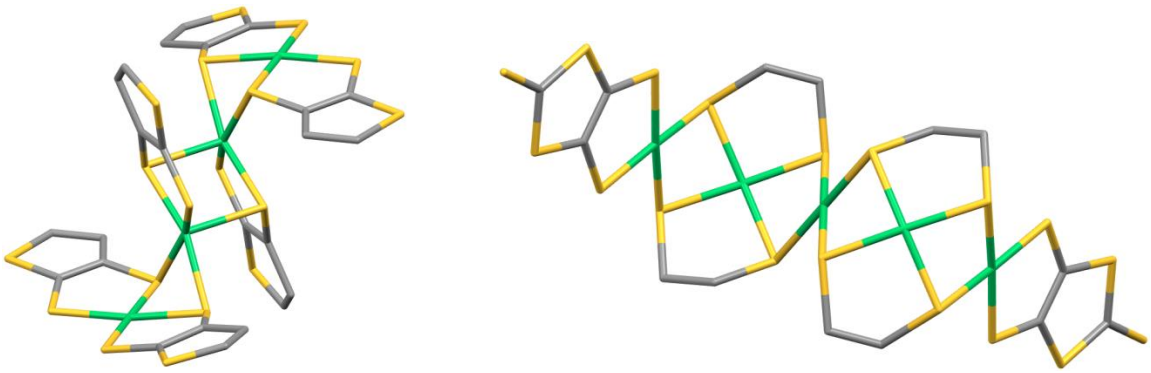

(a) **(b)**

Figure 2.8 Structures of the **(a)** tetranuclear and **(b)** pentanuclear nickel dithiolene complexes. Hydrogen atoms have been omitted for clarity.

The first hexanuclear group 10 dithiolene complex was synthesized by Stiefel *et al.*[14] through the dithiolene transfer of (tmeda)$ZnS_2C_2(COOMe)_2$ with $(MeCN)_2PdCl_2$. This reaction gave the $[Pd(S_2C_2(COOMe)_2)]_6$ complex, with six palladium atoms and one dithiolene unit per metal centre and no other ligands. The complex exhibited S_6 symmetry, with an inversion centre (**Figure 2.9a**). Following our report of a hexameric cage exhibiting noncrystallographic C_2 symmetry,[15] which will be expanded upon in section **2.1.2.b** of this thesis, Fekl and coworkers[16] explored the possible isomers that may exist for these complexes. The $[Pd(tfd)]_6$ complex (**Figure 2.9b**) which they synthesized also showed C_2 symmetry, and after examining the possible binding modes for the dithiolenes they concluded that these hexameric complexes will only exist as the S_6- or C_2-symmetric isomers. For all three hexamers reported, the metal centres form an octahedron, and an imaginary cube may be imposed onto the structures, with the six palladium atoms sitting on each face of the cube and the sulfur atoms at the midpoints of each cube edge.

2.1.2 Phosphine Ligands

Phosphines are neutral 2-electron donors containing phosphorus atoms of the form PR_3. These compounds can be monodentate (containing one P donor), bidentate (containing two P donors), or polydentate (containing more than two P donors that can bind to the metal). Phosphines bind to metals through both σ donation from a phosphorus lone pair into an empty metal orbital and π back-bonding from a filled metal *d* orbital into empty

ligand orbitals.[17] They have been widely used as ligands in coordination chemistry. In group 10 metal dithiolene complexes, phosphines are useful as they are classified as soft bases,[18] so will bind well to the soft Ni^{2+}, Pd^{2+}, and Pt^{2+} centres. Phosphorus serves as a good reporter group, allowing ^{31}P NMR to be used to monitor and analyze the reactions of these complexes. In addition, both their steric and electronic contributions can be tailored to influence the structures and bonding within these complexes (see Sections **2.1.2.a – b**).

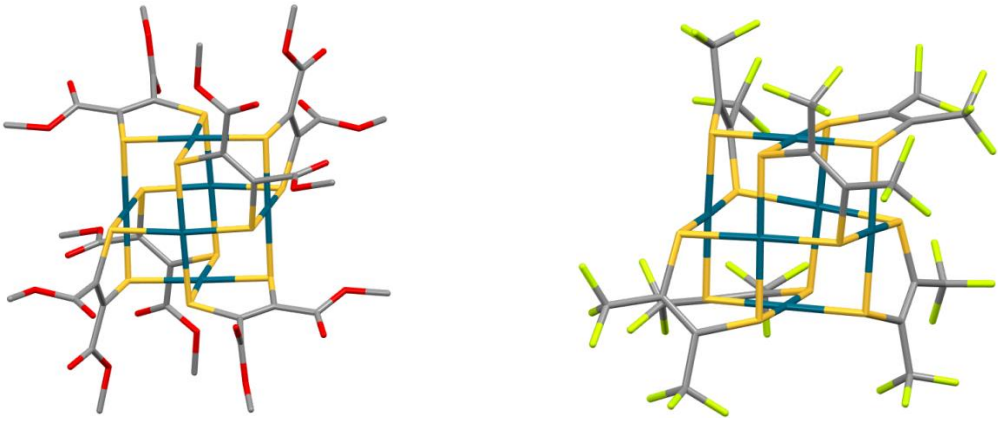

(a) **(b)**

Figure 2.9 Structures of two hexanuclear palladium dithiolates reported in literature. Hydrogen atoms have been omitted for clarity.

2.1.2.a Tolman cone angles

In his review in the 1970s,[19] Tolman described the steric effects of phosphine ligands on metal complexes. Among his findings was that the bulkiness of the phosphine substituents influence the phosphine's binding affinity to the metal centre. This bulkiness was described by the ligand cone angle parameter, θ, which is the angle at the apex of an imaginary cone which can be drawn around a phosphine ligand that is bound to a metal (**Figure 2.10**).

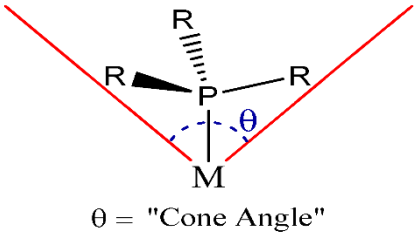

Figure 2.10 Representation of the Tolman cone angle. *Diagram reproduced from reference 4.*

Using molecular modeling kits, Tolman measured these angles for a number of phosphines. He found that phosphines with larger cone angles had a lower binding affinity for the metal. As is shown in **Table 2.2**, as the angle θ increases, the M-P bond length increases, indicating a decrease in bond strength. Studies into dissociation equilibria showed that the rate of ligand dissociation was 100 to 1000 times faster for $P(O\text{-}o\text{-tol})_3$ than for the less bulky $P(O\text{-}p\text{-tol})_3$ at 25 °C. Similar studies in $CuXL_3$ complexes (where X = halogen and L = phosphine) showed that ligand dissociation increased with steric bulk in the order $PMe_2Ph \sim PMePh_2 < PPh_3$.[20]

Table 2.1 Some cone angles reported by Tolman.[19]

Phosphine	Cone angle (°)
PH_3	87
PH_2Ph	101
PMe_3	118
PMe_2Ph	122
$PMePh_2$	136
$P(p\text{-tol})_3$	145
P^tBu_3	182
$P(o\text{-tol})_3$	194
$P(\text{mesityl})_3$	212

Table 2.2 Influence of cone angle on M-P bond length.[19]

Complex	Phosphine ligand cone angle (°)	M-P bond length (Å)
$Cu(NO_3)(PPh_3)_2$	145	2.256(3)
$Cu(NO_3)(PCy_3)_2$	170	2.29(1)

Steric crowding on the phosphine ligands affects ^{31}P NMR chemical shift.[19] Upon coordination, the R-P-R angle opens, which decreases the *s* character in the P lone pair and increases it in the P-R bonds. This usually leads to a downfield shift of $\delta(^{31}P)$. The magnitude of the shift tends to be less for more bulky ligands, because R-P-R angles open less upon coordination (**Table 2.3**).

Table 2.3 ^{31}P NMR chemical shift with increasing bulkiness. *Table reproduced from reference 4.*

Phosphine	δ_P (ppm)
PH_3	–239
$PMeH_2$	–163.5
PMe_2H	–99
PMe_3	–62.2
P^tBuCl_2	198.6
P^tBu_2Cl	145
P^tBu_3	63
$PPhCl_2$	165
PPh_2Cl	81.5
PPh_3	–6

2.1.2.b Phosphine control

Previous studies by Wrixon in this group on phosphine control of metal dithiolene complexes showed that the structures of these complexes seem to be sensitive to the cone angle of the phosphine co-ligand used (**Figure 2.11**).[15] Reaction of bis-(dimethoxybenzo)-1,2,5,6-tetrathiocin with Pd_2dba_3 and bidentate phosphines such as dppe, dppm, and dppf persistently gave mononuclear square planar structures, with one dithiolene and one bidentate phosphine coordinated on either side of the metal centre. The 'bite' of the bidentate phosphine had an influence on bond lengths and angles, with the smaller bite of dppm giving a more strained structure (smaller P-Pd-P angle of 73.29(4) – 73.50(4)° versus 84.98(3)° in dppe complex), and the larger bite of dppf leading to a longer Pd-P length (2.280(3) – 2.321(3) Å versus 2.2739(6) Å in dppe complex) and larger P-Pd-P angle (96.7(1) – 97.4(1)° versus 84.98(3)° in dppe complex).

In contrast, the monodentate PPh_3 (cone angle = 145°) led to formation of the dimer, $[(dmobdt)Pd(PPh_3)]_2$ (**Figure 2.11b**) in which two of the four sulfur atoms adopt a μ_2-bridging mode between the two palladium centres, reflected in their longer Pd-S lengths of 2.3246(5) Å. Using $Pt(PPh_3)_4$ instead of Pd_2dba_3 as the starting material gave a similar platinum dinuclear complex, $[(dmobt)Pt(PPh_3)]_2$, but also allowed for the isolation of a mononuclear intermediate, in which two PPh_3 groups are coordinated to the metal.[3]

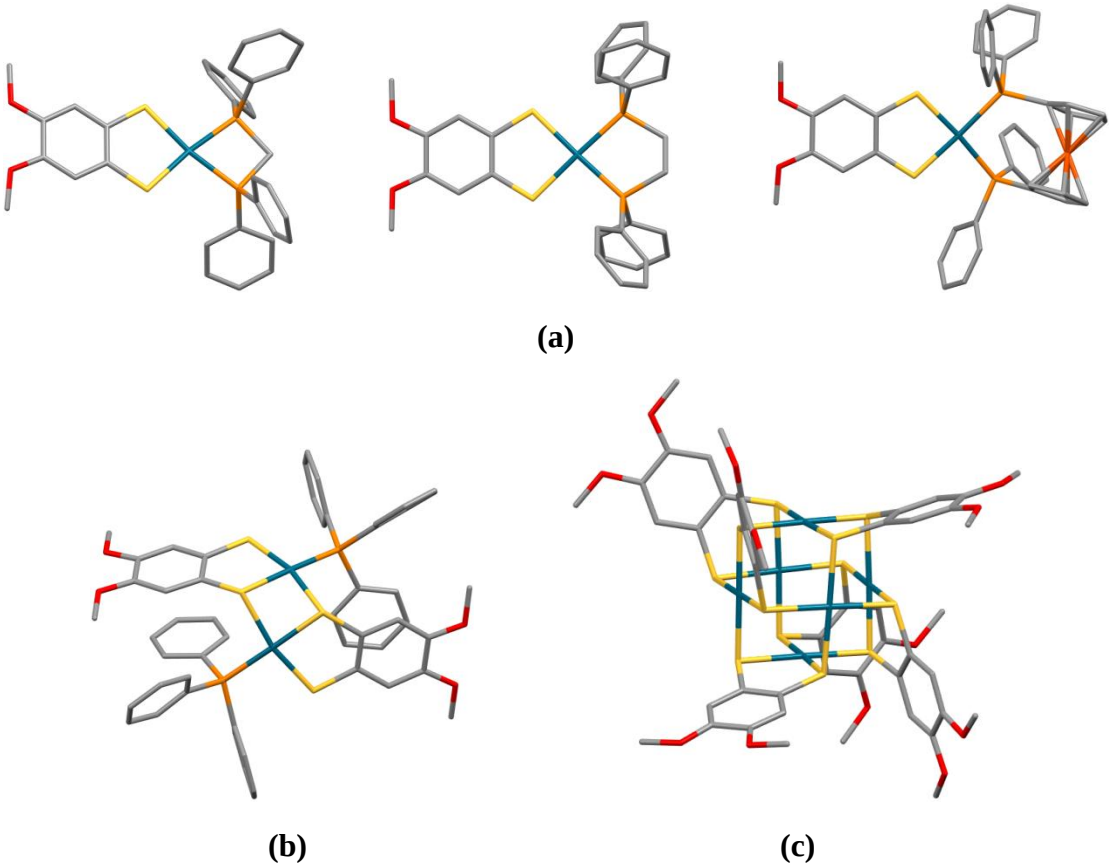

(a)

(b) **(c)**

Figure 2.11 Products of the reaction of bis-(dimethoxybenzo)-1,2,5,6-tetrathiocin, Pd_2dba_3 and PR_3, giving: **(a)** mononuclear structures when PR_3 = dppm (R' = CH_2), dppe (R' = CH_2CH_2), dppf (R' = $(C_5H_5)_2Fe$), **(b)** a dinuclear structure when $PR_3 = PPh_3$, **(c)** a hexanuclear structure when $PR_3 = P^tBu_3$. Hydrogen atoms have been omitted for clarity.

Reaction of the tetrathiocin and Pd_2dba_3 with the even more sterically demanding phosphine P^tBu_3 (cone angle = 182°) produced a hexanuclear complex, $[Pd(dmobdt)]_6$ (**Figure 2.11c**), with one dithiolene ligand per metal centre and no phosphine in the final structure. The bulky P^tBu_3 was too large to remain coordinated to the metal atom. As was found in a previous structure reported by Stiefel[14] (mentioned in section **2.1.1**), each

sulfur atom was μ_2-bridging between two adjacent palladium atoms. However, instead of having S_6 symmetry, this complex contained a non-crystallographic two-fold rotation axis passing through the two axial palladium atoms. This rotation axis leads to three different coordination geometries for the dithiolene ligands, as reflected in the ^{1}H NMR where six distinct peaks can be observed for the methoxy protons, each coordination geometry giving two different proton environments.

2.1.3 Project Objectives

Our previous studies showed that changing the phosphine co-ligand will have a marked effect on the structures of palladium dithiolene complexes. Going from bidentate phosphines dppm, dppe, and dppf to the bulky monodentate PPh_3 to the bulkier P^tBu_3 yielded mono-, di-, and hexanuclear complexes, respectively.[15] These complexes are of general form $[ML(PR_3)_y]_n$ where the solutions are: mononuclear (n = 1, y = 2); dinuclear (n = 2, y = 1) and hexanuclear (n = 6, y = 0). The goal of this project was to further explore these complexes and to identify if other clusters of general formula $M_xL_y(PR_3)_z$ could be isolated from these reactions. Specifically, these studies aimed to probe the likely methods for monomer-dimer conversion and to identify any additional polynuclear structures (x = 3, 4, 5) which would provide structural insight into any other intermediates en route to the hexamer.

2.2. Results and Discussion

2.2.1 Synthesis of 2',3',8',9'-tetramethoxy-dibenzo-1,2,5,6-tetrathiocin $[(MeO)_2C_6H_2S_2]_2$ (1)

Our studies into tetrathiocins began with looking at them as precursors to dithiazolyl radicals.[21] Following the literature procedure,[4,5] tetrathiocin **1** was produced by reacting 1,2-dimethoxybenzene with S_2Cl_2 in degassed glacial acetic acid at room temperature under nitrogen atmosphere, followed by treatment with a methanolic tin chloride solution to discharge the intense blue colour associated with even small quantities of poly-sulfur cations. The resultant tetrathiocin was isolated as a yellow solid in moderate yield (55%).

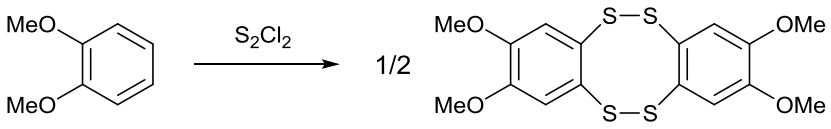

1

Scheme 2.1 Synthesis of tetrathiocin **1**.

The low solubility of tetrathiocins in organic solvents makes characterization methods such as NMR spectroscopy difficult to carry out. Mass spectrometry measurements were conducted and the molecular ion peak for $[M+H]^+$ was observed at *m/z* = 401.0010. A small amount of tiny crystals suitable for X-ray diffraction were obtained through the slow diffusion of diethyl ether into a saturated CH_2Cl_2 solution.[3] The tetrathiocin crystallized in the monoclinic space group $P2_1/c$ and adopts a chair conformation similar to many other tetrathiocins reported in literature.[22] The C-S bond lengths of 1.772(4) Å and 1.775(4) Å are intermediate between a single bond[23] (1.82 Å) and a double bond (1.60 Å), showing the delocalized nature of the compound. The C-C bond lengths ranging from 1.384(3) Å to 1.412(3) Å are shorter than a single C-C bond (1.513 – 1.588 Å) and longer than a double C=C bond (1.299 – 1.345 Å) further supporting the delocalized character.

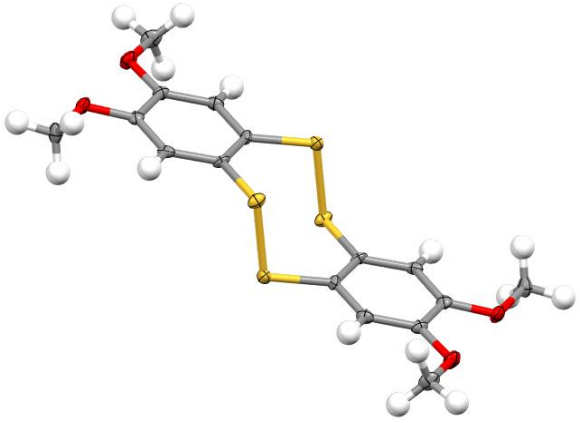

Figure 2.12 Crystal structure of tetrathiocin **1** with thermal ellipsoids drawn at the 50% probability level.

2.2.2 Kinetics of Formation of the Palladium Dimer [(dmobdt)Pd(PPh$_3$)]$_2$ (2)

Previously, the dinuclear palladium dithiolate $[(dmobdt)Pd(PPh_3)]_2$ **2** was synthesized by the oxidative addition of tetrathiocin **1** to Pd_2dba_3 in the presence of the labile phosphine

PPh_3.[15] This reaction was conducted in dry toluene at 150 °C over a period of 40 minutes under microwave irradiation to give a green solution from which crystals of **2** were grown (**Scheme 2.2**).

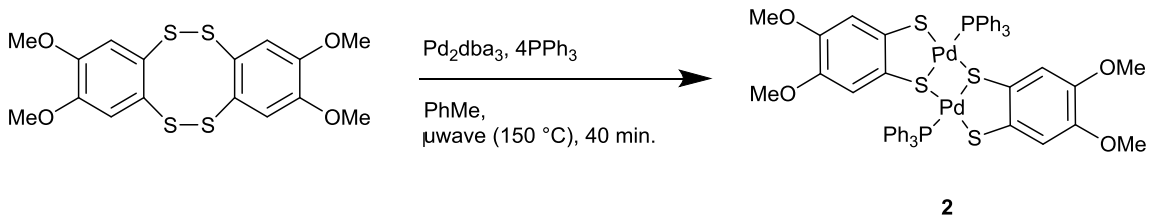

2

Scheme 2.2 Previously reported synthesis of palladium dimer **2**.[15]

Microwave procedures provide a faster, cleaner, and more selective method for synthesis.[6] The slower kinetics of Pt^{II} chemistry, in relation to Pd^{II}, allowed for the isolation of the monomeric intermediate $(dmobdt)Pt(PPh_3)_2$ shown in **Figure 2.13** from reaction of $Pt(PPh_3)_4$ with the tetrathiocin under otherwise similar conditions.[3]

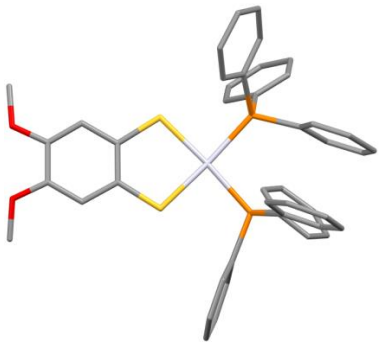

Figure 2.13 Monomeric intermediate isolated from the reaction of $Pt(PPh_3)_4$ with tetrathiocin **1**.[3] Hydrogen atoms have been omitted for clarity.

As a consequence, we wanted to see if this mononuclear intermediate could be obtained for palladium through either a reduction in reaction temperature and/or reaction time. Reaction of Pd_2dba_3 with tetrathiocin **1** and PPh_3 was carried out in an oven-dried microwave vial under inert atmosphere. After one minute, a 0.2 mL sample of the green reaction mixture was removed. The solvent was evaporated through rotary evaporation and the green solid dissolved in $CDCl_3$ so that NMR studies could be conducted.

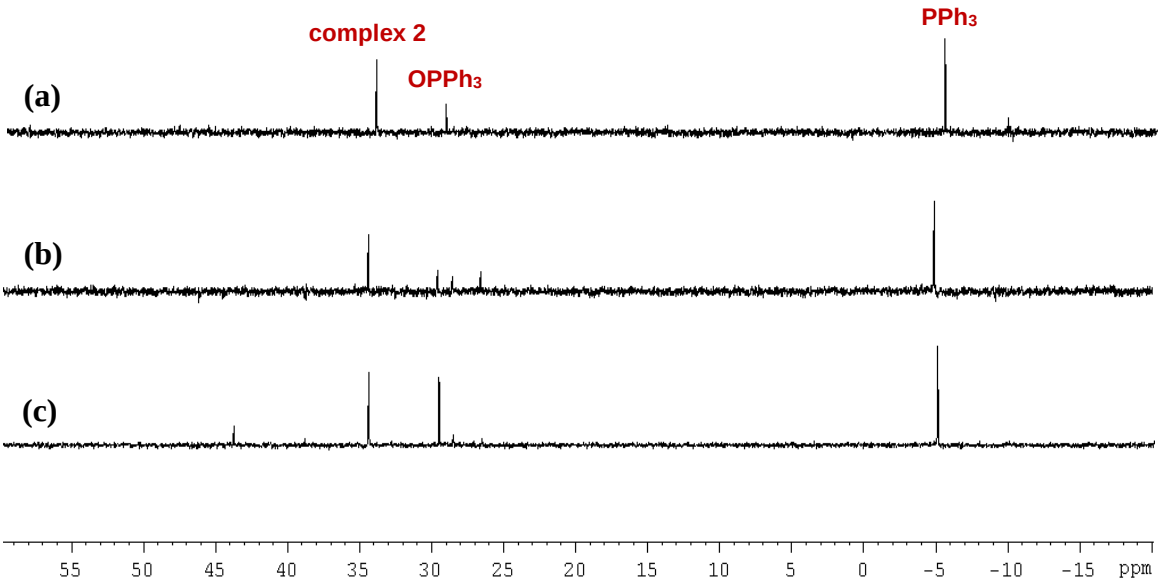

Figure 2.14 ^{31}P NMR spectra in $CDCl_3$ for the reaction of Pd_2dba_3, tetrathiocin **1** and PPh_3 at: **(a)** 150 °C, microwave conditions, 1 min; **(b)** 60 °C, microwave conditions, 5 min; **(c)** 90 °C, thermal conditions, 1 h.

As shown in **Figure 2.14a** and **Figure 2.15a**, peaks belonging to the dinuclear complex $[(dmobdt)Pd(PPh_3)]_2$ (**2**) can be observed in the ^{31}P NMR spectrum ($\delta(^{31}P)$ = 34.40 ppm) and in the ^{1}H NMR spectrum (two peaks for the benzo protons at $\delta(^{1}H)$ = 6.09 ppm and 5.80 ppm and two peaks for the methoxy protons at $\delta(^{1}H)$ = 3.60 ppm and 2.90 ppm). These match closely to the peaks previously found for this complex at $\delta(^{31}P)$ = 34.63 ppm and proton peaks at $\delta(^{1}H)$ = 6.09 and 5.80 ppm and 3.60 and 2.91 ppm.[15] The two distinct resonances for the benzo protons and for the methoxy protons clearly indicate retention of the dimeric structure in solution with two different sets of ^{1}H signals for each chemical environment in the complex (MeO or aromatic CH of the $dmobdt^{2-}$ ligand), consistent with these protons being located on 'the same side' or 'opposite side' to the μ_2-S atom (shown in **Figure 2.15**).

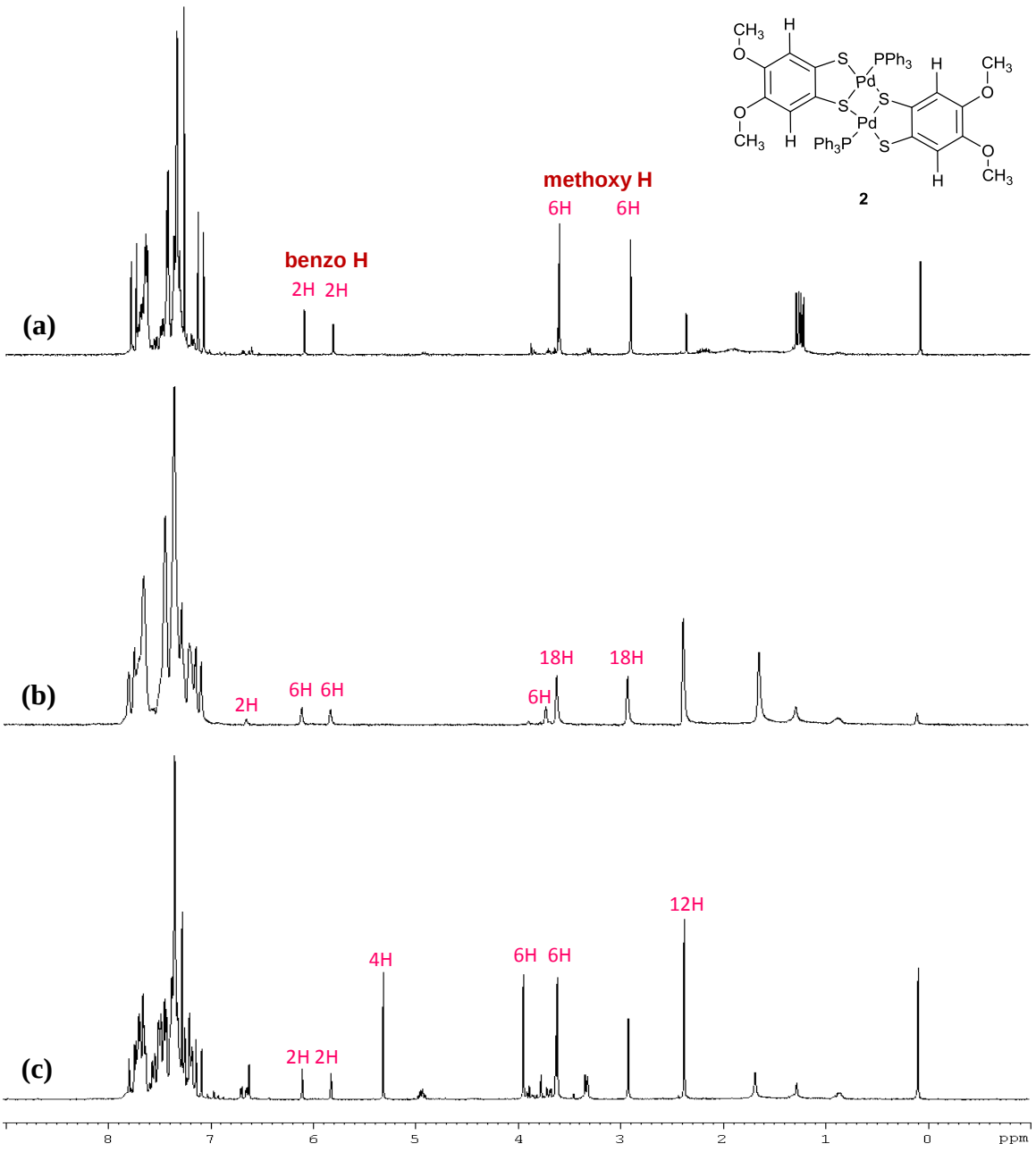

Figure 2.15 ^{1}H NMR spectra in $CDCl_3$ for the reaction of Pd_2dba_3, tetrathiocin **1** and PPh_3 at: **(a)** 150 °C, microwave conditions, 1 min; **(b)** 60 °C, microwave conditions, 5 min; **(c)** 90 °C, thermal conditions, 1 h.

No evidence for the formation of a monomer is seen in the NMR spectra (expected: a peak near the dimer ^{31}P peak of 34 ppm; a single benzo ^{1}H peak around 5 – 7 ppm and a single methoxy ^{1}H peak around 3 – 4 ppm would be expected). The reaction was then carried out in the microwave at 60 °C and under conventional thermal conditions at 90 °C to see if lowering the temperature or if conducting the reaction outside of the microwave

would slow it down sufficiently to isolate a monomer. Samples were analyzed at 5 minutes and 1 hour, respectively, into the reaction, and complex **2** was again seen in both the ^{31}P and ^{1}H NMR spectra (**Figures 2.14b–c** and **2.15b–c**). The ^{1}H NMR spectra of these two reactions showed the presence of peaks which may correspond to a monomeric structure; however, these peaks appear at different shifts in each reaction: around 6.6 ppm and 3.8 ppm in the 60 °C reaction and around 5.3 ppm and 2.4 ppm in the thermal reaction (**Figure 2.15b–c**).

In a second set of experiments $Pd(PPh_3)_4$ was used as the starting material instead of Pd_2dba_3/PPh_3 and reacted with tetrathiocin **1** under similar conditions previously used with $Pt(PPh_3)_4$.[3] Two equivalents of $Pd(PPh_3)_4$ and one equivalent of the tetrathiocin were stirred in dry toluene in the microwave at 150 °C, and a 0.2 mL sample of the reaction mixture was collected after one minute. Again, the NMR spectra of this sample (**Figure 2.16**) showed evidence of the dinuclear complex with a ^{31}P peak at 34.47 ppm and ^{1}H peaks at 6.19 and 5.91 ppm for the benzo protons and 3.69 and 3.00 ppm for the methoxy protons. Two additional small ^{31}P peaks at 26.63 ppm and 23.72 ppm, which were not present in the Pd_2dba_3 reaction shown in **Scheme 2.2** after one minute (see **Figure 2.14a**), could be observed (**Figure 2.16**). Again, the ^{1}H NMR spectrum shows the possibility of monomer formation, with peaks at 6.73 ppm and 3.80 ppm, but the amount present appears minimal.

From these studies, there was circumstantial but ultimately inconclusive evidence for monomer formation and it was concluded that the formation of the dimeric $[(dmobdt)Pd(PPh_3)]_2$ **2** must occur rapidly, as indicated by its appearance as the major product in the NMR spectra one minute into the reaction under all the reaction conditions tried.

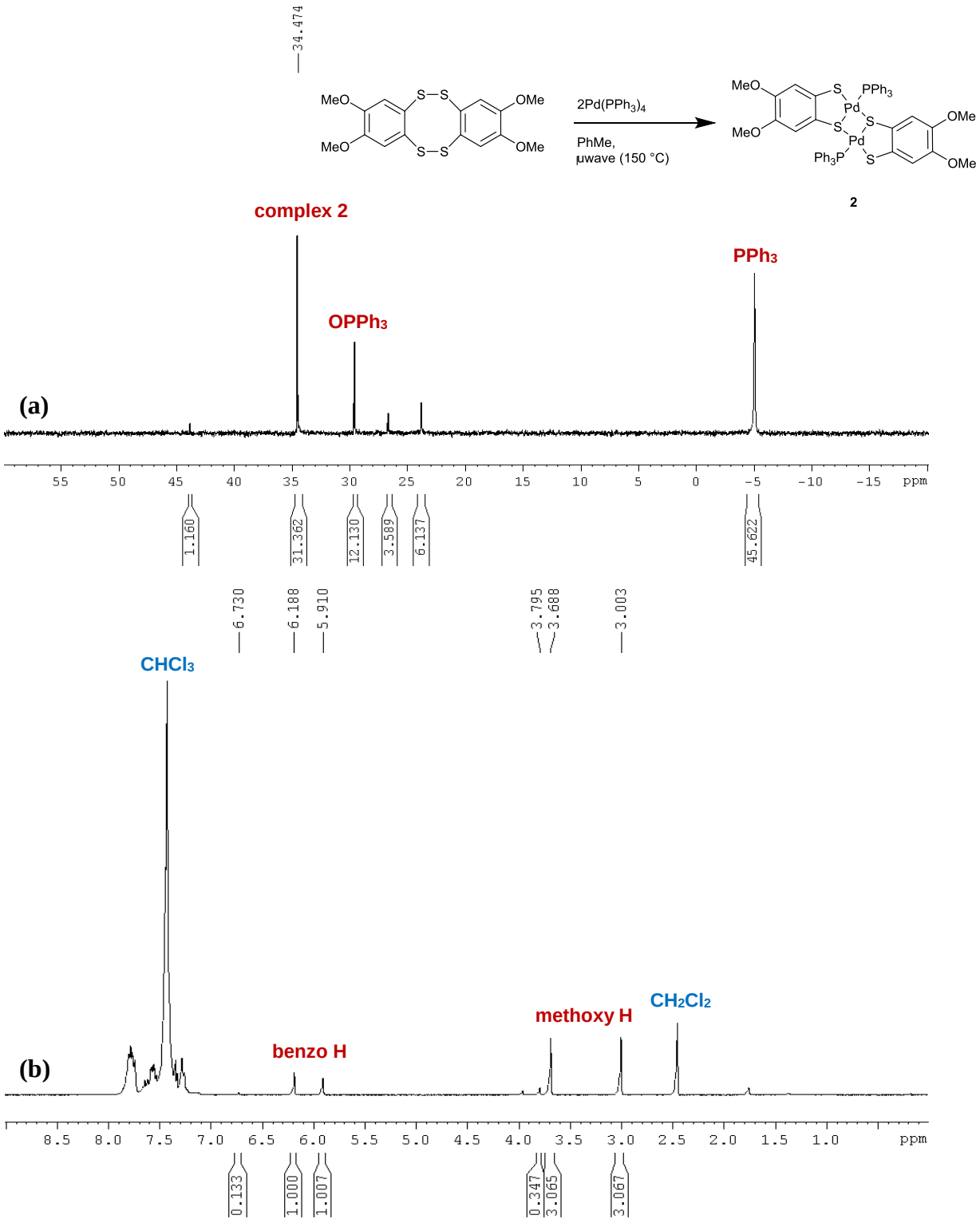

Figure 2.16 NMR spectra in $CDCl_3$ for the reaction of $Pd(PPh_3)_4$ and tetrathiocin **1** at 1 min: **(a)** ^{31}P NMR (121 MHz), **(b)** ^{1}H NMR (300 MHz).

2.2.3 Synthesis and Studies of a Series of Dinuclear Palladium Complexes (3 – 8)

Previous studies into phosphine control showed that the oxidative addition of tetrathiocins to zero-valent palladium can be carefully tuned by intentionally choosing phosphines of various denticities and cone angles to form mononuclear (dppe, dppm, dppf), dinuclear (PPh_3), and hexanuclear (P^tBu_3) complexes (see section **2.1.2.b**). Moving forward, we wanted to see if this approach could be extended to identify intermediate nuclearity clusters (tri-, tetra- and/or penta-nuclear complexes) which might occur between the previously identified dinuclear and hexanuclear derivatives. We therefore set about to examine the reactivity of phosphines with cone angles intermediate between 145° (PPh_3) and 182° (P^tBu_3) (**Table 2.4**). Additionally, we sought to explore the effect of the phosphine cone angle on the kinetics of these reactions.

Table 2.4 Phosphines used and their cone angles.[19,24]

Complex	Phosphine	Cone angle (°)
3	$PPh_2{}^iPr$	150
4	$P(NMe_2)_3$	157
5	P^iPr_3	160
6	$P(m\text{-tol})_3$	165
7	PBn_3	165
8	PCy_3	170

2.2.3.a Synthesis of dinuclear complexes 3 – 8

A procedure similar to that previously used for the palladium dinuclear complex **2** was employed. Tetrathiocin **1**, Pd_2dba_3, and two equivalents of phosphine (**Table 2.4**) were added to an oven-dried microwave vial in the glovebox, to which dry toluene was added. This mixture was stirred in the microwave at 150 °C for 20 minutes to generate green, dichroic red-green, or red solutions. After filtration and evaporation of solvent, NMR analysis of the crude reaction mixtures showed several products had been formed in each reaction.

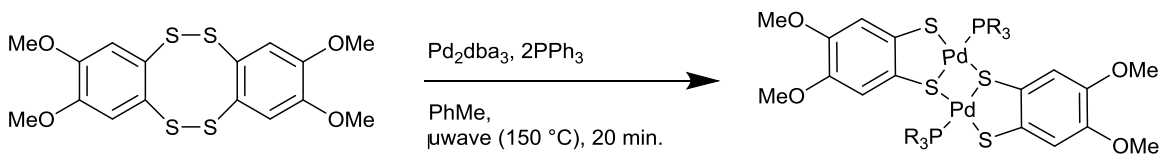

Scheme 2.3 General reaction scheme for the synthesis of complexes **3** to **8**.

Slow diffusion of diethyl ether into a saturated CH_2Cl_2 solution of the crude reaction product in the reaction of $PPh_2{}^iPr$ afforded crystals of the dinuclear complex $[(dmobdt)Pd(PPh_2{}^iPr)]_2$ (**3**) which was similar in structure to the previously reported complex $[(dmobdt)Pd(PPh_3)]_2$ (**2**). In the five remaining reactions, however, recrystallization of the crude reaction mixtures did not yield any crystalline product. In these cases, purification by preparative scale TLC allowed for the isolation of individual products. The reactions with $P(NMe_2)_3$ and P^iPr_3 were eluted in $CHCl_3$, while the remaining reactions were eluted in a 7:3 CH_2Cl_2:hexane mixture and each band was removed from the TLC plate and dissolved in CH_2Cl_2, followed by acetone, with the CH_2Cl_2 and acetone solutions collected separately. In all cases a dinuclear complex (**4** – **8**, **Table 2.4**), similar in structure to complexes **2** and **3**, was isolated. This dimeric structure was supported by high resolution mass spectrometry measurements as well as elemental analysis, ^{31}P and ^1H NMR spectroscopy. An example of the ^1H NMR spectrum of **7** as representative of the behavior of these complexes is shown in **Figure 2.17**. Two benzo and two methoxy environments are observed for the protons consistent with the dimeric structure in which the methoxy and aryl protons are in chemically distinct environments. In addition the relative integrations of dithiolate benzo and methoxy protons to phosphine protons support a structure in which the dithiolate:phosphine ratio is 1:1. Recovered yields for the six complexes were low, ranging from 10% to 31%. For some of the complexes, yield could be improved, sometimes drastically, by either increasing (in the case of complex **8**) or decreasing (in the case of complex **7**) the equivalents of phosphine used.

2.2.3.b Crystallographic studies of complexes 3 – 8

Recrystallization was carried out in various solvents. For complexes **4** to **8**, the reactions produced very low yields after purification so these reactions were repeated two or three times and the combined yields of the two or three trials used for recrystallization.

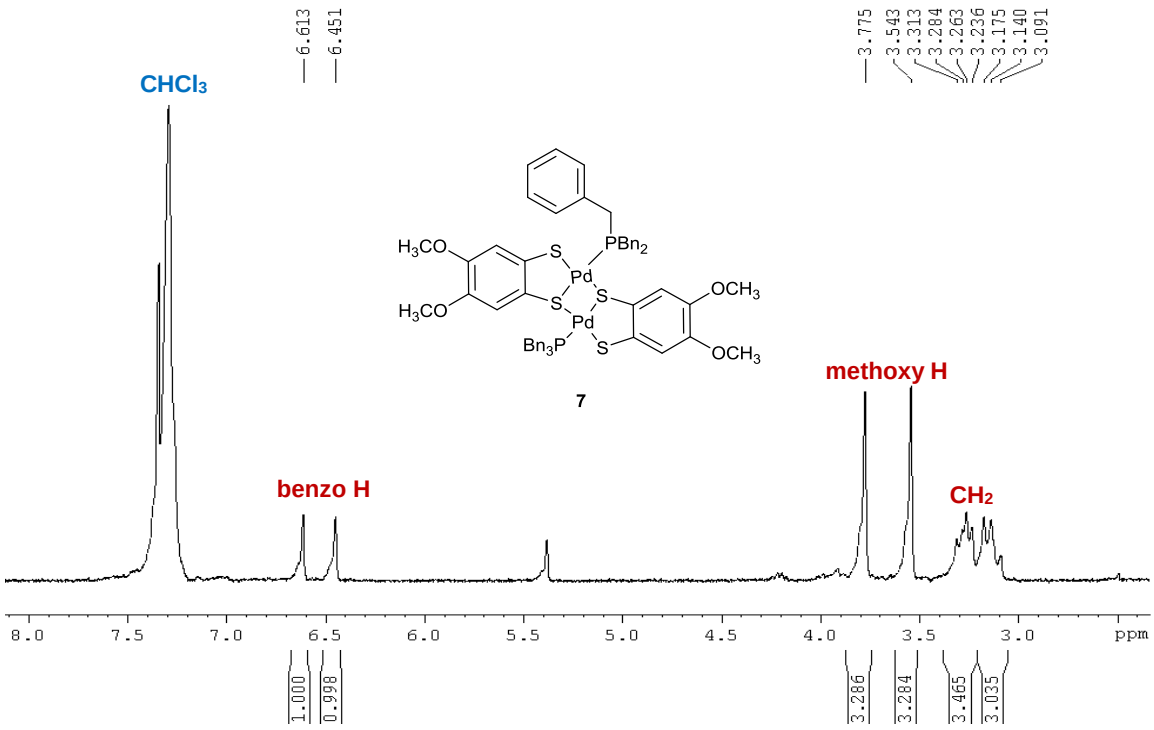

Figure 2.17 ^{1}H NMR spectrum of complex **7**.

Some disorder was present for complexes **6** and **7**. As was seen with complex **2**,[4,15] complexes **3** to **8** exist as dimers with a 2-fold rotation axis. Selected bond lengths and angles are shown in **Table 2.5** and **Table 2.6**. In the complexes studied, Pd1-P1 bond lengths are in the range 2.291(2) – 2.3056(5) Å, compared to the shorter 2.2742(5) Å for complex **2**. The non-bridging Pd1-S1 bonds are 2.280(3) – 2.298(2) Å and the bridging Pd1-S bonds are 2.326(6) – 2.384 Å (for the sulfur on the same dithiolene as the non-bridging sulfur, S2) and 2.360(1) – 2.384(7) Å (for the sulfur on the other dithiolene, S12), versus 2.3246(5) Å and 2.3600(5) Å in complex **2**. S1-Pd1-S2 angles of 88.29(2)° – 90.74(3)° are indicative of square planar geometry, but there are distortions in the other angles. S2-Pd1-S12 angles in the Pd_2S_2 core range from 75.37(1)° to 77.96(2)°, which is lower than those for **2** at 79.57(2)°, and the Pd1-S2-Pd2 angles are in the range 76.26(2)° – 78.4(2)°. The sum of internal angles at Pd ranges from 359.97(4)° – 360.37(6)° for **3** to

8, indicating square planar geometry at the metal centres. In all six complexes, just as in complex **2**, there is a bending between the planes formed by the three sulfurs and phosphorus atoms bound to each palladium centre. The angles between these planes were measured, and found to be 73.42° – 77.98°, compared to the larger angle of 78.54° for complex **2**.

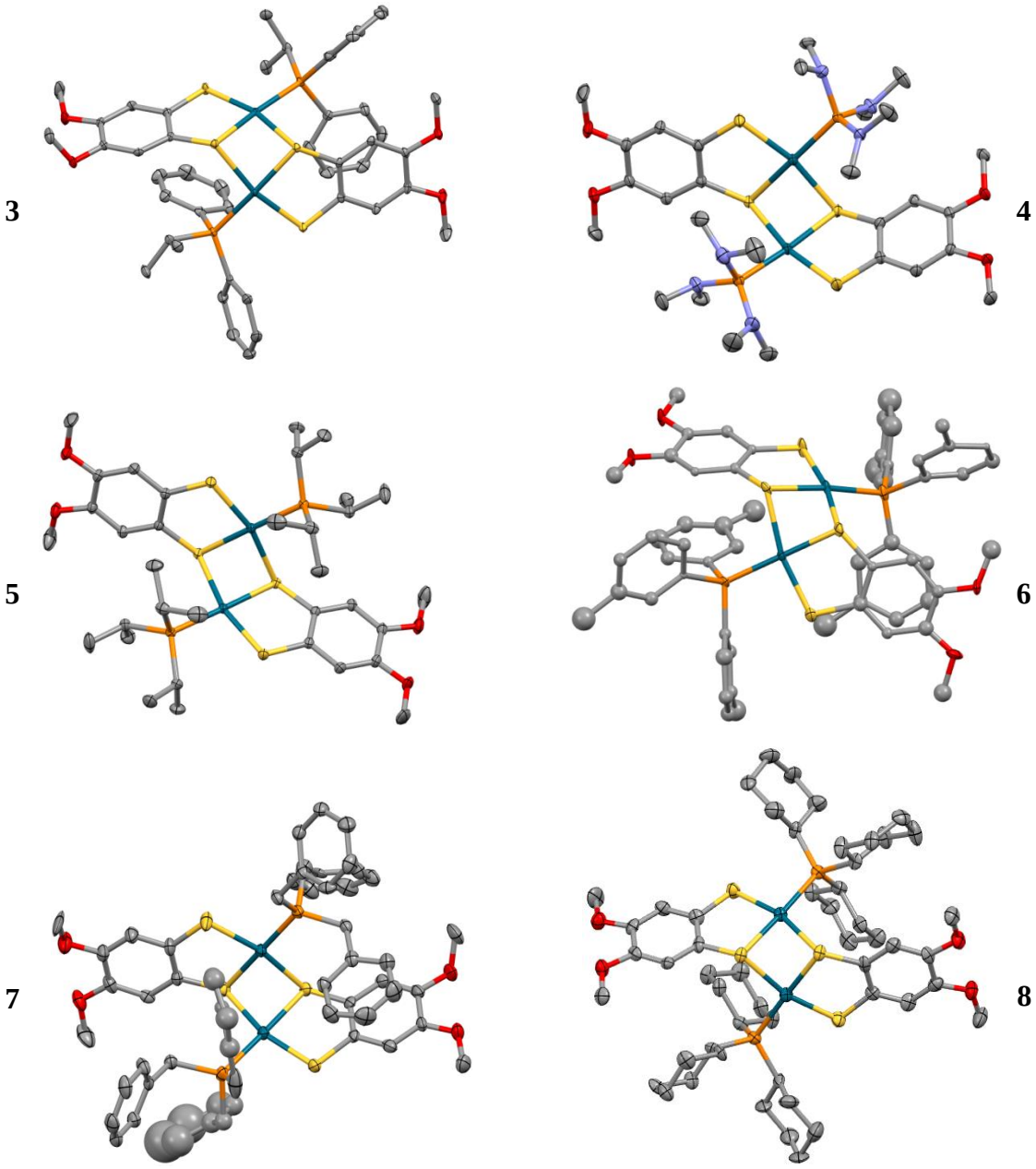

Figure 2.18 Crystal structures of complexes **3** to **8** with thermal ellipsoids drawn at the 50% probability level. Hydrogen atoms have been omitted for clarity.

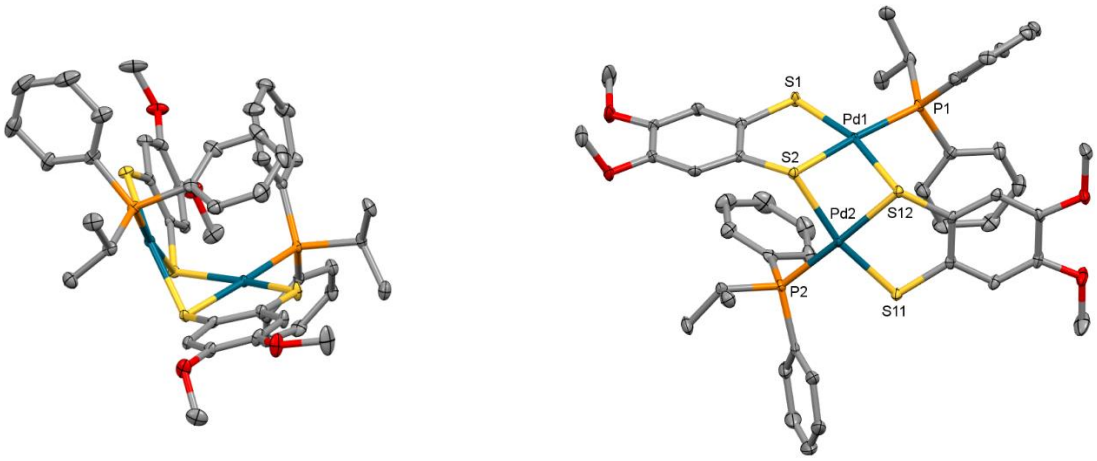

Figure 2.19 Crystal structure of **3** showing the bending between the S_3P1 and S_3P2 planes in these complexes (left) and atom labelling (right).

Comparing complexes **2**, **3**, and **5**, we see the effects of steric bulk on the structures as the bound phosphine becomes progressively larger (PPh_3 < $PPh_2{}^iPr$ < P^iPr_3). All bonds around Pd lengthen as the phosphine becomes bulkier, indicating a weakening of bond strength to both the phosphine and the dithiolene ligands. The S1-Pd1-S2 and S2-Pd1-S12 angles shrink to accommodate the increased size of the phosphine, while the Pd1-S2-Pd2 angle becomes larger. The sum of internal angles around Pd are almost invariant (359.74(4)°, 360.06(6)° and 359.97(4)°), indicating a strong preference for retention of planarity as the phosphine becomes larger. The bending angle between the two S_3P coordination planes decreases with increasing phosphine bulk according to the data from complexes **2**, **3**, and **5**.

Table 2.5 Selected bond lengths for complexes **3** to **8** (Å).

Complex	Space group	Pd1-P1	Pd1-S1	Pd1-S2	Pd1-S12
3	$P2_1/n$	2.302(1)	2.290(1)	2.328(1)	2.371(1)
4	$P2_1/c$	2.303(1)	2.283(1)	2.384(1)	2.360(1)
5	$C2/c$	2.3056(5)	2.2907(6)	2.3330(5)	2.3800(5)
6	P-1	2.291(6)	2.287(8)	2.339(6)	2.384(7)
7	Pbca	2.291(2)	2.298(2)	2.326(2)	2.360(2)
8	P-1	2.297(3)	2.280(3)	2.335(3)	2.414(3)

Table 2.6 Selected angles for complexes **3** to **8** (°).

Complex	S1-Pd1-S2	S1-Pd1-P1	P1-Pd1-S12	S2-Pd1-S12	Pd1-S2-Pd2	S_3P1-S_3P2
3	88.36(3)	96.46(3)	97.28(3)	77.96(2)	77.19(2)	77.98
4	90.74(3)	90.68(3)	101.11(3)	77.84(3)	76.26(2)	73.42
5	88.29(2)	92.46(2)	103.85(2)	75.37(1)	77.49(2)	77.11
6	89.3(2)	91.6(2)	101.5(2)	77.6(2)	78.4(2)	75.30
7	88.47(7)	91.03(8)	104.53(8)	76.00(7)	76.51(6)	76.75
8	88.6(1)	90.0(1)	104.9(1)	76.7(1)	78.4(1)	74.01

2.2.3.c Isolation of other products

The complexity of the crude ^{1}H NMR spectra made it difficult to determine the number and nature of products present and attention was turned to ^{31}P NMR spectroscopy to probe reactivity. The ^{31}P NMR spectra of the crude reaction mixtures reveal that for the five reactions that were purified by preparative TLC, the dinuclear complex was the major phosphorus-containing product (54 – 60% on the basis of ^{31}P NMR). However, other peaks in the spectra suggests the presence of several other unidentified products, albeit in low yield (typically < 5%, **Table 2.7**). It is possible that some of these minor products may be alternative oligomers to the mono-, di- or hexanuclear structures previously observed. Attempts were made to isolate and identify these other products. For each reaction, all bands were isolated from the TLC plate and dissolved in CH_2Cl_2 or acetone. Recrystallization of the major products as well as comparison to their known ^{31}P NMR values allowed us to determine the identities of some peaks. A summary of the observed ^{31}P NMR data for the separated reaction products is presented in **Table 2.7**, revealing that *ca.* 75% of the phosphorus-containing material present in the reaction mixture comprised the dimetallic complexes **4** – **8**, the free phosphine (PR_3), and/or the corresponding phosphine oxide, (OPR_3). There was no evidence for monometallic structures based on the ^{31}P NMR data. For the reactions of $P(NMe_2)_3$, P^iPr_3, PBn_3 and PCy_3, resonances were observed at 24 ppm, 59 ppm, 41 ppm and 53 ppm, respectively, which were attributed to the oxidized phosphines based on literature data.[25] In the case of $OPBn_3$, the structure was additionally determined by X-ray diffraction after recrystallization. In the reactions of PBn_3 and PCy_3, it was determined that peaks at 46 ppm and 63 ppm respectively were contained in the yellow bands found at the top of the TLC plates; however, these bands also contained dba starting material. Recrystallization

of these bands yielded only crystals of dba and all efforts to separate these products from dba were unsuccessful.

Table 2.7 Observed peaks in ^{31}P NMR spectra of the crude reaction mixtures for complexes **4** to **8**. Percentages indicate what fraction of the mixture each product accounts for, and is based on integration of the NMR peaks. The major product is highlighted in blue for each reaction.

Phosphine	Identified peaks, ppm[25]	Unidentified peaks, ppm
$P(NMe_2)_3$	**104** (60% – *complex **4***), 24 (14% – *$OP(NMe_2)_3$*)	97 (3%), 82 (4%), 38 (4%), 31 (3%), 26 (10%), –6 (3%)
P^iPr_3	**50** (58% – *complex **5***), 21 (7% – *P^iPr_3*), 59 (19% – *OP^iPr_3*)	76 (1%), 75 (0.8%), 73 (4%), 63 (2%), 52 (1%), 44 (5%), 42 (0.9%)
P(*m*-tol)$_3$	**35** (57% – *complex **6***), –5 (19% – *P(m-tol)$_3$*)	58 (1%), 44 (5%), 30 (15%), 28 (1%), 27 (1%)
PBn_3	41 (21% – *$OPBn_3$*), **12** (54% – *complex **7***)	74 (0.3%), 53 (0.3%), 48 (2%), 46 (3%), 11 (9%)
PCy_3	**41** (58% – *complex **8***), 53 (25% – *$OPCy_3$*)	119 (2%), 68 (3%), 63 (12%)

To ensure that the reason no other oligomers were isolated was not simply because of the stoichiometry used in these reactions, the phosphines with the largest cone angles, PBn_3 and PCy_3, were reacted with tetrathiocin **1** and Pd_2dba_3 in various ratios. Using 0.75 to 5 equivalents of phosphine, one equivalent of the tetrathiocin, and one equivalent of Pd_2dba_3, the reactions were carried out in otherwise identical conditions. As can be seen in **Figures 2.20** and **2.21**, the same products can be found in all reactions, albeit in different amounts. In all cases, dimers **7** and **8** were the major products.

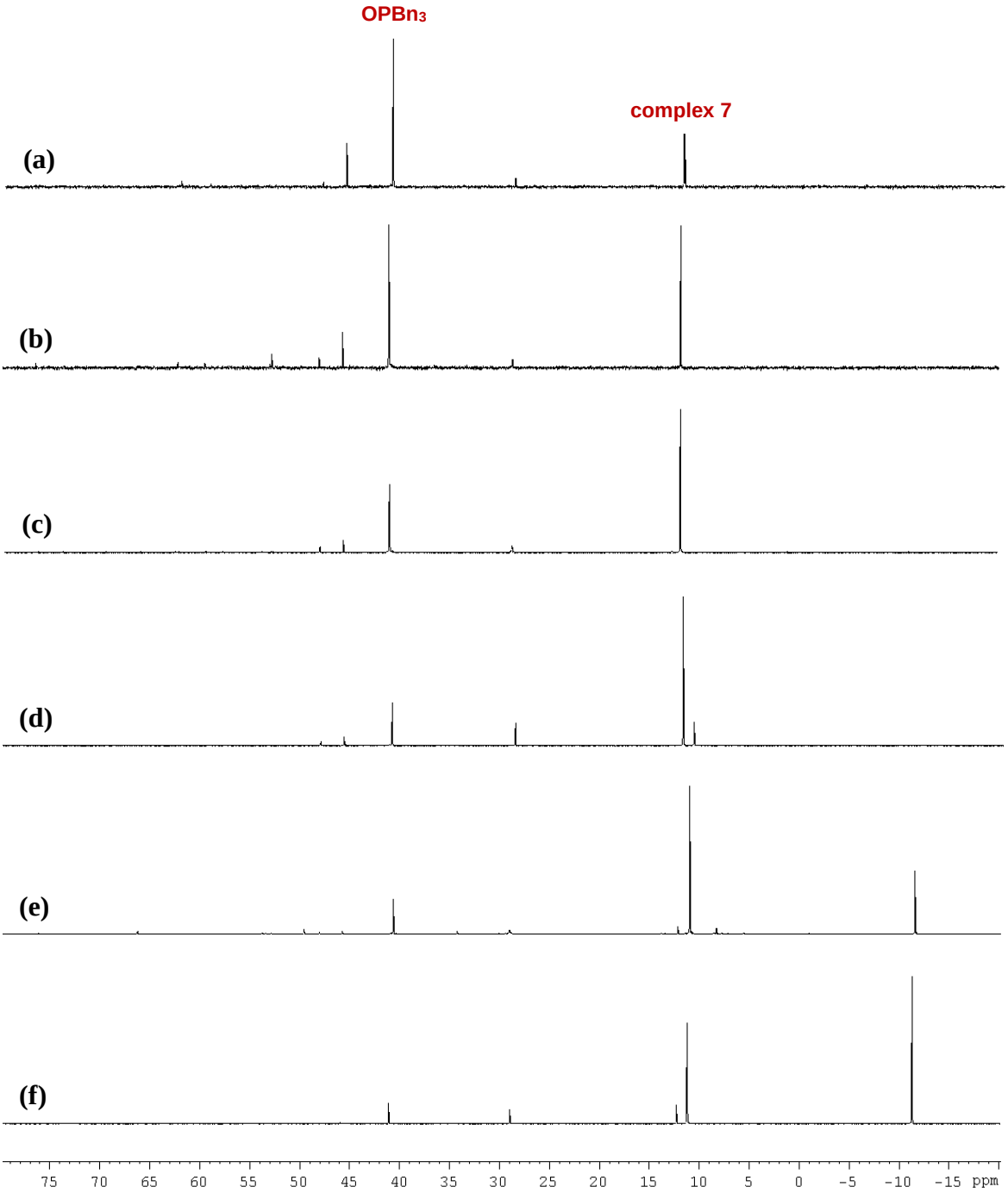

Figure 2.20 ^{31}P NMR spectra of the crude reaction mixture for the reaction of tetrathiocin **1**, Pd_2dba_3, and PBn_3 at: **(a)** 0.75 equiv., **(b)** 1 equiv., **(c)** 1.5 equiv., **(d)** 2 equiv., **(e)** 4 equiv., and **(f)** 5 equiv. of phosphine.

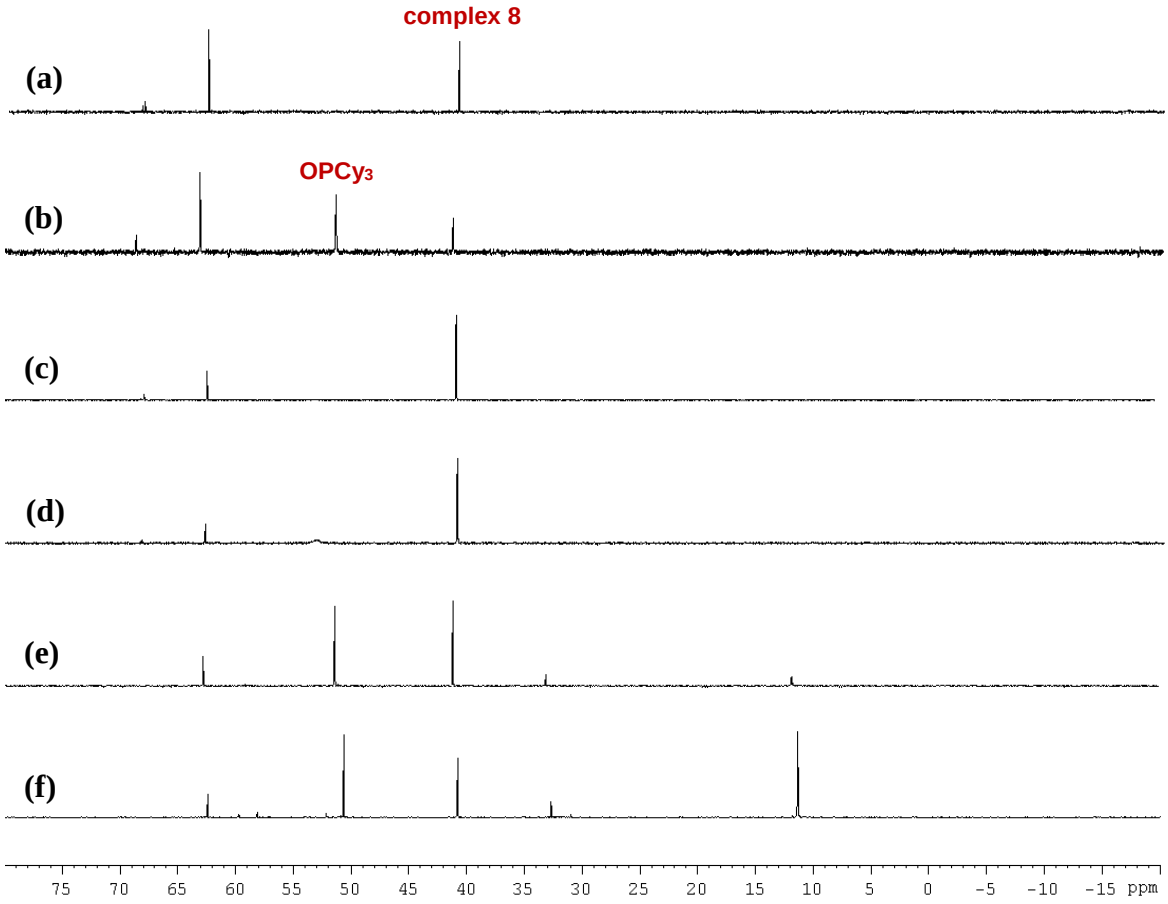

Figure 2.21 ^{31}P NMR spectra of the crude reaction mixture for the reaction of tetrathiocin **1**, Pd_2dba_3, and PCy_3 at: **(a)** 0.75 equiv., **(b)** 1 equiv., **(c)** 1.5 equiv., **(d)** 2 equiv., **(e)** 4 equiv., and **(f)** 5 equiv. of phosphine.

2.2.4 Phosphine Requirement for the Palladium Hexamer [Pd(dmobdt)]$_6$ (9)

The extremely large cone angle of P^{t}Bu$_3$ (182°) means that in the synthesis of the hexanuclear cage [Pd(dmobdt)]$_6$, the phosphine is too bulky to remain coordinated to the metal centre, giving a structure in which no phosphine was present.[15] In this original synthesis the yield was reported to be 12%. In these studies, the absence of phosphine in the final complex suggested that this complex might be produced by reacting Pd_2dba_3 with tetrathiocin **1**, without addition of phosphine.

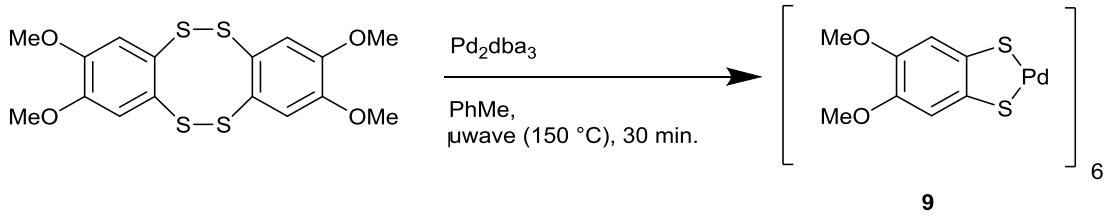

9

Scheme 2.4 Synthesis of **9** without addition of phosphine.

The resultant brown solution was filtered from a small amount of black precipitate (possibly Pd^0). Purification by preparative TLC yielded a brown solid which showed no ^{31}P peak. However, six distinct ^1H NMR resonances could be observed in both the aryl and alkyl regions of the spectrum, indicating that complex **9** had successfully been synthesized without phosphine. In addition, the yield increased from 12%[15] to 39%.

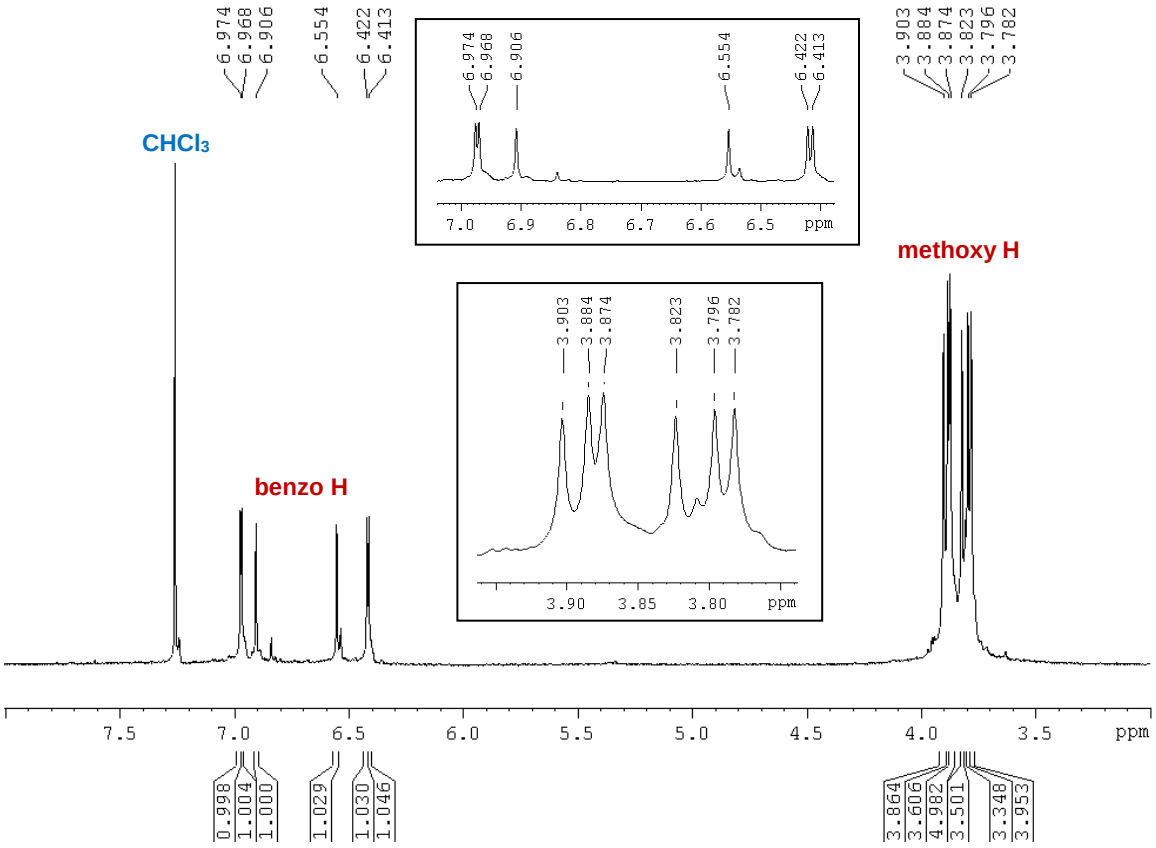

Figure 2.22 ^1H NMR spectrum of complex **9** in $CDCl_3$, showing six resonances for the benzo protons and six for the methoxy protons.

2.2.5 Kinetics of Formation of the Platinum Dimer [(dmobdt)Pt(PPh$_3$)]$_2$ (10)

Previous studies had revealed that while the chemistry of platinum and palladium appear similar, the kinetics of Pt are typically slower than Pd.[26] Thus while reaction of tetrathiocin **1** with Pd_2dba_3 amd PPh_3 formed only the dimer $[(dmobdt)Pd(PPh_3)]_2$, the corresponding reaction of $Pt(PPh_3)_4$ with **1** permitted the isolation of both the dinuclear complex $[(dmobdt)Pt(PPh_3)]_2$ (**10**) and the monometallic complex $(dmobdt)Pt(PPh_3)_2$ (**11**).[3] Initial studies revealed that when $Pt(PPh_3)_4$ was stirred with tetrathiocin **1** in dry toluene at 150°C under microwave conditions for 30 minutes, a mixture of the dinuclear complex **10** and the mononuclear complex **11** were produced. Extending the reaction time to 60 minutes yielded only the dinuclear complex. From this, the mechanism of the reaction was proposed as follows: firstly the monomeric structure (**11**) is formed, followed by (solvent assisted) dissociation of a labile PPh_3 and dimerization to give the dimer (**Scheme 2.5**).

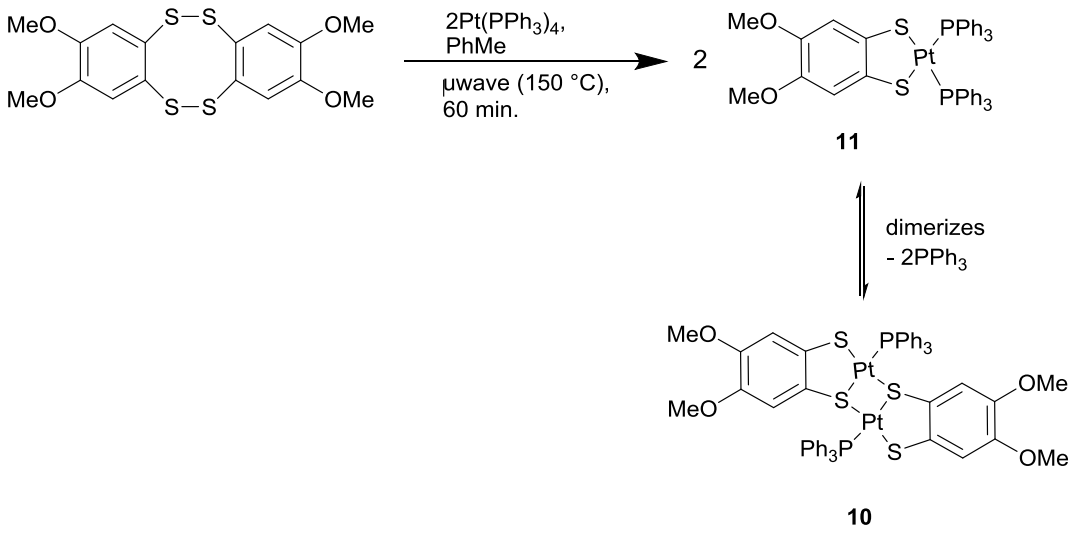

Scheme 2.5 Proposed mechanism for the formation of platinum dimer **10**.[3]

However, in the current studies, when the experiment was conducted again under identical conditions, similar results were not observed, suggesting the initial observations were not reproducible. After 60 minutes, a mixture of complexes **10** and **11** could still be seen by ^{31}P and ^{1}H NMR, but with a larger amount of the mononuclear complex than the dimer present. Extending the reaction times further yielded similar results, with very little

additional conversion to the dimer. At 90 minutes, a yellow solid precipitated out of the orange solution, and was filtered out and washed with hexane and identified as the mononuclear complex **11** based on NMR analysis. The reaction was repeated four times, each time affording similar results, with complex **11** precipitating at various points in the reaction (after 15, 50, 60, 80, 90 minutes) and in varying yields (a few milligrams up to 0.174 g).

To confirm that the mononuclear complex **11** was generated en route to **10**, the isolated complex **11** was heated with stirring at 150 °C in the microwave for 60 minutes in dry toluene. The yellow solution was evaporated and dissolved in $CDCl_3$, and NMR analysis (**Figure 2.23**) showed that no conversion to the dimer had taken place. A peak at 19.998 ppm with satellites at 31.91 and 8.09 ppm was observed in the ^{31}P spectrum. In the ^{1}H spectrum, a single resonance at 6.80 ppm could be seen for the benzo protons and one resonance in the alkyl region at 3.72 ppm was observed for the methoxy protons, matching reported values.[3] These observations suggested that either water and/or oxygen and/or solvent likely played a pivotal role in the conversion of mononuclear complex to dinuclear complex. To test this hypothesis the reaction was conducted in wet toluene but yielded similar results, suggesting water did not play a role in this transformation.

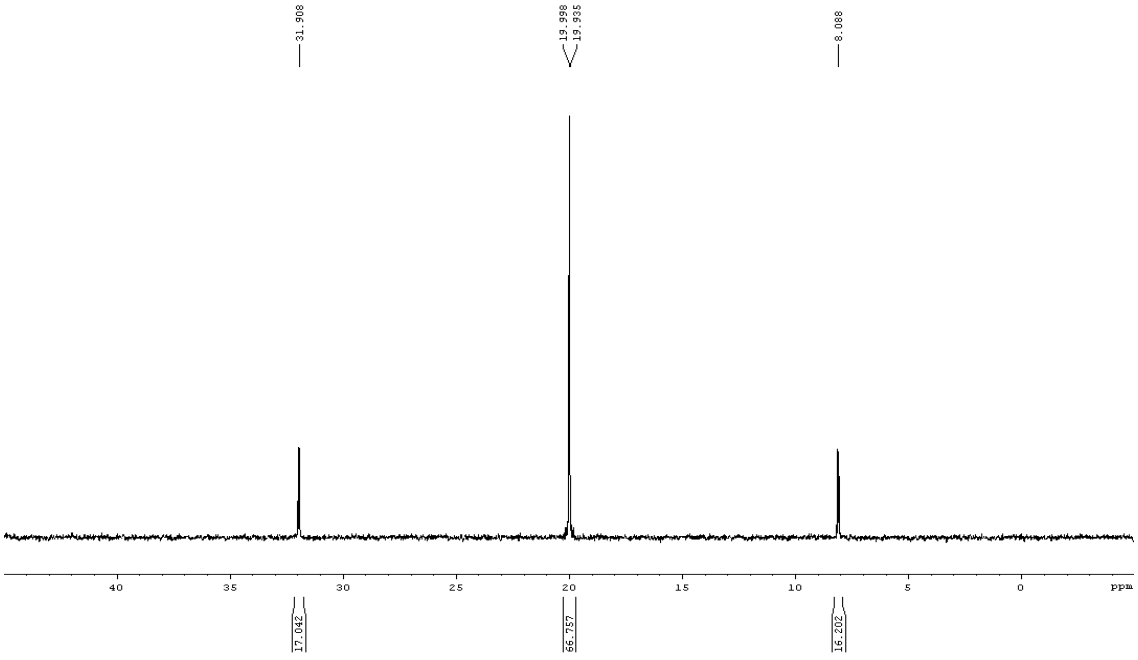

Figure 2.23 ^{31}P NMR spectrum after **11** was heated in dry toluene at 150 °C for 60 min.

Performing the reaction in wet, dry, and degassed THF, under otherwise similar conditions, provided greater insight into the monomer to dimer conversion. A 10 mg sample of complex **11** was heated in the microwave at 150 °C in 0.5 mL of degassed, dry, or wet THF, and NMR studies were conducted after 60 minutes. In both dry and wet THF, there was a change in colour of solution from yellow to orange. The emergence of resonances attributed to the dimer (21 ppm) were identified in addition to the monomer (19 ppm), suggesting oxygen present in both mixtures plays a role in the reaction. An additional ^{31}P peak at 29 ppm can be observed in each reaction, corresponding to the oxidized phosphine $OPPh_3$. The presence of both monomer and dimer was additionally confirmed by the ^{1}H NMR spectra. This was confirmed using degassed THF when no colour change was observed and no dimer signals identified by NMR spectroscopy (**Figure 2.24**). Comparing the three reactions, conversion to dimer seems to increase as conditions which favour phosphine oxidation are present. The monomer:dimer:$OPPh_3$ ratio was 1:0:0 in degassed THF, 5:1:2.78 in dry THF, and 1:1:3.5 in wet THF according to ^{31}P NMR. These ratios were supported by ^{1}H NMR measurements. These results indicate that the conversion of monomer to dimer may be driven by oxidation of the phosphine. As this oxidation takes place and PPh_3 is removed, the equilibrium shifts towards the products according to Le Chatelier's principle, driving the formation of complex **10** (**Scheme 2.6**).

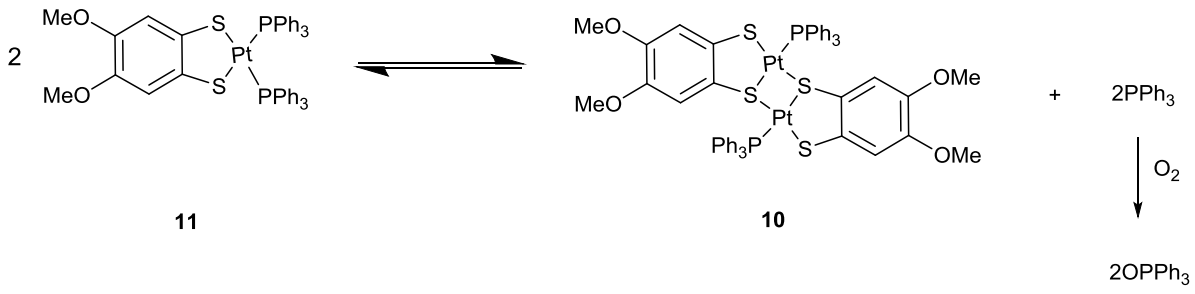

Scheme 2.6 Reaction equilibrium shifted by oxidation of PPh_3.

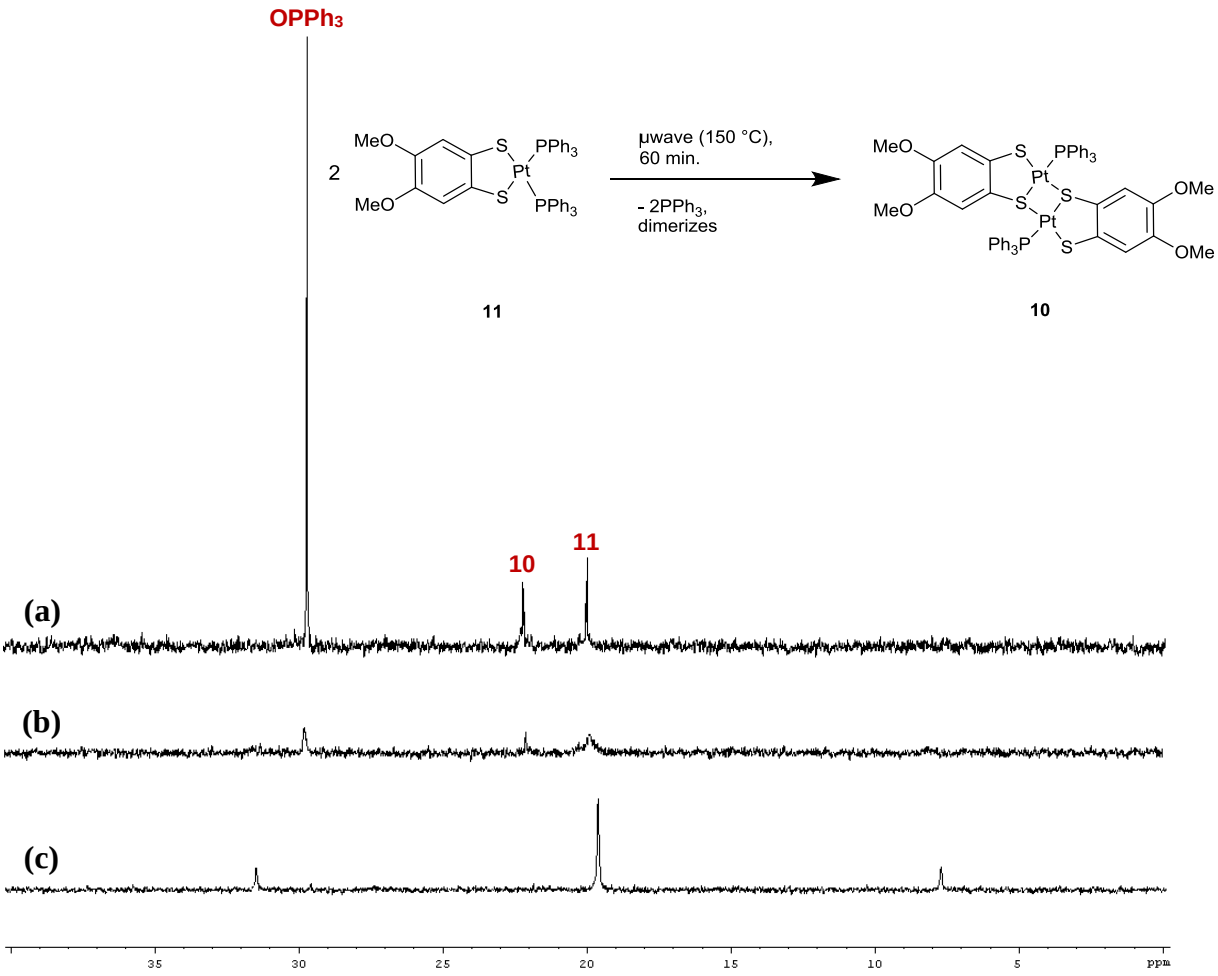

Figure 2.24 ^{31}P NMR after heating **11** at 150 °C in the microwave for 60 min in: **(a)** wet THF, **(b)** dry THF, and **(c)** degassed (wet) THF.

Attempts to conduct kinetic measurements in wet THF were unsuccessful, with percentage of monomer to dimer conversion ranging widely and no pattern observed with changes in concentration. It is possible that other factors which are difficult to measure, such as amount of oxygen or water present in the atmosphere, play a role in the rate of reaction.

2.2.6 Synthesis of a Platinum Hexamer [Pt(dmobdt)]$_6$ (12)

The slower kinetics of platinum described in section **2.2.5** provided an alternative potential strategy (to tuning the phosphine descrbed in section **2.2.3**) to isolate intermediate nuclearity complexes between the dimer and hexamer. The Pd hexamer was

previously prepared from Pd_2dba_3, P^tBu_3 and tetrathiocin **1**. As a consequence, the related Pt^0 chemistry was examined. Unlike Pd which forms analytically pure Pd_2dba_3, dibenzylideneacetone complexes of Pt rnge from the stochiometric Pt_1dba_3 through to the non-stoichiometric $Pt_{2-x}dba_3$ depending on preparative procedure.[27] A sample of $Pt_{2-x}dba_3$ was prepared according to the literature procedure[27a] to compare with the Pd_2dba_3 chemistry with microanalytical data confurming the compoisition to be x = 0.1, i.e. $Pt_{1.9}dba_3$.

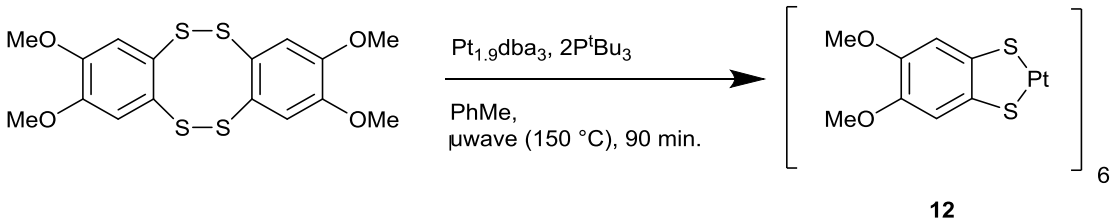

12

Scheme 2.7 Synthesis of platinum hexamer **12**.

Tetrathiocin **1** was combined with $Pt_{1.9}dba_3$ and P^tBu_3 in dry toluene and stirred at 150 °C under microwave conditions for 1.5 hours (**Scheme 2.7**). The resultant brown solution was purified by preparative TLC methods, and a yellow band isolated and extracted into CH_2Cl_2. ^1H NMR analysis of this band showed that a hexameric complex had been successfully synthesized based on the observation of six resonances corresponding to the benzo protons and six resonances for the methoxy protons, consistent with a hexanuclear structure similar to the previously described palladium hexamer, $[Pd(dmobdt)]_6$ (**9**).

Orange crystals of complex **12** could be grown from layering of diethyl ether onto a saturated CH_2Cl_2 solution, however they were not good enough for X-ray diffraction. Recrystallization by layering diisopropyl ether onto a CH_2Cl_2 solution afforded good crystals, which crystallized in the orthorhombic $P2_12_12$ space group. Just as was observed in the palladium hexamer $[Pd(dmobdt)]_6$ **9**,[15] complex **12** contained six metal centres arranged in an octahedron, with six dithiolenes adopting μ_2-bridging modes between the metals, and a noncrystallographic 2-fold rotation axis going through the two axial Pt1 and Pt6 atoms. The Pt-S bond lengths were comparable to the Pd-S lengths in complex **9** (2.303(5) – 2.363(5) Å vs 2.294(2) – 2.361(2) Å). The sum of internal angles around the

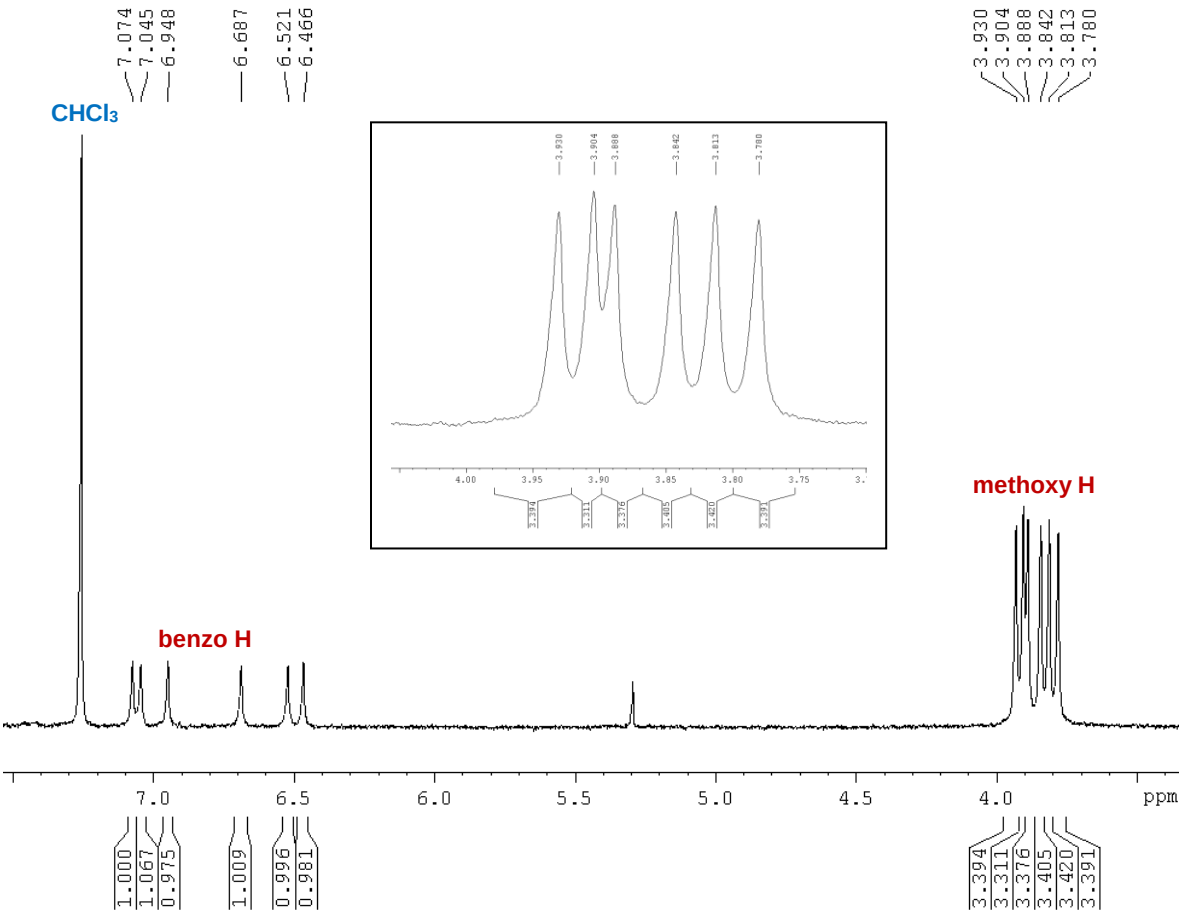

Figure 2.25 ^{1}H NMR spectrum of complex **12** with an inset showing six resonances for the methoxy protons.

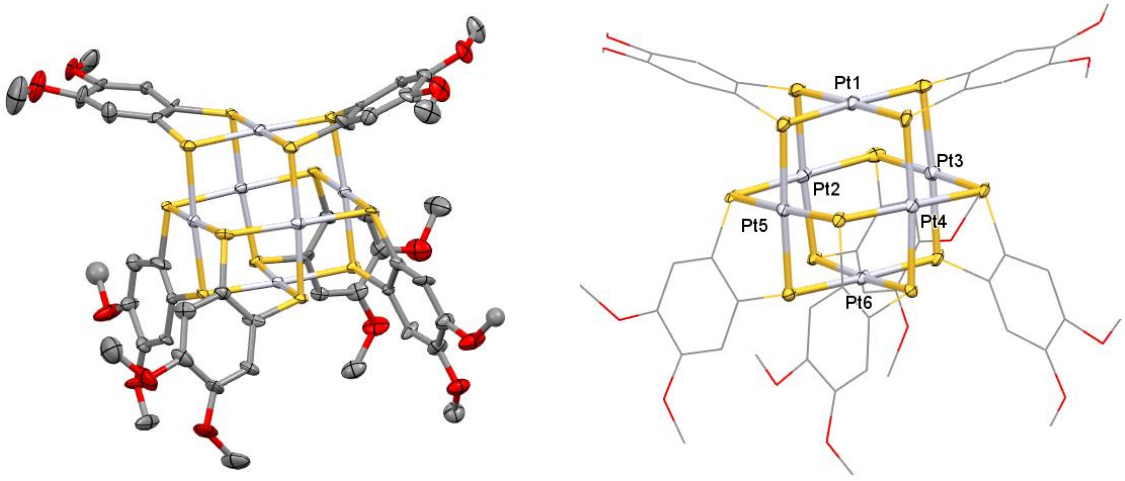

Figure 2.26 Crystal structure of complex **12** (left), and platinum atom labelling (right). Hydrogen atoms have been omitted for clarity.

Pt atoms was invariant at 359.8(4) – 359.9(4)°, consistent with square planar geometries at the metal centres. To our knowledge, this is the first report of a hexameric platinum dithiolene complex.

An additional orange band was collected from the TLC plate. The ^{31}P spectrum (**Figure 2.27**) appeared similar to previous spectra observed for the mixture of dimeric and monomeric complexes **10** and **11**, with two major products observed with ^{195}Pt satellites at 57.36 ppm ($^{1}J_{Pt-P}$ = 1294 Hz) and 52.83 ppm ($^{1}J_{Pt-P}$ = 1735 Hz). The ^{1}H spectrum (**Figure 2.28**) appeared consistent with the possible presence of a dimer [benzo protons at 6.99 and 6.96 ppm and methoxy peaks at 3.87 and 3.85 ppm with benzo:methoxy proton ratio of 1:3] as well as a possible monomer [methoxy peak at 3.82 ppm and a possible peak at 1.58 ppm coming from the ^{t}Bu groups].

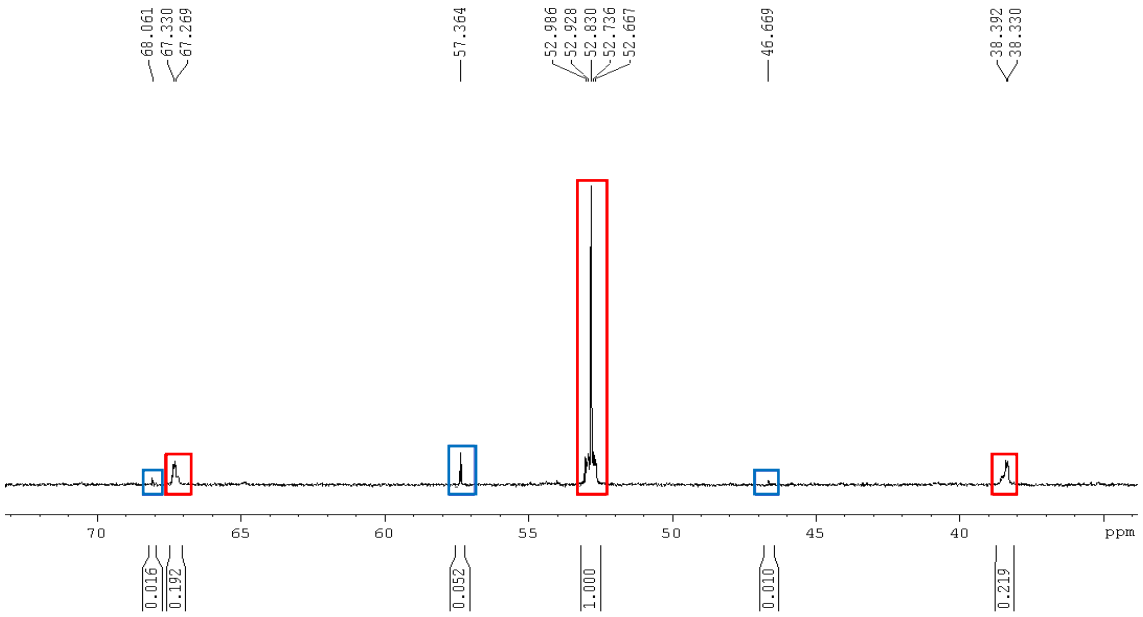

Figure 2.27 $^{31}P\{^{1}H\}$ NMR spectrum of the orange band showing a possible mixture of dimeric (red) and monomeric (blue) products.

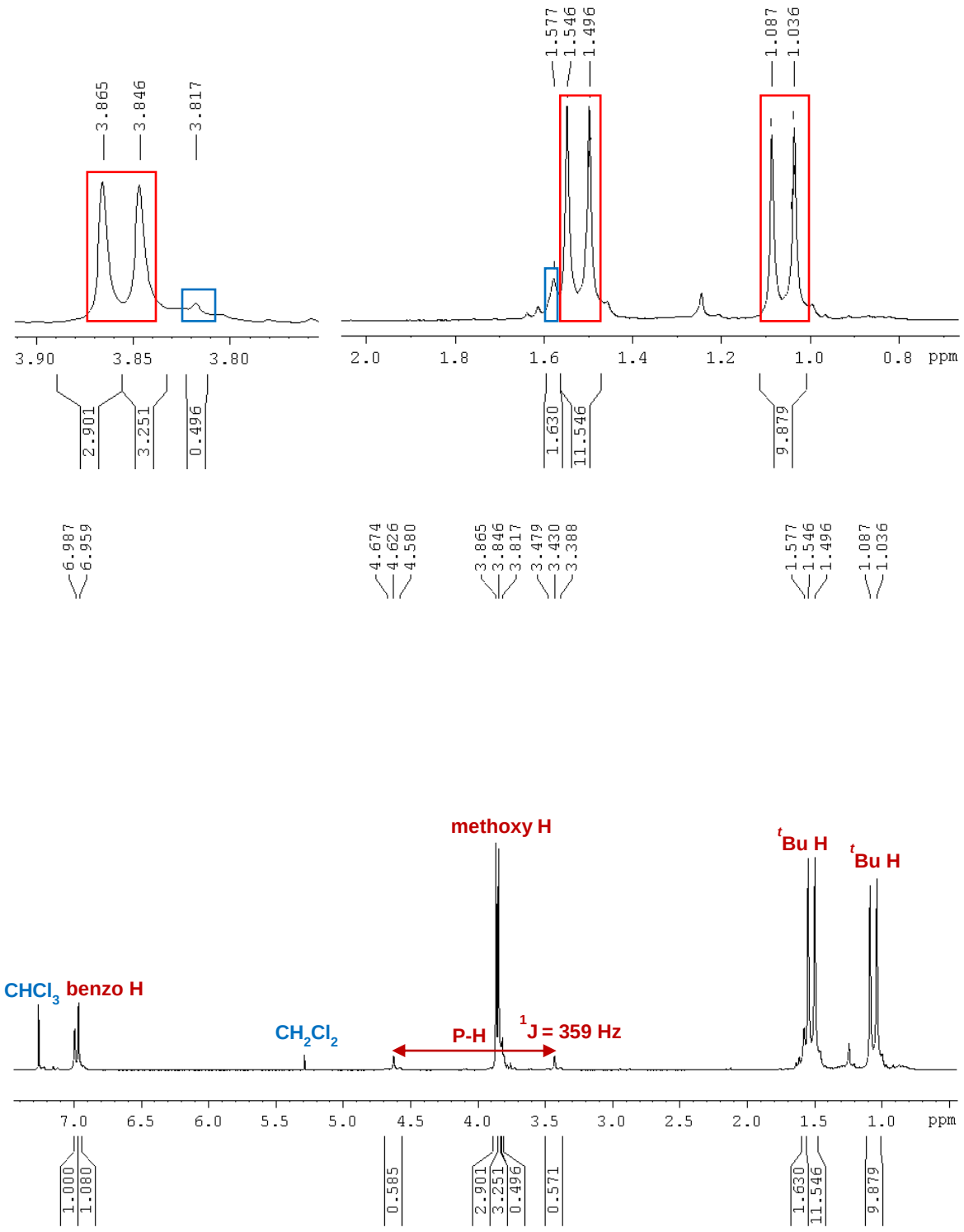

Figure 2.28 ^{1}H NMR spectra of the orange band showing a possible mixture of products, including possible monomer (blue) and dimer (red) formation shown in the methoxy and ^{t}Bu regions (above).

Recrystallization of this orange band by slow diffusion of diethyl ether into a CH_2Cl_2 solution afforded large orange-red blocks, which were identified by X-ray diffraction as the dimeric $[(dmobdt)Pt(PH^tBu_2)]_2$ **13** (shown in **Figure 2.29**). Complex **13** crystallizes in the monoclinic $P2_1/n$ space group. The Pt-P distance is 2.260(1) Å and the Pt-S bonds are in the range 2.282(1) – 2.367(1) Å, with the μ_2-bridging sulfurs having longer Pt-S distances (between 0.038(1) and 0.085(1) Å longer) than the non-bridging sulfurs. The sum of internal angles at the platinum centres are 359.94(7)° and 360.01(7)°, indicating square planar geometry, although the S-Pt-S angles in the Pt_2S_2 core are small (77.34(3)° and 77.63(3)°). The dihedral angle between the two S_3P planes is 72.60°. NMR analysis of this complex confirmed the tentative assignment of the dimer to the peak at 52 ppm in the ^{31}P NMR spectrum (**Figure 2.27**).

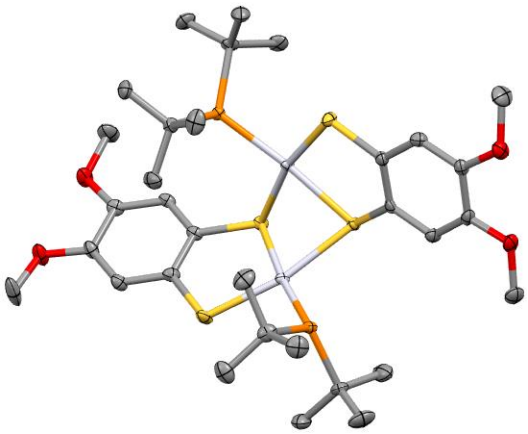

Figure 2.29 Crystal structure of complex **13** with thermal ellipsoids drawn at the 50% probability level. Hydrogen atoms have been omitted for clarity.

This type of phosphine reactivity in these oxidative addition reactions was entirely unexpected. However, previous examples exist in the literature for the conversion of P^tBu_3 to PH^tBu_2 upon metal coordination;[28] in the reaction of $Re_3(CO)_{12}(\mu\text{-}H)_3$ with P^tBu_3, two of the five products isolated were $Re_2(CO)_7(\mu\text{-}P^tBu_2)(PH^tBu_2)(\mu\text{-}H)$ and $Re_2(CO)_5(P^tBu_3)(PH^tBu_2)(\mu\text{-}OP^tBu_2)(\mu\text{-}H)$. It was postulated that this conversion may have involved the evolution of isobutene, but this was not confirmed. Future efforts to study this dimeric complex further and to separate and isolate each of the products in this reaction may prove useful in identifying possible intermediates and studying the mechanism of this reaction.

2.3. Conclusions

In this chapter, the formation of dinuclear complexes [(dmobdt)Pd(PPh_3)]$_2$ (**2**) and [(dmobdt)Pt(PPh_3)]$_2$ (**10**), as well as the possible effect of phosphine co-ligand on kinetics of [(dmobdt)Pd(PR_3)]$_2$ formation, were re-examined. Initial studies revealed that a series of dinuclear palladium complexes could be prepared as the major product from Pd_2dba_3 and tetrathiocin in the presence of monodentate phosphines, PR_3 with different Tolman cone angles. The structures of the dimetallic complexes **3** – **8** were determined by X-ray diffraction and showed geometric changes in the dimeric cage structure related to the steric demand of the phosphine. Although there was evidence for formation of other (minor) species based on TLC and ^{31}P NMR studies, no other oligomers were unambiguously identified in these reactions apart from the hexameric [Pd(dmobdt)]$_6$ when using P^{t}Bu$_3$. Studies on the kinetically slower platinum chemistry showed that the mononuclear intermediate (dmobdt)Pt(PPh_3)$_2$ **11** could be isolated as well as the dinuclear complex [(dmobdt)Pt(PPh_3)]$_2$. The conversion of **11** to **10** was found not to simply involve liberation of free phosphine but required the presence of dissolved oxygen which appears to facilitate removal of coordinated PPh_3 as $OPPh_3$ during dimer formation. Using the more sterically demanding P^{t}Bu$_3$ permitted the first hexanuclear homoleptic platinum dithiolate complex [Pt(dmobdt)]$_6$ **12** to be prepared, as well as the possible dinuclear intermediate [(dmobdt)Pt(PH^{t}Bu$_2$)]$_2$ **13** in which, for the first time, the phosphine shows non-innocent behavior.

2.4. Experimental

2.4.1 Crystallographic Studies

Crystals were mounted on a cryoloop with paratone oil and examined on a Bruker D8 Venture diffractometer equipped with a Photon 100 CCD area detector and an Oxford Cryostream cooler. Data were measured using graphite-monochromated Mo-Kα radiation (λ = 0.71073 Å) or Cu-Kα radiation (λ = 1.54178 Å) using the APEX-II software.[29] Final cell constants were determined from full least squares refinement of all observed reflections. The data were collected for absorption (sadabs)[30] and the structures solved by intrinsic phasing. Any remaining heavy atom positions were located in subsequence difference maps and the structure refined with full least squares refinement on F^2 within the SHELXTL suite.[31] Hydrogen atoms were placed at calculated positions and refined isotropically with a riding model. Structure solution, refinement and preparation of final cif files were undertaken using the SHELXTL package.

2.4.2 General Experimental Procedures

NMR spectra were recorded on a Bruker DPX300 300 MHz or a Bruker UltraShield 300 MHz spectrometer with a Broadband AX Probe using $CDCl_3$ (^1H δ = 7.26 ppm, s) as an internal reference point relative to Me_4Si (δ = 0 ppm). ^{31}P NMR spectra were referenced to 85% H_3PO_4 (δ = 0 ppm). IR spectra were obtained using a Bruker Alpha FT-IR spectrometer equipped with a Platinum single reflection diamond ATR module. Elemental compositions were determined on a PerkinElmer 2400 Series II Elemental Analyzer. Mass spectra were recorded on a Waters XEVO G2-XS Time Of Flight (TOF) mass spectrometer using Electrospray Ionization Time of Flight (ESI-TOF) operated in positive mode or Atmospheric Solids Analysis Probe (ASAP) operated in positive techniques. Microwave syntheses were carried out in sealed vessels using a Biotage Initiator+ microwave with continuous stirring.

The following reagents were prepared using the procedures reported in literature: 2′,3′,8′,9′ -tetramethoxy-dibenzo-1,2,5,6-tetrathiocin (**1**)[4,5], $Pd_2dba_3{\cdot}CHCl_3$[32], and $[(dmobdt)Pd(PPh_3)]_2$ (**2**)[15].

2.4.3 Preparation of [(dmobdt)Pd(PPh$_3$)]$_2$, (2), through reaction with Pd(PPh$_3$)$_4$.

$Pd(PPh_3)_4$ (0.252 g, 0.218 mmol) and tetrathiocin **1** (0.044 g, 0.109 mmol) were placed in an oven dried microwave vial under an inert nitrogen atmosphere. Dry toluene (5 mL) was added to the vial and the suspension was placed in the microwave at 150 °C. After 1 minute, a 0.2 mL sample was removed from the green solution and evaporated by rotary evaporation, then dissolved in $CDCl_3$ for NMR analysis.

NMR (ppm) ($CDCl_3$)**: δ_H** (300 MHz) = 6.16 (2H, s, benzo C–H), 5.89 (2H, s, benzo C–H), 3.66 (6H, s, O–CH_3), 2.98 (6H, s, O–CH_3); **$\delta_P\{^1H\}$** (121 MHz) = 34.47.

2.4.4 Preparation of [(dmobdt)Pd(PPh$_2$^{i}Pr)]$_2$, (3).

Pd_2dba_3 (0.100 g, 0.109 mmol), $PPh_2{}^iPr$ (0.050 g, 0.218 mmol) and tetrathiocin **1** (0.044 g, 0.109 mmol) were placed in an oven dried microwave vial under an inert nitrogen atmosphere. Dry toluene (5 mL) was added to the vial and the suspension was placed in the microwave for 20 minutes at 150 °C to afford a dark green solution. The solution was filtered from a small amount of black precipitate and evaporated by rotary evaporation. The solid was recrystallized by slow diffusion of Et_2O into a saturated CH_2Cl_2 solution affording dichroic green-orange plates suitable for X-ray diffraction (0.012 g, 10% yield).

NMR (ppm) ($CDCl_3$)**: δ_H** (300 MHz) = 6.46 (2H, s, benzo C–H), 5.92 (2H, s, benzo C–H), 5.30 (s, CH_2Cl_2), 3.79 (6H, s, O–CH_3), 3.30 (6H, s, O–CH_3), 1.59 (16H, s, CH–CH_3), 0.92 (0.99–0.84, 12H, m, CH–CH_3); **$\delta_P\{^1H\}$** (121 MHz) = 37.73.

HRMS (ESI-TOF) *m/z*: calc. for $C_{46}H_{50}O_4P_2S_4Pd_2$ 1070.0155; found 1070.0187.

Elemental Analysis calc. for $C_{46}H_{50}O_4P_2S_4Pd_2 \cdot ½CH_2Cl_2$: C 50.21; H 4.62%; found: C 50.10; H 4.68%.

IR (cm^{-1}): $\tilde{\nu}$ = 3050(w), 2958(w), 2926(w), 2865(w), 2831(w), 1583(w), 1474(s), 1456(m), 1430(vs), 1365(w), 1341(w), 1235(vs), 1200(vs), 1175(s), 1155(s), 1092(s), 1035(vs), 1006(m), 921(w), 878(w), 846(m), 783(m), 774(m), 740(vs), 692(vs), 681(vs), 639(s), 615(m), 575(w), 527(vs), 511(vs), 490(m), 475(vs), 447(m), 414(w).

2.4.5 Preparation of [(dmobdt)Pd(P(NMe$_2$)$_3$)]$_2$, (4).

Pd_2dba_3 (0.100 g, 0.109 mmol), $P(NMe_2)_3$ (0.04 mL, 0.218 mmol) and tetrathiocin **1** (0.044 g, 0.109 mmol) were placed in an oven dried microwave vial under an inert nitrogen atmosphere. Dry toluene (5 mL) was added to the vial and the suspension was placed in the microwave for 20 minutes at 150 °C. The resultant dark red solution was isolated from a small amount of black solid by filtration. The solvent was evaporated by rotary evaporation and the residue dissolved in a small amount of CH_2Cl_2, and was then purified by preparative TLC (eluted in $CHCl_3$). The orange band (R_f = 0.34) was removed from the silica plate and extracted into CH_2Cl_2. Evaporation of the solvent resulted in a red-orange solid (0.0198 g, 19% yield) and recrystallized by layering pentane onto a saturated $CHCl_3$ solution followed by slow evaporation to produce orange crystals suitable for X-ray diffraction. The crystals were washed with hexane and dried in air.

NMR (ppm) ($CDCl_3$)**: δ_H** (300 MHz) = 6.81 (2H, s, benzo C–H), 6.78 (2H, s, benzo C–H), 3.83 (6H, s, O–CH_3), 3.80 (6H, s, O–CH_3), 2.73 (18H, s, N–CH_3), 2.70 (18H, s, N–CH_3); **$\delta_P\{^1H\}$** (121 MHz) = 104.52.

HRMS (ESI-TOF) *m/z*: calc. for $C_{28}H_{52}N_6O_4P_2S_4Pd_2$ 940.0489; found 904.0511.

Elemental Analysis calc. for $C_{28}H_{52}N_6O_4P_2S_4Pd_2 \cdot CH_2Cl_2$: C 33.99; H 5.31; N 8.20%; found: C 33.60; H 4.81; N: 7.82%.

IR (cm^{-1}): $\tilde{\nu}$ = 3000(w), 2920(vs), 2851(s), 2794(w), 1644(w), 1584(w), 1556(w), 1483(vs), 1462(vs), 1434(vs), 1343(w), 1242(vs), 1202(s), 1169(vs), 1107(w), 1058(w), 1030(vs), 952(vs), 842(s), 782(m), 745(m), 718(m), 702(m), 682(s), 661(s), 573(w), 509(m), 453(m), 413(w).

2.4.6 Preparation of [(dmobdt)Pd(P^{i}Pr$_3$)]$_2$, (5).

Pd_2dba_3 (0.100 g, 0.109 mmol), P^iPr_3 (0.04 mL, 0.218 mmol) and tetrathiocin **1** (0.044 g, 0.109 mmol) were placed in an oven dried microwave vial under an inert nitrogen atmosphere. Dry toluene (5 mL) was added to the vial and the suspension was placed in the microwave for 20 minutes at 150 °C. The resultant dark green-red solution was isolated from a small amount of black solid by filtration. The solvent was evaporated by

rotary evaporation and dissolved in a small amount of CH_2Cl_2, and was then purified by preparative TLC (eluted in $CHCl_3$). The green band (R_f = 0.34) was removed from the silica plate and extracted into CH_2Cl_2. Evaporation of the solvent resulted in a green solid (0.0356 g, 35%), recrystallization by layering pentane onto a saturated CH_2Cl_2 solution followed by slow evaporation afforded green crystals suitable for X-ray diffraction. The crystals were washed with hexane and dried in air.

NMR (ppm) ($CDCl_3$)**:** δ_H (300 MHz) = 6.82 (2H, s, benzo C–H), 6.73 (2H, s, benzo C–H), 3.82 (6H, s, O–CH_3), 3.79 (6H, s, O–CH_3), 1.42 (1.45–1.38, 18H, m, C–CH_3), 2.40 (2.44–2.35, 6H, m, P–CH), 1.12 (1.16–1.09, 18H, m, C–CH_3); $\delta_P\{^1H\}$ (121 MHz) = 50.26.

HRMS (ESI-TOF) ***m/z*****:** $[M+H]^+$ calc. for $C_{34}H_{59}O_4P_2S_4Pd_2^+$ 935.0855; found 935.0850.

Elemental Analysis calc. for $C_{34}H_{58}O_4P_2S_4Pd_2 \cdot C_7H_8$: C 48.00; H 6.48%; found: C 47.94; H 6.26%.

2.4.7 Preparation of [(dmobdt)Pd(P(m-tol)$_3$)]$_2$, (6).

Pd_2dba_3 (0.100 g, 0.109 mmol), P(*m*-tol)$_3$ (0.066 g, 0.218 mmol) and tetrathiocin **1** (0.044 g, 0.109 mmol) were placed in an oven dried microwave vial under an inert nitrogen atmosphere. Dry toluene (5 mL) was added to the vial and the suspension was placed in the microwave for 20 minutes at 150 °C. The resultant dark green-red solution was isolated from a small amount of black solid by filtration. The solvent was evaporated by rotary evaporation and the reaction mixture dissolved in a small amount of $CHCl_3$, and was then purified by preparative TLC (7:3 mixture of CH_2Cl_2 and hexane). The green band (R_f = 0.58) was removed from the silica plate and extracted into CH_2Cl_2. The solution was concentrated by evaporation of solvent, then further purified by preparative TLC (eluted in $CHCl_3$). The green band (R_f = 0.34) was removed from the silica plate and extracted into CH_2Cl_2. Evaporation of the solvent resulted in a green solid (0.042 g, 31% yield) which could be purified by dissolving in $CHCl_3$ and layering hexane, giving a globular green solid. A small amount of crystals suitable for X-ray diffraction were grown by evaporation. The crystals were washed with hexane and dried in air.

NMR (ppm) ($CDCl_3$)**:** δ_H (300 MHz) = 6.03 (2H, s, benzo C–H), 5.84 (2H, s, benzo C–H), 3.70 (6H, s, O–CH_3), 2.91 (6H, s, O–CH_3), 2.33 (18H, s, CH_3); $\delta_P\{^1H\}$ (121 MHz) = 34.81.

HRMS (ESI-TOF) ***m/z*****:** $[M+H]^+$ calc. for $C_{58}H_{59}O_4P_2S_4Pd_2^+$ 1223.0864; found 1223.0841.

Elemental Analysis calc. for $C_{58}H_{58}O_4P_2S_4Pd_2$: C 57.00; H 4.78%; found: C 57.82; H 4.95%.

IR (cm^{-1}): $\tilde{\nu}$ = 3049(w), 2996(w), 2948(w), 2922(w), 2831(w), 1672(w), 1651(w), 1617(w), 1589(m), 1556(w), 1486(s), 1457(s), 1435(s), 1405(m), 1337(m), 1241(vs), 1201(vs), 1173(s), 1104(s), 1062(m), 1035(vs), 989(m), 924(w), 877(w), 841(m), 775(s), 764(s), 688(vs), 554(s), 543(s), 505(w), 467(vs), 451(vs).

2.4.8 Preparation of [(dmobdt)Pd(PBn_3)]$_2$, (7).

Protocol #1: Pd_2dba_3 (0.100 g, 0.109 mmol), PBn_3 (0.066 g, 0.218 mmol) and tetrathiocin **1** (0.044 g, 0.109 mmol) were placed in an oven dried microwave vial under an inert nitrogen atmosphere. Dry toluene (5 mL) was added to the vial and the suspension was placed in the microwave for 20 minutes at 150 °C. The resultant dark green-red solution was isolated from a small amount of black solid by filtration. The solvent was evaporated by rotary evaporation and the reaction mixture dissolved in a small amount of $CHCl_3$, and was then purified by preparative TLC (7:3 mixture of CH_2Cl_2 and hexane). The green band (R_f = 0.20) was removed from the silica plate and extracted into CH_2Cl_2. Evaporation of the solvent resulted in a green solid (0.021 g, 16% yield) that was recrystallized by slow evaporation of a saturated CH_2Cl_2 solution, affording green crystals suitable for X-ray diffraction.

Protocol #2: Pd_2dba_3 (0.100 g, 0.109 mmol), PBn_3 (0.017 g, 0.055 mmol) and tetrathiocin **1** (0.044 g, 0.109 mmol) were placed in an oven dried microwave vial under an inert nitrogen atmosphere. Dry toluene (5 mL) was added to the vial and the suspension was placed in the microwave for 20 minutes at 150 °C. The resultant brown solution was isolated from a small amount of black solid by filtration.

The solvent was evaporated by rotary evaporation and dissolved in a small amount of $CHCl_3$, and was then purified by preparative TLC (7:3 mixture of CH_2Cl_2 and hexane). The green band (R_f = 0.60) was removed from the silica plate and dissolved in CH_2Cl_2, then acetone (collected separately). Evaporation of the solvent from the acetone washings resulted in a green solid (0.032 g, 96% yield), which was recrystallized by layering hexane onto a saturated CH_2Cl_2 solution to produce green crystals suitable for X-ray diffraction. The crystals were washed with hexane and dried in air.

NMR (ppm) ($CDCl_3$)**: δ_H** (300 MHz) = 6.53 (2H, s, benzo C–H), 6.36 (2H, s, benzo C–H), 3.69 (6H, s, O–CH_3), 3.46 (6H, s, O–CH_3), 3.19 (3.23–3.15, 6H, m, CH_2), 3.04 (3.09–3.00, 6H, m, CH_2); **$\delta_P\{^1H\}$** (121 MHz) = 12.15.

HRMS (ESI-TOF) ***m/z*****:** $[M+H]^+$ calc. for $C_{58}H_{59}O_4P_2S_4Pd_2^+$ 1223.0864; found 1223.0835.

Elemental Analysis calc. for $C_{58}H_{58}O_4P_2S_4Pd_2$: C 57.00; H 4.78%; found: C 56.94; H 4.34%.

IR (cm^{-1}): $\tilde{\nu}$ = 3059(w), 3021(w), 2992(w), 2930(w), 2895(w), 2831(w), 1599(w), 1582(w), 1546(w), 1493(s), 1485(s), 1474(vs), 1464(s), 1450(vs), 1429(vs), 1403(m), 1341(m), 1341(m) 1329(w), 1238(vs), 1202(vs), 1174(s), 1159(s), 1103(m), 1071(m), 1035(vs), 1015(s), 917(w), 862(s), 842(vs), 775(vs), 766(s), 741(m), 719(m), 694(vs), 681(vs), 641(m), 619(w), 586(w), 569(w), 561(w), 556(w), 532(w), 514(w), 473(s), 462(s), 451(m), 440(w), 431(w), 412(w).

2.4.9 Preparation of [(dmobdt)Pd(PCy_3)]$_2$, (8).

Protocol #1: Pd_2dba_3 (0.100 g, 0.109 mmol), PCy_3 (0.061 g, 0.218 mmol) and tetrathiocin **1** (0.044 g, 0.109 mmol) were placed in an oven dried microwave vial under an inert nitrogen atmosphere. Dry toluene (5 mL) was added to the vial and the suspension was placed in the microwave for 20 minutes at 150 °C. The resultant dark green solution was isolated from a small amount of black solid by filtration. The solvent was evaporated by rotary evaporation and dissolved in a small amount of $CHCl_3$, and was then purified by preparative TLC (7:3 mixture of CH_2Cl_2 and hexane). The

green band (R_f = 0.75) was removed from the silica plate and extracted into $CHCl_3$. The solution was concentrated by evaporation of solvent and was further purified by preparative TLC (eluted in toluene), and the green band (R_f = 0.26) was removed from the silica plate and extracted into CH_2Cl_2. Evaporation of the solvent resulted in a green solid (0.014 g, 11% yield), which was recrystallized from slow diffusion of Et_2O into a saturated CH_2Cl_2 solution to produce green crystals suitable for X-ray diffraction. The crystals were washed with hexane and dried in air.

Protocol #2: In otherwise similar conditions as above, but using 0.122 g (0.436 mmol) of PCy_3, the solvent was evaporated and dissolved in a small amount of $CHCl_3$, and was then purified by preparative TLC (7:3 mixture of CH_2Cl_2 and hexane). The green band (R_f = 0.40) was removed from the silica plate and extracted into CH_2Cl_2 and then in acetone (collected separately). The solvent from both washings was evaporated and dissolved in a small amount of $CHCl_3$, then further purified by preparative TLC (CH_2Cl_2 washings eluted in toluene, acetone washings eluted in 7:3 mixture of CH_2Cl_2 and hexane). The green bands (R_f = 0.35 for CH_2Cl_2 washings and R_f = 0.32 for acetone washings) were extracted from the silica plates in CH_2Cl_2. Evaporation of the solvent resulted in a green solid (0.028 g, 22% yield), which was recrystallized from slow diffusion of Et_2O into a saturated CH_2Cl_2 solution to produce green crystals suitable for X-ray diffraction.

NMR (ppm) ($CDCl_3$)**: δ_H** (300 MHz) = 6.91 (2H, s, benzo C–H), 6.75 (2H, s, benzo C–H), 3.82 (6H, s, O–CH_3), 3.81 (6H, s, O–CH_3), 2.05 (12H, m, PCy_3), 1.79 (12H, s, PCy_3), 1.65 (18H, m, PCy_3), 1.57 (6H, s, PCy_3), 1.25 (18H, s, PCy_3); **$\delta_P\{^1H\}$** (121 MHz) = 40.92.

HRMS (ASAP) *m/z*: $[M+H]^+$ calc. for $C_{52}H_{83}O_4P_2S_4Pd_2^+$ 1175.2739; found 1175.2733.

Elemental Analysis calc. for $C_{52}H_{82}O_4P_2S_4Pd_2 \cdot CH_2Cl_2$: C 53.19; H 7.04%; found: C 52.88; H 6.54%.

IR (cm^{-1}): $\tilde{\nu}$ = 2986(w), 2929(s), 2917(s), 2842(m), 1583(w), 1553(w), 1498(w), 1482(s), 1464(vs), 1435(vs), 1427(vs), 1339(m), 1326(w), 1298(w), 1232(vs), 1200(vs), 1173(vs), 1153(m), 1125(m), 1107(m), 1074(w), 1047(vs), 1036(vs), 1020(m), 1002(s),

917(m), 888(m), 847(vs), 821(m), 780(vs), 743(s), 709(w), 683(s), 641(w), 573(w), 530(w), 518(s), 488(m), 450(w), 418(w).

2.4.10 Preparation of [Pd(dmobdt)]$_6$, (9).

Pd_2dba_3 (0.100 g, 0.109 mmol) and tetrathiocin **1** (0.044 g, 0.218 mmol) were combined in dry toluene (5 mL) in an oven-dried microwave vial under inert nitrogen atmosphere. The suspension was placed in the microwave for 30 minutes at 150 °C. The resultant brown solution was filtered, and the filtrate evaporated by rotary evaporation and dissolved in a small amount of $CHCl_3$. This solution was purified by preparative TLC (7:3 mixture of CH_2Cl_2 and hexane) and the brown band ($R_f = 0$) removed from the silica plate and dissolved in a CH_2Cl_2 and MeCN mixture, and the solvent evaporated to give a brown solid (0.026 g, 39% yield).

NMR (ppm) ($CDCl_3$)**: δ_H** (300 MHz) = 6.97 (2H, s, benzo C–H), 6.97 (2H, s, benzo C–H), 6.91 (2H, s, benzo C–H), 6.55 (2H, s, benzo C–H), 6.42 (2H, s, benzo C–H), 6.41 (2H, s, benzo C–H), 3.90 (6H, s, O–CH_3), 3.88 (6H, s, O–CH_3), 3.87 (6H, s, O–CH_3), 3.82 (6H, s, O–CH_3), 3.80 (6H, s, O–CH_3), 3.78 (6H, s, O–CH_3).

2.4.11 Preparation of [(dmobdt)Pt(PPh_3)]$_2$ (10) and (dmobdt)Pt(PPh_3)$_2$ (11).

$Pt(PPh_3)_4$ (0.500 g, 0.402 mmol) and tetrathiocin **1** (0.080 g, 0.200 mmol) were combined in an oven dried microwave vial under an inert nitrogen atmosphere. Dry toluene (5 mL) was added to the vial and the suspension was placed in the microwave for 60 minutes at 150 °C. A 0.2 mL sample was removed from the orange solution and evaporated by rotary evaporation to be analyzed by ^{31}P and ^{1}H NMR, and the remaining solution placed in the microwave for an additional 30 minutes. A yellow solid (complex **11**) was filtered from the orange solution, washed with hexane, and dried in air (0.095 g, 26 % yield). The orange filtrate was evaporated by rotary evaporation to be analyzed by ^{31}P and ^{1}H NMR (was a mixture of complex **10** and **11**). Yield of **11** was improved using 0.400 g $Pt(PPh_3)_4$, 0.064 g tetrathiocin **1**, and 4 mL dry toluene, with **11** precipitating after 60 minutes (0.174 g, 59% yield).

Complex 10:

NMR (ppm) ($CDCl_3$)**:** δ_H (300 MHz) = 6.12 (2H, s, benzo C–H), 5.87 (2H, s, benzo C–H), 3.55 (6H, s, O–CH_3), 2.81 (6H, s, O–CH_3); $\delta_P\{^1H\}$ (121 MHz) = 21.78.

Complex 11:

NMR (ppm) ($CDCl_3$)**:** δ_H (300 MHz) = 6.80 (2H, s, benzo C–H), 3.72 (6H, s, CH_3); $\delta_P\{^1H\}$ (121 MHz) = 19.69 ($^1J_{Pt-P}$ = 1441 Hz).

2.4.12 Preparation of $Pt_{1.9}dba_3{\cdot}CH_2Cl_2$. [27a]

Sodium acetate (2.8 g, 34.1 mmol), dibenzylideneacetone (3.1 g, 13.2 mmol), and Bu_4NCl (1.6 g, 13.2 mmol) were combined in a two-necked round bottom flask, and dissolved by refluxing in MeOH (160 mL) open to air. Finely ground K_2PtCl_4 (0.79 g, 1.9 mmol) dissolved in 10 mL hot H_2O was slowly added to the solution. The mixture was stirred at 80 °C for 2 hours, then was concentrated to approx. 50 mL by cannula filtration. A brown solid was filtered out of the solution and was washed with H_2O (2 × 25 mL) and MeOH (2 × 25 mL), then washed into a new beaker through dissolving in 150 mL hot THF. The dark purple solution was concentrated to approx. 10 mL by rotary evaporation. MeOH (approx. 20 mL) was layered slowly, and the solution was cooled in the fridge for 1.5 hours. A dark brown solid was filtered and washed with MeOH, then recrystallized by layering MeOH onto a saturated CH_2Cl_2 solution, followed by slow evaporation (0.400 mg, 35% yield by Pt).

Elemental Analysis calc. for $C_{52}H_{44}Cl_2O_3Pt_{1.9}$: C 53.91; H 3.83%; found: C 53.91; H 3.82%.

2.4.13 Preparation of $[Pt(dmobdt)]_6$ (12) and $[(dmobdt)Pt(PH^tBu_2)]_2$ (13).

$Pt_{1.9}dba_3{\cdot}CH_2Cl_2$ (0.132 g, 0.114 mmol), P^tBu_3 (0.044 g, 0.218 mmol), and tetrathiocin **1** (0.044 g, 0.109 mmol) were combined in an oven-dried microwave vial under intert nitrogen atmosphere. Dry toluene (5 mL) was added and the vial was placed in the microwave for 1.5 hours at 150 °C. The resultant brown solution was filtered from a small amount of insoluble black solid, and the filtrate evaporated by rotary evaporation. The brown solid obtained by evaporation was dissolved in a small amount of $CHCl_3$ and

purified by prep TLC (eluted in a 7:3 mixture of CH_2Cl_2 and hexane). A yellow band (R_f = 0.46) and an orange band (R_f = 0.07) were extracted into CH_2Cl_2 then evaporated to yield a yellow-orange solid (complex **12**) (0.0037 g, 4% yield) from the yellow band and an orange solid (mixture of complex **13** and another product) (0.0258 g) from the orange band. Orange crystals suitable for X-ray diffraction of these complexes could be obtained by layering diisopropyl ether onto a saturated CH_2Cl_2 solution of **12** or through the slow diffusion of Et_2O into a saturated solution of **13** (yield of **13**: 0.0069 g, 6% yield by Pt).

Complex 12:

NMR (ppm) ($CDCl_3$)**: δ_H** (300 MHz) = 7.07 (2H, s, benzo C–H), 7.05 (2H, s, benzo C–H), 6.95 (2H, s, benzo C–H), 6.69 (2H, s, benzo C–H), 6.52 (2H, s, benzo C–H), 6.47 (2H, s, benzo C–H), 3.93 (6H, s, O–CH_3), 3.90 (6H, s, O–CH_3), 3.89 (6H, s, O–CH_3), 3.84 (6H, s, O–CH_3), 3.81 (6H, s, O–CH_3), 3.78 (6H, s, O–CH_3).

Complex 13:

NMR (ppm) ($CDCl_3$)**: δ_H** (300 MHz) = 6.99 (2H, s, benzo C–H), 6.96 (2H, s, benzo C–H), 4.03 (2H, 4.63–3.43, d, P–H, $^1J_{PH}$ = 359 Hz), 3.87 (6H, s, O–CH_3), 3.85 (6H, s, O–CH_3), 1.57 (18H, 1.58–1.55, d, ^{t}Bu–CH_3, ^2J = 9.3 Hz), 1.07 (18H, 1.09–1.04, d, ^{t}Bu–CH_3, ^2J = 15 Hz); **$\delta_P\{^1H\}$** (121 MHz) = 52.83 ($^1J_{Pt\text{-}P}$ = 1735 Hz).

2.5. References

1. *Dithiolene chemistry: Synthesis, properties, and applications*, ed. E. I. Stiefel, Interscience: Hoboken, New Jersey, 2003.

2. **(a)** E. Cerrada, A. Moreno and M. Laguna, *Dalton Trans.*, 2009, 6825–6835; **(b)** T. R. Miller and I. G. Dance, *J. Am. Chem. Soc.*, 1973, **95**, 6970–6979.

3. J. D. Wrixon, Z. S. Ahmed, M. U. Anwar, Y. Beldjoudi, N. Hamidouche, J. J. Hayward and J. M. Rawson, *Polyhedron*, 2016, **108**, 115–121.

4. J. D. Wrixon, *Reactivity of 1,2,5,6-Tetrathiocines*, University of Windsor, 2015.

5. K. W. Stender, N. Wolki and G. Klar, *Phos, Sulf., Sil and Rel. Elts*, 1989, **42**, 111–114.

6. J. D. Wrixon, J. J. Hayward, O. Raza and J.M. Rawson, *Dalton Trans.*, 2014, **43**, 2134–2139.

7. **(a)** J. R. Nicholson, G. Christou, J. C. Huffman and K. Folting, *Polyhedron*, 1987, **6**, 863–870; **(b)** F. Pop, D. G. Branzea, T. Cauchy and N. Avarvari, *C. R. Chimie*, 2012, **15**, 904–910; **(c)** Z. Biao, O. Satomi, L. Q. Zhi, K. Hidetaka, N. Eiji and K. Akiko, *Chem. Lett.*, 2016, **45**, 303–305; **(d)** M. Bousseau, L. Valade, J. P. Legros, P. Cassoux, M. Carbauskas and L. V. Interrante, *J. Am. Chem. Soc.*, 1986, **108**, 1908–1916; **(e)** K. W. Browall, T. Bursh, L. V. Interrante and J. S. Kasper, Inorg. Chem., 1972, **11**, 1800–1806; **(f)** D. Simao, H. Alves, D. Belo, S. Rabac, E. B. Lopes, I. C. Santos, V. Gama, M. T. Duarte, R. T. Henriques, H. Novais and M. Almeida, *Eur. J. Inorg. Chem.*, 2001, 3119–3126; **(g)** N. Kobayashi, T. Naito and T. Inabe, *Mol. Cryst. Liq. Cryst.*, 2002, **376**, 233–238; **(h)** X. X. Chen, F. Qiao, C. F. Wang, Y. H. Chi, E. Cottrill, N. Pan, J. M. Shi, W. W. Zhu-Ge, Y. X. Fu, J. Xu and X. P. Qian, *J. Molecular Structure*, 2016, **1107**, 157–161.

8. J. R. Nicholson, G. Christou, J. C. Huffman and K. Folting, *Polyhedron*, 1987, **6**, 863–870.

9. M. Cha, J. Sletten, S. Critchlow and J. A. Kovacs, *Inorg. Chim. Acta*, 1997, **263**, 153–159.

10. E. Cerrada, A. Moreno and M. Laguna, *Dalton Trans.*, 2009, 6825–6835.

11. T. Sheng, W. Zhang, X. Gao and P. Lin, *Chem. Commun.*, 1998, 263–264.

12. D. Shimizu, N. Takeda and N. Tokitoh, *Chem. Commun.*, 2006, 177–179.

13. A. I. S. Neves, I. C. Santos, L. C. J. Pereira, C. Rovira, E. Ruiz, D. Belo and M. Almeida, *Eur. J. Inorg. Chem.*, 2011, 4807–4815.

14. C. L. Beswick, R. Terroba, M. A. Greaney and E. I. Stiefel, *J. Am. Chem. Soc.*, 2002, **124**, 9664–9665.

15. J. D. Wrixon, J.J. Hayward and J.M. Rawson, *Inorg. Chem.*, 2015, **54**, 9384–9386.

16. J. Moscattini, A. J. Lough and U. Fekl, *Acta Cryst.*, 2017, **E73**, 957–962.

17. N. Fey, A. G. Orpen and J. N. Harvey, *Coord. Chem. Rev.*, 2009, **253**, 704–722.

18. **(a)** R. G. Pearson, *J. Chem. Ed.*, 1968, **45**, 581–587; **(b)** R. G. Pearson, *J. Chem. Ed.*, 1968, **45**, 643–648.

19. C. A. Tolman, *Chem. Rev.*, 1977, **77**, 313–348.

20. S. J. Lippard and J. J Mayerle, *Inorg. Chem.*, 1972, **11**, 753–759.

21. A. Alberola, D. Eisler, R. J. Less, E. Navarro-Moratalla and J. M. Rawson, *Chem. Commun.*, 2010, **46**, 6114–6116.

22. **(a)** C. Vinas, W. M. Butler, F. Teixidor and R. W. Rudolph, *Inorg. Chem.*, 1986, **25**, 4369–4374; **(b)** X. F. Hou, S. Liu, P. C. Zhang and G. X. Jin, J. Organomet. Chem., 2007, 692, 1766–1770; **(c)** K. Zong, W. Chen, M. P. Cava and R. D. Rogers, *J. Org. Chem.*, 1996, **61**, 8117–8124; **(d)** X. Yang, T. B. Rauchfuss and Scott Wilson, *J. Chem. Soc., Chem. Commun.*, 1990, 34–36; **(e)** M. C. Aragoni, M. Arca, F. A. Devillanova, F. Isaia, V. Lippolis, A. Mancini, L. Pala, A. M. Z. Slawin and J. D. Woollins, *Chem. Commun.*, 2003, 2226–2227.

23. F. H. Allen, O. Kennard and D. G. Watson, *J. Chem. Soc. Perkin Trans. II*, 1987, S1–S19.

24. **(a)** J. A. Bilbrey, A. H. Kazez, J. Locklin and W. D. Allen, *J. Comput. Chem*., 2013, **34,** 1189–1197; **(b)** A. Muller and R. Meijboom., *Acta Cryst*, 2010, **E66**, m1463.

25. **(a)** R. Bosque and J. Sales, *J. Chem. Inf. Comput. Sci*., 2001, **41**, 225–232; **(b)** T. T. Derencsenyi, *Inorg. Chem.*, 1981, **20**, 665–670.

26. *Chemical Kinetics and Inorganic Reaction Mechanisms*, 2nd ed., S. Asperger, Springer Science and Business Media: New York, 2003.

27. **(a)** L. N. Lewis, T. A. Krafft and J. C. Huffman, *Inorg. Chem.*, 1992, **31**, 3555–3557; **(b)** K. Moseley and P. M. Maitlis, *J. Chem. Soc. D*, 1971, 982–983; **(c)** P. D. Harvey, F. Adar and H. B. Gray, *J. Am. Chem. Soc.*, 1989, **111**, 1312–1315; **(d)** H. Tanaka and H. Kawazura, *Bull. Chem. Soc. Jpn.*, 1979, **52**, 2815–2818.

28. R. D. Adams, B. Captain and P. J. Pellechia, *Organometallics*, 2007, **26**, 6564–6575.

29. APEX-II, Bruker AXS Inc., Madison, Wisconsin, USA.

30. Sadabs, Bruker AXS Inc., Madison, Wisconsin, USA.

31. SHELXTL package for crystal structure solution and refinement, Bruker AXS Inc., Madison, Wisconsin, USA.

32. Y. Ishii, *Ann. N.Y. Acad. Sci.*, 1974, **239**, 114–128.

CHAPTER 3. Towards the rational design of hetero-multimetallic dithiolene complexes: Synthesis and reactivity of cobalt dithiolates

3.1. Introduction

Previous work in the Rawson group on the oxidative addition chemistry of tetrathiocins has focused exclusively on their reactivity towards the group 10 metals, Ni, Pd and Pt, with either phosphine co-ligands (see Chapters 1 and 2) or, in the case of nickel, N,N′-chelate ligands such as bipyridine and its derivatives. In this Chapter, the reactivity is extended towards the synthesis of the group 9 metal, cobalt.

3.1.1 Cobalt Dithiolene Complexes

Compared to the group 10 dithiolenes, group 9 complexes comprise a much smaller number of reported structures. Of the 125 cobalt dithiolene complexes reported in the CSD, 81 are mononuclear, with 70% of them containing one dithiolene ligand and a non-dithiolene co-ligand. Over half of the bis(dithiolene) cobalt complexes are dimeric, with the metal centre adopting a pentacoordinate square pyramidal geometry. One example of a tris(dithiolene) complex of octahedral geometry has been reported.[1] Amongst these 125 cobalt dithiolene complexes, almost 50% (60 structures) comprise benzo-fused cobalt dithiolene complexes, half of which are unsubstituted benzenedithiolates.

Over 90% of the tricoordinate cobalt dithiolene complexes reported in the CSD contain a cyclopentadienyl (Cp) ligand. Due to their strong electron donor ability, Cp ligands afford dithiolene complexes with a rich redox and chemical reactivity.[1] Dithiolenes containing Cp ligands have been used in ligand-transfer reactions, and in the synthesis of 1,2-dithietes (and even 1,2,5,6-tetrathiocins) through oxidation by sulfuryl chloride.

The variation in metal binding is reflected in a series of three coordinate metal complexes, CpCo(dithiolene). King[2] employed oxidative addition of the dithiete bis(trifluoromethyl)dithietene to $CpCo(CO)_2$ in refluxing methylcyclohexane to produce the cobalt dithiolene complex CpCo(tfd) containing a Cp co-ligand which had a

tricoordinate metal centre. This monomeric complex was diamagnetic according to ^{19}F NMR and had a weak band at 1480 cm^{-1} in the IR spectrum which could be attributed to a delocalized C=C bond, and it was proposed that the complex adopted a dithiolate structure with the C=C bond of the dithiolene π-bonded to the metal centre. Subsequent structural studies by Baird and White[3] on the same complex led to a different conclusion. Their analysis of the C-S and C-C bond distances obtained from X-ray diffraction led them to conclude that this complex adopted a Co(I) dithioketone, rather than Co(III) dithiolate structure (**Scheme 3.1**).

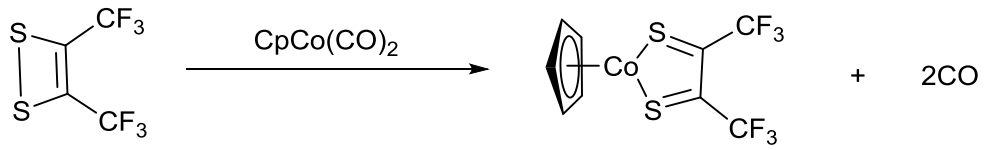

Scheme 3.1 Synthesis of a cobalt dithiolene complex from oxidative addition of the dithiete $S_2C_2(CF_3)_2$.

Conversely, Miller and coworkers[4] synthesized a cobalt dithiolate, CpCo(bdt) which could be recrystallized from evaporation of a 1:1 hexane and CH_2Cl_2 solution. In the monomer, the CoS_2C_2 ring is nearly planar and lies perpendicular to the Cp ring, and according to C-S bond distances obtained from X-ray diffraction, the complex takes on a Co(III) dithiolate, rather than Co(I) dithioketone, structure with single bond C-S lengths of 1.729(7) – 1.748(6) Å.

This compound exhibited an unusual solid state reactivity;[4] when these crystals sat at room temperature for a few weeks, dimerization was observed. This dimer could be converted back to the monomer either by heating at 150 °C or by dissolving in a non-coordinating organic solvent. Rate of evaporation also played a role, wherein slow evaporation over a period of 24 hours of a CH_2Cl_2 solution of either the monomer or dimer yields crystals of the dimer, while more rapid evaporation (such as rotary evaporation) affords crystals of the monomer. It was found that other factors could lead to inter-conversion as well: sublimation of the monomer or the dimer both gave crystals of the monomer which would be very slow to dimerize.

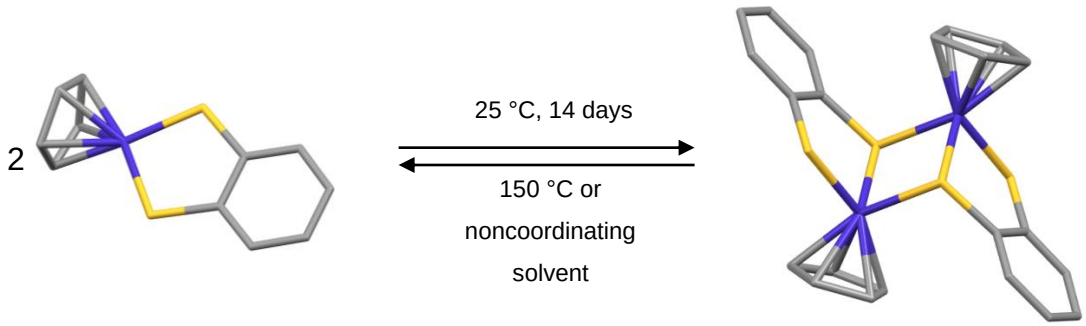

Scheme 3.2 Reaction equilibrium between the monomer CoCp(bdt) and the dimer $[CoCp(bdt)]_2$.

Upon dimerization, one of the sulfur atoms of the dithiolene becomes μ_2-bridging between the cobalt centres, and changes in the structure occurs, with the ring no longer planar (with an angle of 20.9° between the S_2C_2 and CoS_2 planes), and an additional tilting of around 45° for the Cp. The geometry goes from a two-legged piano stool in the monomer to three-legged in the dimer, and all Co-S bonds are lengthened upon dimerization. The S-C bond lengths remained similar in the monomer and dimer.

3.1.2 Crown Ethers

Charles Pedersen was awarded the 1987 Nobel Prize in Chemistry based on his discovery of crown ethers in the 1960s and his work on this class of compounds over the next two decades.[5] While studying the effects of multidentate phenol-based ligands on the catalytic properties of VO, he obtained a small amount of white crystals which were insoluble in hydroxylic solvents. Elemental analysis and molecular weight measurements revealed that these crystals were the 18-membered ring dibenzo-18-crown-6 shown in **Figure 3.1a**, the first crown ether to be discovered. The name "crown ether" was used due to the crown-like structure of the polyether ring in molecular models, and a naming system was created for this class of compounds, based on the substituents attached to the ring, the number of oxygen atoms in the ring, and the size of the ring (**Figure 3.1b**). This discovery revealed a method to produce large rings in moderate yields (approx. 45%) in a single reaction; in most organic reactions, only 5, 6, or 7-membered rings are easily formed. The crown ethers are neutral, white compounds which are sparingly soluble in water and alcohols, moderately soluble in aromatic solvents, and very soluble in

chloroform. Since Pedersen's initial discovery, thousands of structures belonging to this class of compounds have been reported.[6]

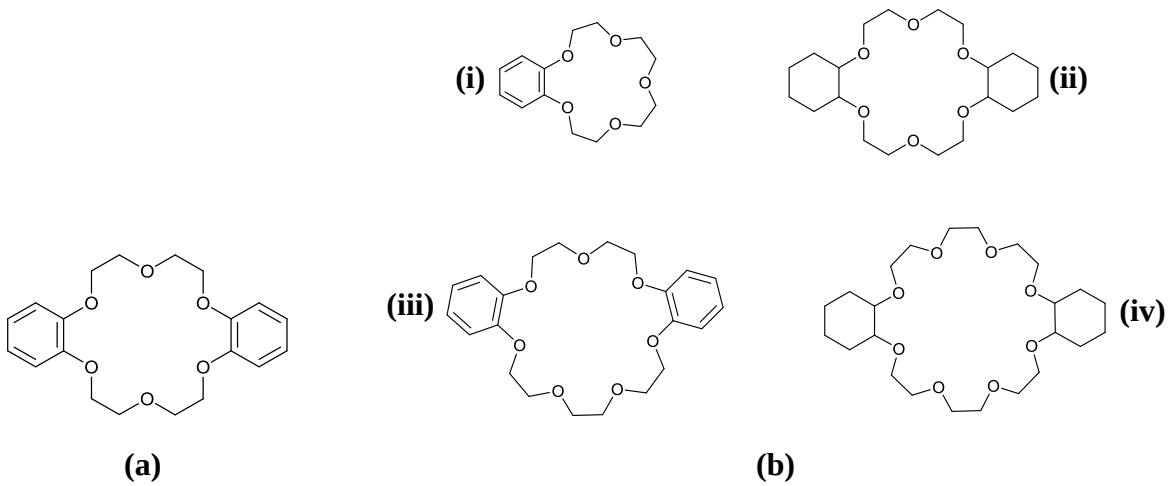

Figure 3.1 (a) The first crown ether discovered by Pedersen[5] and **(b)** some examples of crown ethers: (i) benzo-15-crown-5, (ii) perhydrodibenzo-18-crown-6, (iii) dibenzo-21-crown-7, and (iv) perhydrodibenzo-24-crown-8.

The crown ether crystals were sparingly soluble in methanol, but their solubility greatly increased with the addition of sodium salts to the solution with the sodium ion located in the center of the crown, forming electrostatic $Na^{+}\cdots O^{\delta-}$ interactions. This could be extended to allow other metals, such as other alkali and alkaline earth ions and ammonium ion, into the crown cavity, and therefore led to the first discovery of a neutral compound forming stable complexes with alkali ions. It was proposed that the presence of these alkalis could help in the synthesis of these crown ethers, wherein the oxygen atoms wrap around the cation to form a three-quarter circle, then dispose of the cation in the ring-closing step, in a mechanism similar to porphyrin formation.[5]

The discovery of crown ethers meant the development of a new method to trap alkali cations. These cations are hard acids according to Pearson's hard and soft acid base theory,[7] so they less readily form complexes with many of the ligands used for the transition metals. Pedersen synthesized around 60 crown ethers and their analogues, ranging in size from 12-membered to 60-membered rings, with between 4 and 10 oxygen atoms, and some containing nitrogen or sulfur donors.[5] He found that the best cation complexing agents were compounds that contained 15- or 24-membered rings with 5 to

10 oxygen atoms, each oxygen atom separated from the next by an ethane bridge. The stability of these complexes depended on both the size of the cation and the ring size, such that each metal cation has an optimal crown with which it will form its most stable complex (**Table 3.1)**. For example, for sodium the optimal sizes are 15 to 18-membered rings, 18 for potassium, and 18 to 21 for cesium. Crown ethers may form complexes with cations of other sizes, giving sandwich-type structures with bigger cations (crown to cation ratio is 2:1) or fitting multiple ions into the cavity with smaller cations (crown to cation ratio is 1:2). Complexes with crown to cation ratios of 3:2 have also been prepared. Crown ethers have been used as cationic complexing agents by Visser and coworkers, where 18-crown-6 and other crowns were used to extract sodium, cesium, and strontium cations from aqueous solutions.[8]

Table 3.1 Ratio of crown to cation for 15-crown-5 and 18-crown-6, with approximate size of the crowns and cations specified. *Table reproduced from data found in references 5 and 6.*

Ion	**Ionic Radius (**Å)	**15-crown-5** (1.7 – 2.2 Å)	**18-crown-6** (2.6 – 3.2 Å)
Li^+	1.36	-	-
Na^+	1.94	1:1	-
K^+	2.66	2:1	1:1
Rb^+	2.94	2:1	1:1 or 2:1
Cs^+	3.34	-	2:1 or 3:2

Crown ethers have been used in the development of sensors. Pedersen found that crowns containing benzo groups will have a maximum absorption at 275 mμ in methanol, and that by adding salts to the crown pocket, the shape of the absorption curve will change.[5] Crown ether based dyes, which are insoluble in aqueous solution, have been used to detect the presence of cations at organic/aqueous interfaces.[6] The crown extracts ions at this interface, leading to a colour change which can be monitored by spectrophotometry. An example of one of these dyes is shown in **Figure 3.2**, which undergoes a colour change from orange to red when it binds K^+ or Rb^+ in a sandwich-type structure. Dyes prepared by Kaneda *et al.*[9] selectively detected the presence of Li^+ down to 25–250 ppb, giving a change in colour from purple to red. Crowns have also been used for

fluorescence sensing. Bourson and coworkers[10] observed that the emission spectra of fluoroionophores made from the laser dye coumarin 153 bound to crown ethers was red shifted upon cation binding, with the extent of the shift reflecting the charge density, and therefore identity, of the cation.

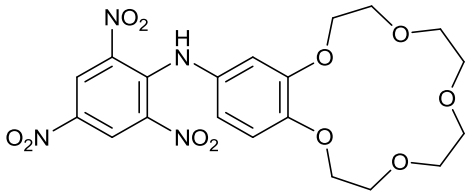

Figure 3.2 An example of a crown ether used as a dye reported by Gokel.[6]

Pilkington and coworkers[11] reported the synthesis of a crown ether complex containing the large oxophilic lanthanide Dy^{3+} ion. The complex exhibits a pseudo-sandwich structure, with the Dy^{3+} cation bound to one crown and four H_2O molecules, three of which are hydrogen bonded to a second crown (**Figure 3.3a**), reflecting both the large size of the Dy^{3+} cation which cannot be accommodated within the cavity of the crown and competition between water and the O-donor crown as coordinating ligands. The related benzo-15-crown-5 complex[12] consists of a $[Dy(H_2O)_8]^{3+}$ hydrogen bonded to three benzo-15-crown-5 ethers, forming a supramolecular capsule (**Figure 3.3b**). Both compounds were found to exhibit single molecule magnetic (SMM) behaviour as well as luminescence. Ding and coworkers also studied a series of crown ethers of various sizes with Dy^{3+} for their possible SMM properties.[13] The sandwich-type structure of these complexes, with the macrocyclic crown ethers above and below the metal centres, are useful for SMMs as they may enhance the anisotropy of the system, helping to slow down magnetic relaxation.

Crown ethers have also found use in photochemical[14] and electrochemical[15] switching, molecular mouse traps,[16] and in biological applications such as modeling ion channels in cell membranes,[17] enhancing enzyme activity,[18] DNA binding[19] and intercalation,[20] and as antimicrobial agents.[21]

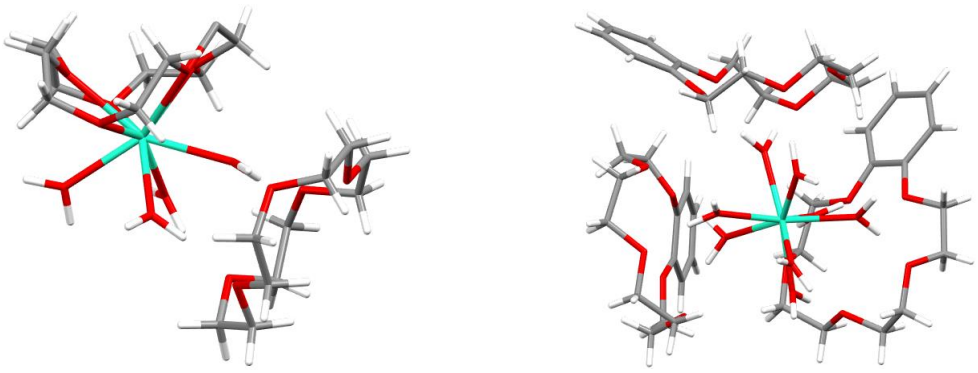

(a) **(b)**

Figure 3.3 Crown ether complexes exhibiting magnetic properties reported by Pilkington and coworkers.[11,12]

3.1.3 Crown Ethers in Metal Dithiolene Complexes

The possibility to create transition metal dithiolene complexes incorporating crown ethers into their structures allows for the creation of multi-functional materials displaying the properties of both dithiolates and crown ethers described in sections **3.1.1** and **3.1.2**. There is only one previous series of studies investigating benzo-fused dithiolene ligands containing crown ether groups. Garner and coworkers reported[22] a series of benzo-fused dithiolene complexes bearing 15-crown-5 and 18-crown-6 side groups (**Figure 3.4**). The dithiol precursors were prepared from benzo-15-crown-5 and benzo-18-crown-6, through a four-step process comprising (i) bromination; (ii) substitution to form the *o*-bis(*n*-butylthioethers); (iii) conversion to the alkali dithiolates and finally; (iv) acidification to form the corresponding dithiols. These dithiols were then reacted with $MoCl_5$ or WCl_6 (to form complexes I, II, and III), reacted with Cp_2TiCl_2 in the presence of triethylamine (generating complexes IV and V). Alternatively, they were converted to alkali metal dithiolates and reacted with either $NiCl_2{\cdot}6H_2O$ (forming complexes VI and VII), (dppe)$NiCl_2$ (complexes VIII and IX), or $CpCo(CO)I_2$ (complexes X and XI). Formation of the final complex therefore required up to five steps with a linear synthetic strategy. Although crystals were grown for the molybdenum and some nickel complexes, no crystal structures were reported; instead, identification of all complexes was based on spectroscopic and electrochemical studies.

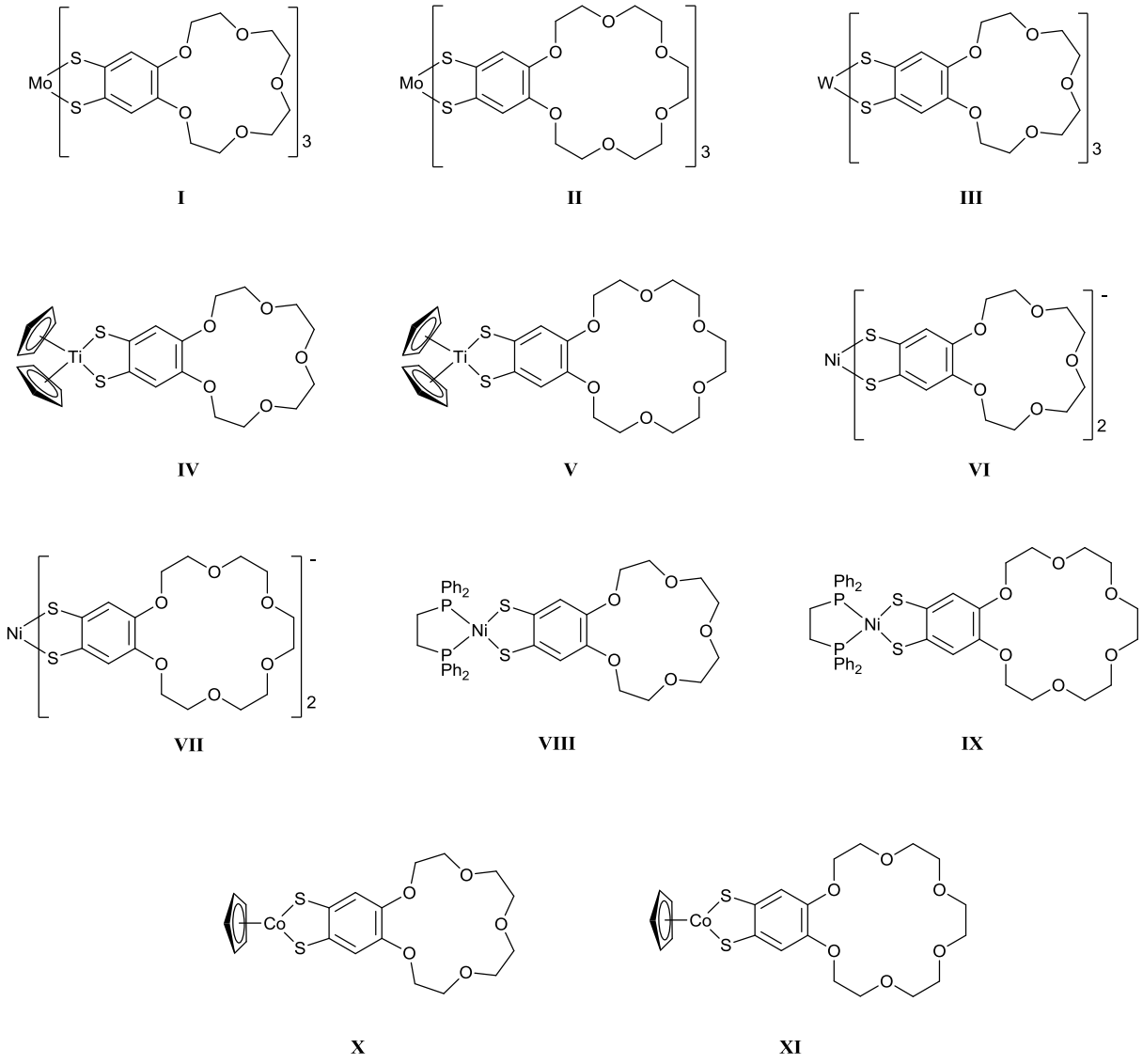

Figure 3.4 The range of transition metal dithiolene complexes produced by Lowe and Garner[22] which incorporated crown ethers into their structures.

Subsequent studies[23] examined the effects of binding alkali cations into the crown pockets of these complexes. Addition of Li^+, Na^+, or K^+ salts to solutions of most of the complexes shown in **Figure 3.4** led to a colour change, which was attributed to cation complexation into the crown pocket. The shift in λ_{max} to higher energy upon complexation of alkali cation (**Table 3.2**) was consistent with a primarily ligand-to-metal charge transfer nature for the UV/vis transitions.

Cyclic voltammetry measurements after adding the alkali salts also showed a positive shift in the redox potential upon complexation (**Table 3.3**). Mass spectrometry measurements of the complexes derived from I, III, and X supported 1:1 cation-binding by the dithiolene complex but no crystal structures were reported.

Table 3.2 Shift in wavelength of maximum absorption in UV/vis upon complexation of alkali metals into some of the crown ether metal dithiolene complexes reported by Lowe and Garner. *Table reproduced from reference 23.*

		Shift in λ_{max} (cm^{-1}) upon complexation		
Complex	**λ_{max} (cm^{-1})**	**$Li[ClO_4]$**	**$Na[ClO_4]$**	**$K[PF_6]$**
I	20800, 12900	580, 430	620, 430	620, 290
IV	21450, 15750	230, 250	190, 200	140, 100
X	15750	440	490	280
XI	15800	180	180	230

Table 3.3 Shift in redox potential (mV) according to cyclic voltammetry upon complexation of alkali metals into some of the crown ether metal dithiolene complexes reported by Lowe and Garner. *Table reproduced from reference 23.*

Complex	**$Li[ClO_4]$**	**$Na[ClO_4]$**	**$K[PF_6]$**
I	+ 40, + 50	+ 30, + 50	-
IV	+ 50	+ 50	+ 10
X	+ 40, + 70	+ 50, + 30	+ 10, + 40
XI	+ 10, + 50	+ 20, + 70	+ 30, + 100

As mentioned in Chapter 2, we were previously able to make a diverse array of functionalized tetrathiocins using the literature method,[24] including the benzo-15-crown-5 derivative (see section **2.1**).[25] It was additionally shown that this tetrathiocin could be used as a precursor to the palladium complexes **14** and **15** (**Figure 3.5**) such that the dithiolate complexes could be conveniently prepared in a simple two-step synthetic procedure (tetrathiocin synthesis followed by oxidative addition). Both **14** and **15** were shown to form crown complexes [**14**·Na][BPh_4] and [**15**·Na][BPh_4] respectively, with a single Na^+ cation bound in the crown pocket.

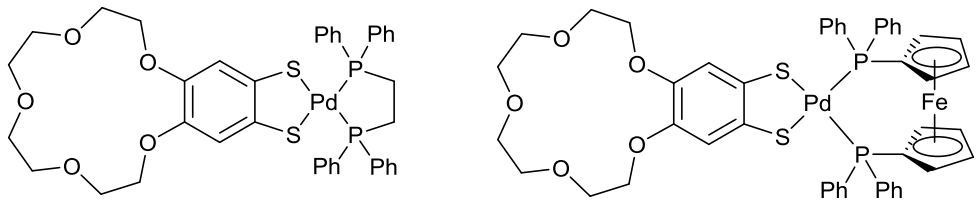

14 15

Figure 3.5 Structures of complexes **14** (left) and **15** (right).

3.1.4 Project Objectives

The goal of this project was to extend the established oxidative addition chemistry of tetrathiocins to group 10 metals to encompass the group 9 metal, cobalt. A first objective was to identify an appropriate low oxidation state cobalt precursor which would facilitate this chemistry, and secondly to extend the reactivity to prepare a cobalt complex bearing a crown ether group, and finally establish its reactivity towards formation of a range of hetero-multi-metallic complexes through binding *s*, *d* or *f*-block metals.

3.2. Results and Discussion

3.2.1 Synthesis of Bis-15-crown-5-dibenzo-1,2,5,6-tetrathiocin (16)

Tetrathiocin **16** was produced by dropwise addition of S_2Cl_2 to benzo-15-crown-5 in 15 mL degassed glacial acetic acid which was stirred for over a week under nitrogen atmosphere, followed by treatment with methanolic tin chloride solution. The yellow solid was obtained in 48% yield, and identity confirmed by ASAP mass spectrometry with a molecular ion peak for $\mathbf{16}^+$ at *m/z* = 661.1269 and satisfactory elemental analysis.

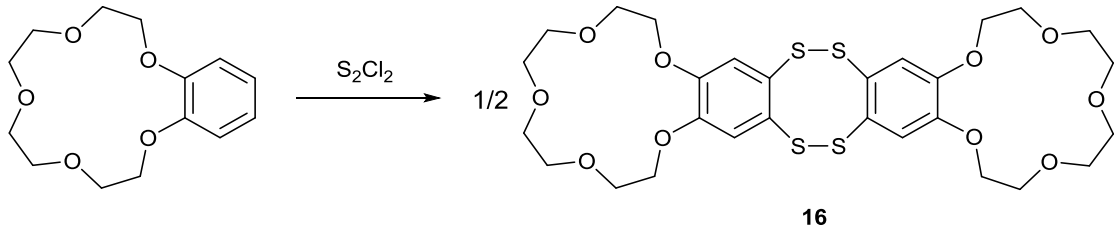

16

Scheme 3.3 Synthesis of tetrathiocin **16**.

3.2.2 Synthesis of [CpCo(dmobdt)]$_2$ (17) and CpCo(b-15-c-5-dt) (18)

The microwave synthesis used for the previous metal dithiolene complexes was employed in these reactions. In contrast to the group 10 metal reactions in which the leaving groups were typically the low volatility ligands COD (Ni), dba (Pd) or PPh_3 (Pt), these studies employed the 18*e*$^-$ cobalt(I) carbonyl complex $CpCo(CO)_2$, in which the leaving group was gaseous CO. The increase in pressure within the sealed microwave reactor was considered but found not to exceed the tolerances of the microwave vials; nevertheless, new microwave vials were used in all experiments to avoid any weaknesses which might be inherent in recycled units. In a typical reaction, 0.5 mmol of tetrathiocin **1** or **16** was combined with 1.0 mmol of $CpCo(CO)_2$ in a new 5 mL microwave vial under inert atmosphere to which 5 mL dry toluene was added. The mixtures were stirred for 30 minutes at 150 °C in the microwave until evolution of CO gas was completed, as shown by a plateau at approximately 6 bar in the pressure reading on the microwave pressure readout.

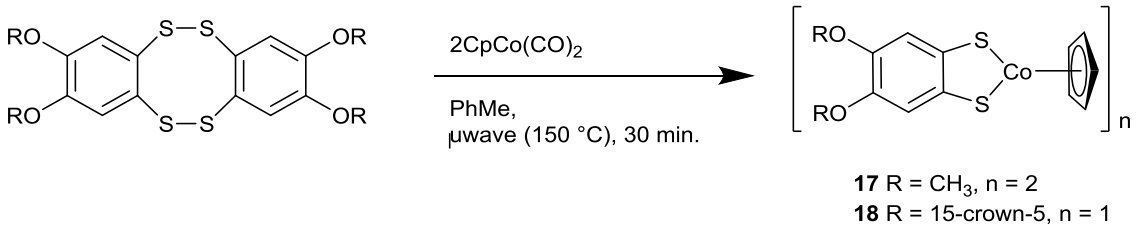

Scheme 3.4 General synthetic procedure for complexes **17** and **18**.

In both cases, a deep blue solution was produced. Microwave caps were removed carefully after slowly releasing pressure through a needle. The solvent was evaporated, the product redissolved in $CHCl_3$, filtered from a small amount of dark grey solid, and the filtrate evaporated. In the case of **17** the sample was washed with Et_2O, filtered, and dried *in vacuo*, whereas for **18** the complex was isolated by addition of hexane to a saturated CH_2Cl_2 solution. Both complexes were collected in good yields (81% for complex **17** and 71% for complex **18**).

^{1}H and ^{13}C NMR studies were conducted for each complex. The product from reaction of the methoxy-functionalized tetrathiocin showed (**Figure 3.6**) a single resonance for the benzo protons at 7.51 ppm and a single resonance for the methoxy protons at 3.85 ppm,

consistent with a symmetric structure in solution [*cf*. two ^{1}H methoxy environments for [(dmobdt)Pd(PPh_3)]$_2$ and six environments for [Pd(dmobdt)]$_6$, (Chapter 2)]. The integral of the dmobdt ligand to the Cp ring protons was consistent with formation of CpCo(dmobdt) (**17**). Complex **18** exhibited a benzo proton peak at 7.47 ppm and peaks for the protons in the crown ether ring in the range 3.74 – 4.05 ppm (**Figure 3.7**). Integration against the Cp ring protons again suggested a composition of CpCo(b-15-c-5-dt).

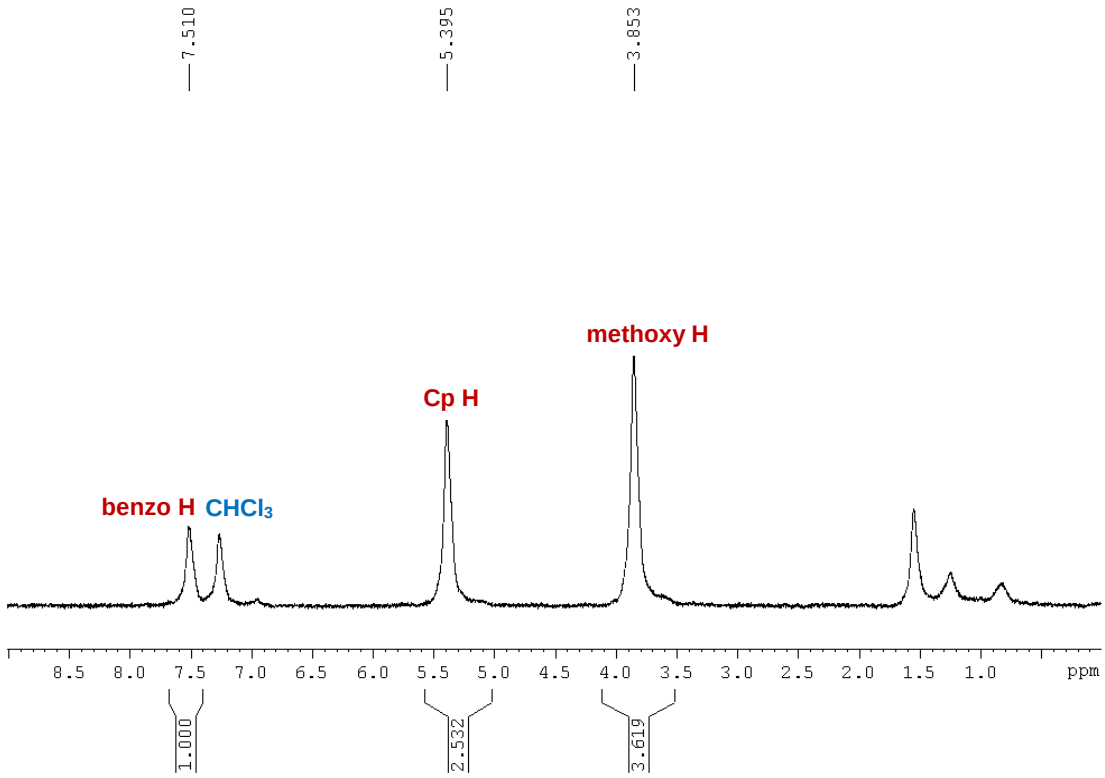

Figure 3.6 ^{1}H NMR spectrum of complex **17**.

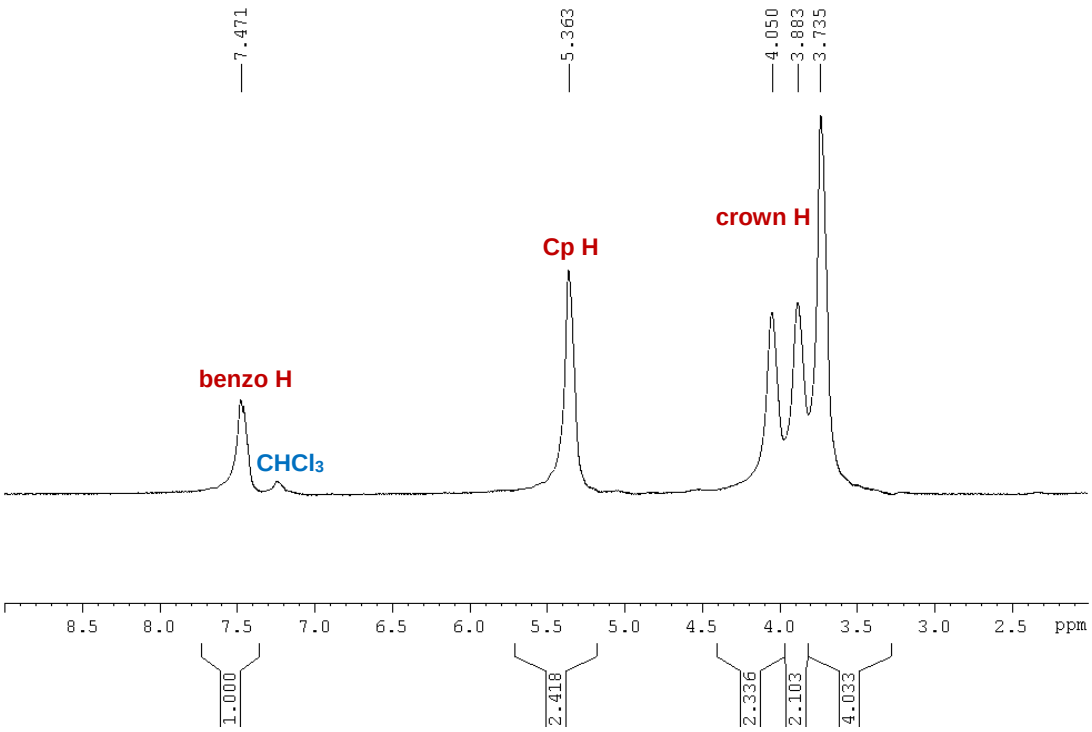

Figure 3.7 ^{1}H NMR spectrum of complex **18**.

3.2.3 Crystal Structures of 17 and 18

Crystals of **17** suitable for X-ray diffraction were obtained by sublimation at temperatures up to 230 °C in dynamic vacuum. Complex **17** crystallizes in the monoclinic $P2_1/n$ space group, with a crystallographic inversion centre. Although **17** appeared monomeric in solution, X-ray crystallography reveals a dimeric structure in which one sulfur of the dithiolene adopts a μ_2-bridging mode to two cobalt centres such that there is one molecule in the unit cell located about an inversion center (half a molecule in the asymmetric unit). These results match the findings of Miller[4] who showed that the dimeric $[CpCo(bdt)]_2$ could be converted to its monomer when dissolved in a non-coordinating solvent. Bond lengths are in the range 2.2309(8) – 2.2672(7) Å for Co-S. The C-S bond length for the bridging sulfur is 0.019 Å longer than that of the non-bridging sulfur, and their values of 1.779(2) Å and 1.760(3) Å are closer to the single bond distance[26] of 1.71 – 1.75 Å than the double bond distance of 1.67 – 1.68 Å, consistent with a dithiolate rather than dithioketone structure. This was supported by the C-C length of 1.384(4) Å on the dithiolene ligand, which matches that of a double bond. All S-Co-S bonds are near 90°, with a three-legged piano stool geometry about the metal

centre. The Co metal is lifted above the plane created by the dithiolene ligand, with an angle of 23.51° between the C_2S_2 and CoS_2 planes. The angle of folding about the bridging sulfur (C-S-Co angle) is 108.54(9)°.

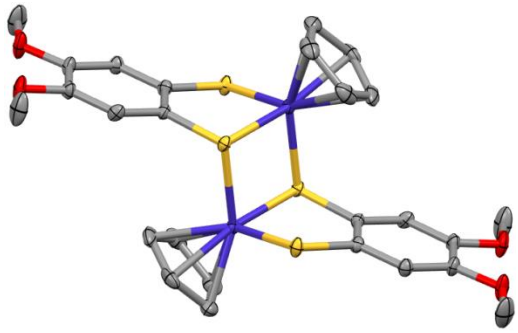

Figure 3.8 Crystal structure of **17** with thermal ellipsoids drawn at the 50% probability level. Hydrogen atoms have been omitted for clarity.

Some crystals of **18** crystallized directly from the reaction mixture; however, better crystals could be obtained by the slow diffusion of pentane into a 1:1 MeOH:CH_2Cl_2 solution (see section **3.2.6**). These dark blue crystals crystallized in the monoclinic space group *C*c. The Co-S bond lengths were in the 2.106(1) – 2.127(1) Å range. The S-C length of 1.728(4) Å and the length of C-C bond for the carbons bound to the sulfur atoms of 1.410(6) Å were consistent with a dithiolate structure. Unlike **17** which dimerizes in the solid state, **18** was found to be monomeric, leading to significantly different aspects to the molecular geometry. The complex adopted a two-legged piano stool geometry, and had a S-Co-S angle of 91.83(5)°. The angle between the C_2S_2 and Co_2S planes was near zero at 0.69°, indicating planarity. The Cp ligand was nearly perpendicular to the C_2S_2 plane, lying at a 89.47° angle.

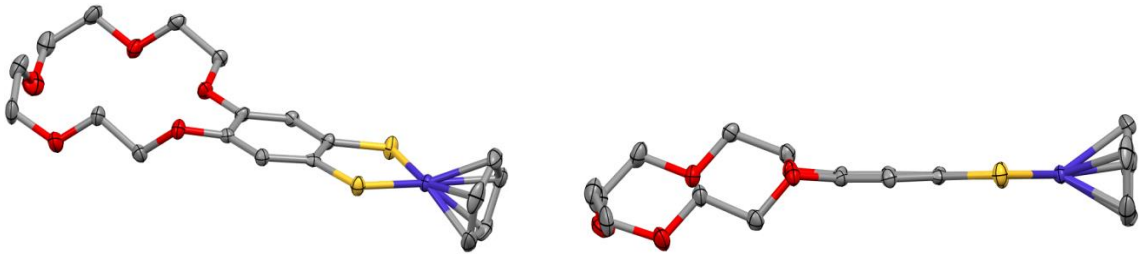

Figure 3.9 Crystal structure of **18** with thermal ellipsoids drawn at the 50% probability level (left) and structure showing planarity at Co (right). Hydrogen atoms have been omitted for clarity.

3.2.4 Complexation of Alkali Metals into Complex 18

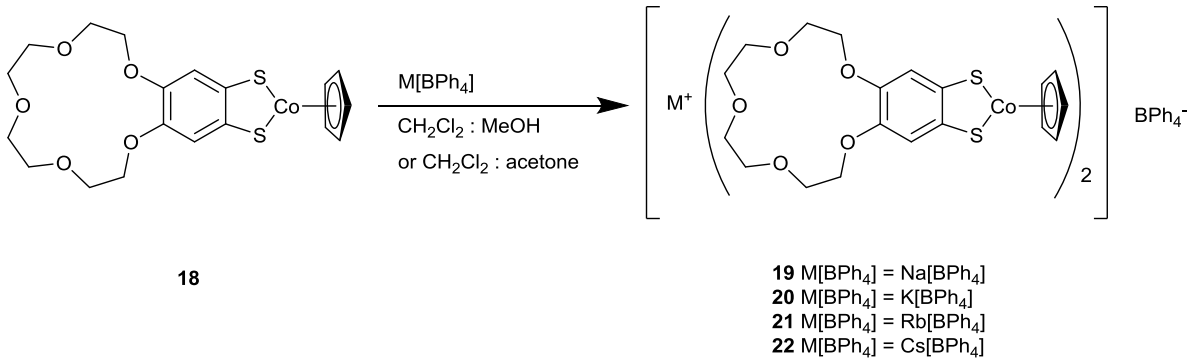

Scheme 3.5 General synthesis of complexes **19** to **22**.

The general procedure for the preparation of complexes **19** – **22** is shown in **Scheme 3.5**. For complexes **19** and **22**, one equivalent of complex **18** and one equivalent of $Na[BPh_4]$ or $Cs[BPh_4]$ were combined in a 1:1 MeOH and CH_2Cl_2 mixture and stirred for one hour under ambient conditions, then layered with hexane to yield dark blue-black crystals in 40% and 18% yield, respectively. Following the same process for $K[BPh_4]$ and $Rb[BPh_4]$ led to an immediate precipitate upon layering with hexane. Instead recrystallization of complexes **20** and **21** was achieved by layering a saturated acetone solution of $K[BPh_4]$ or $Rb[BPh_4]$ onto a saturated CH_2Cl_2 solution of complex **18**, and allowing the two reagents to slowly diffuse for one day. These solutions were then layered with hexane to afford dark blue-black crystals in 40% and 83% yield. The yield could be improved by repeating these procedures with one equivalent of alkali salt and two equivalents of complex **18**.

3.2.5 Crystallographic Studies of Complexes 19 – 22

In all four complexes, the alkali metal was sandwiched between the crown ether rings of two molecules of complex **18**. This 2:1 ratio of complex **18** to alkali metal is in contrast to the 1:1 ratio postulated by Garner[22] based on mass spectrometry measurements. Each alkali metal is bound to the five oxygen atoms on each crown ether ring, making them decacoordinate. Complexes **19** to **22** all crystallize in the monoclinic space group *C*2/*c*. Bond lengths and angles in the cobalt dithiolene complexes remain essentially unchanged

within experimental error upon complexation of alkali metal into the crown pockets; however, the cobalt atom is brought slightly out of plane, sitting between 1.86° and 5.24° above the C_2S_2 plane. The Cp ligands remain roughly perpendicular to the dithiolene planes in most complexes, with a slight shrinking of the angle by up to 8°. However, in **20** there is a larger shrinking of one of the Cp-dithiolene angles by 12°.

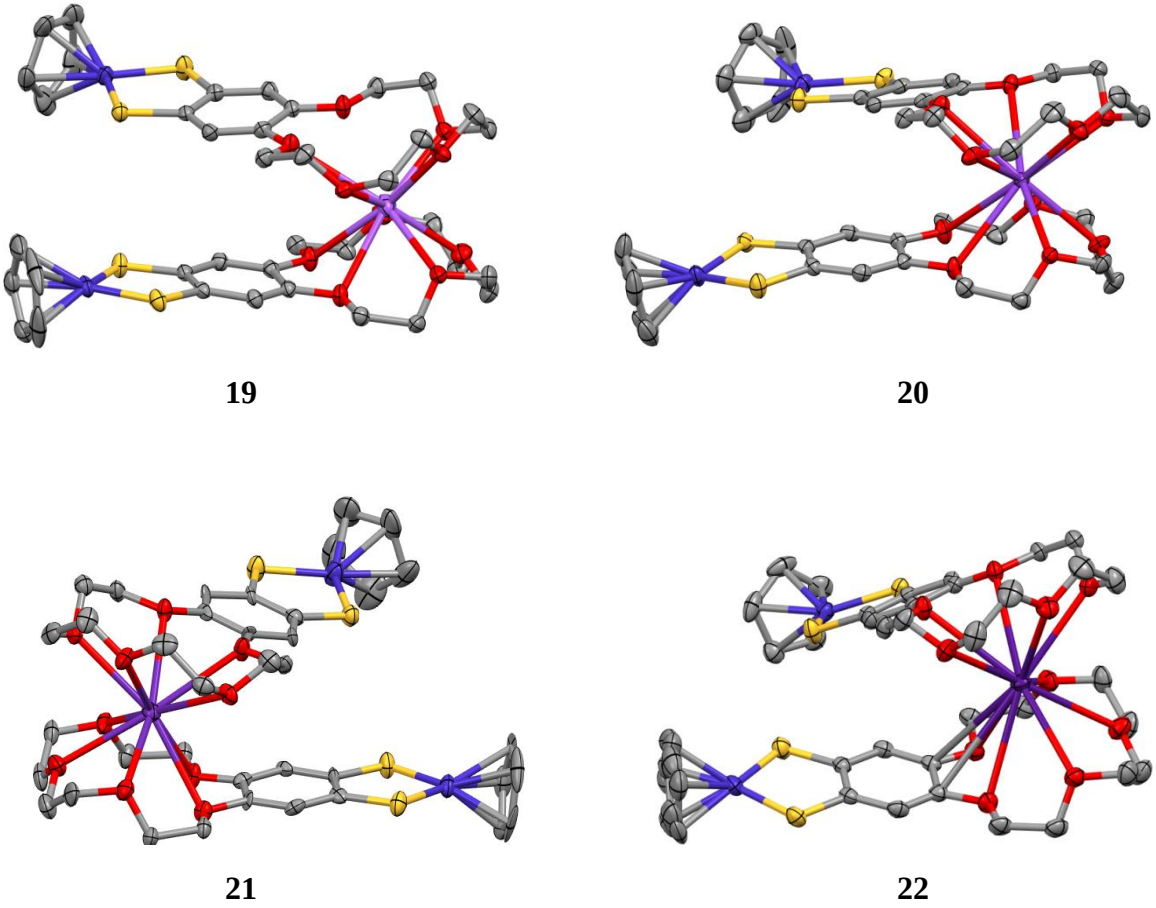

19 **20**

21 **22**

Figure 3.10 Crystal structures of **19** to **22** with thermal ellipsoids drawn at the 50% probability level. Hydrogen atoms, solvent molecules, and BPh_4^- counterions have been omitted for clarity.

As the size of the alkali bound to the crown pocket increases, the sandwich opens up to accommodate the larger size of the metal. This leads to an increase in the angle between the planes defined by the benzene rings of the two dithiolenes, θ, increasing from 10.54° in **19** to 13.67° in **20** to 15.17° in **21** to 36.97° in **22** (**Figure 3.11a**). In all cases, the two dithiolenes above and below the alkali metal are offset from one another, and the angle of offset, Φ, stays roughly constant, with only a very slight increase by less than 2° with

increased alkali size (**Figure 3.11b**). These values for the four complexes are summarized in **Table 3.4**.

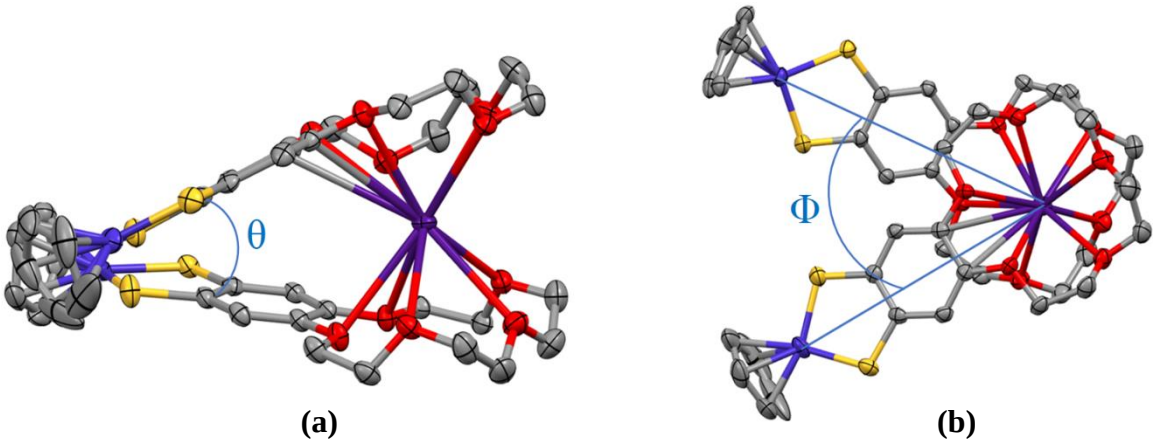

(a) **(b)**

Figure 3.11 Crystal structure of complex **22** showing the **(a)** angle of opening in the sandwich (θ) and **(b)** angle of offset of the dithiolene complexes (Φ).

Table 3.4 Values of θ, Φ, and C_2S_2-CoS_2 angles for complexes **19** to **22** (°). C_2S_2-CoS_2 angle is the angle between the C_2S_2 and CoS_2 planes and indicates deviation from planarity at Co.

Complex	Angle of opening of the sandwich (θ)	Angle of dithiolene offset (Φ)	C_2S_2-CoS_2
19	10.54	55.10(1)	2.47 and 2.25
20	13.67	55.65(1)	2.88 and 5.10
21	15.17	55.78(1)	3.48 and 5.24
22	36.97	56.76(1)	3.18 and 1.86

Previously, we found that reaction of $Na[BPh_4]$ with (b-15-c-5-dt)Pd(dppe) (complex **14**) using the same procedure as that of complex **19** gave the 1:1 complex [Na{(b-15-c-5-dt)Pd(dppe)}][BPh_4] with a 1:1 ratio of dithiolene complex and sodium cation.[25] The 2:1 ratio observed in **19** suggested the potential to form the related sandwich complex [Na{(b-15-c-5-dt)Pd(dppe)}$_2$][BPh_4], [Na(**14**)$_2$][BPh_4]. However, layering the 2:1 reaction mixture of (b-15-c-5-dt)Pd(dppe) with $Na[BPh_4]$ with hexane yielded orange crystals of [**14**·Na][BPh_4], suggesting that the 1:1 complex is the thermodynamically preferred product in this case. Attempts to incorporate other alkali metals into the crown

pocket of **14** were unsuccessful; recrystallization yielded only crystals of the alkali salt starting material, as well as a second polymorph of **14** (see **Table 3.5**) which exhibits some conformational differences in the crown ether backbone (**Figure 3.12**).

Table 3.5 Crystallographic data for the previously found polymorph of **14**[25] versus the new polymorph.

	Previous polymorph of 14	**New polymorph of 14**
Crystal system	Monoclinic	monoclinic
Space group	$P2_1/c$	$P2_1/c$
a (Å)	11.8434(12)	14.064(15)
b (Å)	13.561(3)	19.44(2)
c (Å)	24.616(7)	13.565(15)
α (°)	90	90
β (°)	101.568(14)	100.06(5)
γ (°)	90	90
R-factor (%)	3.16	3.10

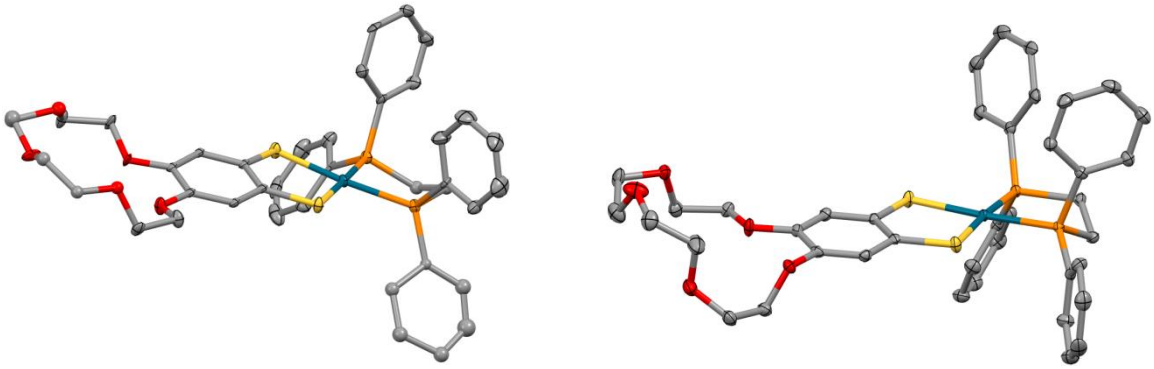

(a) **(b)**

Figure 3.12 Crystal structures of the **(a)** previously reported[25] and **(b)** new polymorph of **14**, with thermal ellipsoids drawn at the 50% probability level. Hydrogen atoms have been omitted for clarity.

3.2.6 Attempts to Incorporate Other Metals into 18

Following the procedures used to prepare complexes **19** and **22** but using $Li[ClO_4]$ instead of $Na[BPh_4]$ or $Cs[BPh_4]$ did not yield any crystals. Further reactivity studies probed the reaction with the first row transition metal salts $Fe(BF_4)_2{\cdot}6H_2O$, $Co(BF_4)_2{\cdot}6H_2O$, $Cu(ClO_4)_2{\cdot}6H_2O$, and $Cu(CF_3SO_3)_2$ in which the counterions are considered weakly interacting. No clear evidence for binding of these *d*-block metals was

observed. However the reaction of one equivalent of $Co(BF_4)_2 \cdot 6H_2O$ with one equivalent of **18** in a 1:1 mixture of MeOH and CH_2Cl_2, followed by recrystallization through the slow diffusion of pentane into the reaction mixture afforded crystals of **23** (**Figure 3.13**). Compound **23** crystallizes in the monoclinic space group *C*2/*c* with half a molecule in the asymmetric unit. Complex **23** is a dimer of complex **18**, reflecting the subtle balance observed elsewhere between monomer and dimer forms of these CpCo(bdt) derivatives

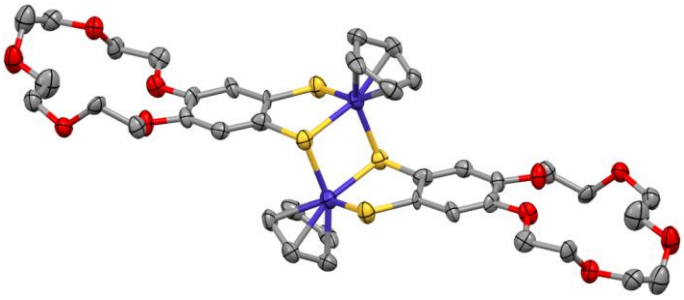

Figure 3.13 Preliminary crystal structure of complex **23** with thermal ellipsoids drawn at the 50% probability level. Hydrogen atoms have been omitted for clarity.

In the case of the $Cu(CF_3SO_3)_2$ reaction, a small number of crystals were obtained suitable for X-ray diffraction. These revealed an unusual dimeric structure of formula $[CpCo(b\text{-}15\text{-}c\text{-}dt)]_2[CF_3SO_3]_2$ in which oxidation appears to have taken place with the formation of a new disulfide bond between two metal dithiolene complexes to give complex **24** (**Figure 3.14**). This can be envisaged as arising from the two half reactions:

$$2\ RS^- \rightarrow RSSR + 2e^-$$

$$2Cu^{2+} + 2e^- \rightarrow 2Cu^+$$

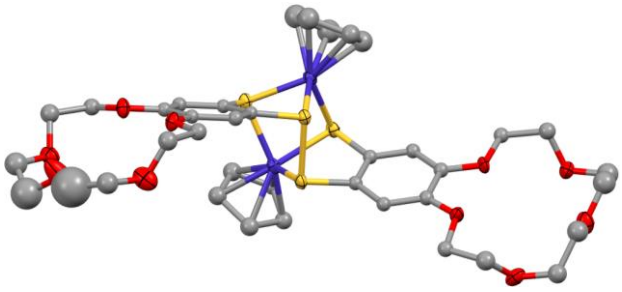

Figure 3.14 Crystal structure of the product of the reaction of **18** and $Cu(CF_3SO_3)_2$ showing possible formation of a new S-S bond. Hydrogen atoms and $CF_3SO_3^-$ counterions have been omitted for clarity.

Similar behavior was not observed for the simpler CpCo(dmobdt) derivative.

Previous studies done by Pilkington[11,12] and Ding[13] have shown that crown ether sandwich complexes containing a lanthanide metal in the pocket may behave as single molecule magnets (SMMs). To probe the possibility of creating multi-functional metal dithiolene complexes which exhibit magnetic properties, we combined the lanthanide salts $Sm(NO_3)_3 \cdot 6H_2O$ and $Yb(CF_3SO_3)_3 \cdot xH_2O$ with complex **18** in 1:1 MeOH and CH_2Cl_2 mixtures, as well as 1:3 mixtures of MeOH and MeCN. No crystals were isolated for the ytterbium reactions, while slow diffusion of pentane into the MeOH:CH_2Cl_2 solution of the samarium reaction mixture afforded crystals of the starting material **18** (see **Figure 3.9** for crystal structure). Following the procedure used by Pilkington,[11,12] we stirred $Dy(ClO_4)_3 \cdot 6H_2O$ and **18** in $CHCl_3$ or CH_2Cl_2 or a 1:3 mixture of MeOH and MeCN at 55 °C. Recrystallization of the latter two by layering of Et_2O afforded branch-like crystals which were unsuitable for X-ray diffraction. Conducting the same reaction with (b-15-c-5-dt)Pd(dppe) (**14**) instead of CpCo(b-15-c-5-dt) (**18**) led to a change in solution colour from pink to blue, indicating a reaction had taken place (**Scheme 3.6**). However, all efforts to recrystallize this solution led to a change in colour back to pink, with the product depositing as an oil at the bottom of the vial. This may indicate that some complexation of Dy^{3+} into the pocket of the crown takes place in solution, leading to the colour change from pink to blue, but that the coordination is weak, so that when recrystallization is attempted, the Dy^{3+} cation is displaced from the crown pocket. Careful tuning of the solvent system used for recrystallization, or PXRD studies may allow for the identification of this product.

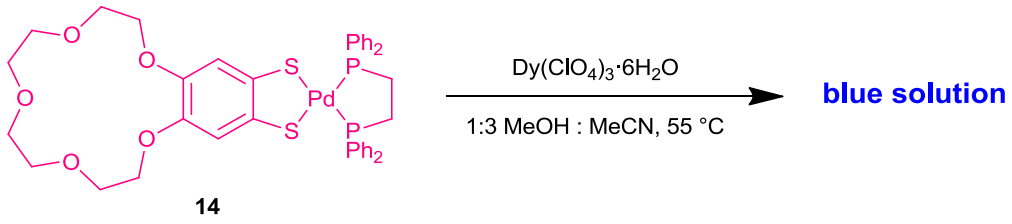

14

Scheme 3.6 The reaction of complex **14** and $Dy(ClO_4)_3 \cdot 6H_2O$.

3.3. Conclusions

In this chapter, the oxidative addition of tetrathiocins to Co(I) has been achieved. The bond lengths in complexes **17** and **18** derived from CpCo(bdt) reflect a formal Co(III)

center with a dithiolate ligand. Complex **17** existed as a dimer in the solid state but could be converted into its monomer when dissolved in the noncoordinating solvent $CDCl_3$, matching previous findings for $[CpCo(bdt)]_2$.[4] Depending on the crystallization method, CpCo(b-15-c-5-dt) could be isolated in two different forms; monomeric **18** and dimeric **23**, reflecting similar thermodynamic stabilities of the two species. Reactivity of **18** with a range of alkali metal salts led to the series of sandwich structures **19** to **22** in which two benzo-crown ligands sandwiched a single alkali metal centre. Interestingly, under similar conditions the palladium dithiolate complex **14** proved more selective with only a 1:1 complex isolated with Na^+ and no complexes isolated for other alkali metals. Extending this reactivity towards *d*- and *f*-block metals proved inconclusive, although there was evidence for Cu^{2+} to promote dithiolate oxidation. These reactions will need to be studied more fully in future.

3.4. Experimental

3.4.1 Crystallographic Studies

Crystals were mounted on a cryoloop with paratone oil and examined on a Bruker D8 Venture diffractometer equipped with a Photon 100 CCD area detector and an Oxford Cryostream cooler. Data were measured using graphite-monochromated Mo-Kα radiation (λ = 0.71073 Å) or Cu-Kα radiation (λ = 1.54178 Å) using the APEX-II software.[27] Final cell constants were determined from full least squares refinement of all observed reflections. The data were collected for absorption (sadabs)[28] and the structures solved by intrinsic phasing. Any remaining heavy atom positions were located in subsequence difference maps and the structure refined with full least squares refinement on F^2 within the SHELXTL suite.[29] Hydrogen atoms were placed at calculated positions and refined isotropically with a riding model. Structure solution, refinement, and preparation of final cif files were undertaken using the SHELXTL package.

3.4.2 General Experimental Procedures

NMR spectra were recorded on a Bruker DPX300 UltraShield 300 MHz spectrometer with a Broadband AX Probe or a Bruker UltraShield 300 MHz spectrometer using $CDCl_3$ (^{1}H δ = 7.26 ppm, s) as an internal reference point relative to Me_4Si (δ = 0 ppm). ^{31}P NMR spectra were referenced to 85% H_3PO_4 (δ = 0 ppm). IR spectra were obtained using a Bruker Alpha FT-IR spectrometer equipped with a Platinum single reflection diamond ATR module. Elemental compositions were determined on a PerkinElmer 2400 Series II Elemental Analyzer. Mass spectra were recorded on a Waters XEVO G2-XS Time Of Flight (TOF) or a Waters Micromass LCT Classic Electrospray Ionization Time of Flight (ESI-TOF) mass spectrometer operated in positive mode**.** Melting points were determined using a Stanford Research Systems MPA 120 EZ-Melt Automated Melting Point Apparatus. Microwave syntheses were carried out in sealed vessels using a Biotage Initiator+ microwave with continuous stirring.

3.4.3 Preparation of bis-15-crown-5-dibenzo-1,2,5,6-tetrathiocin, (16).

In a modification of the literature procedure,[24,25] benzo-15-crown-5 (1 g, 3.73 mmol) was added to 15 mL of degassed glacial acetic acid under nitrogen atmosphere. S_2Cl_2 (0.30 mL, 3.73 mmol) was added dropwise to the solution, and the solution was stirred for seven days, undergoing a change in colour from yellow to blue. A blue solid was isolated by vacuum filtration and washed with Et_2O (2 × 10 mL), then suspended in approx. 5 mL $CHCl_3$. Three drops of methanolic tin chloride solution (3 g anhydrous $SnCl_2$ in 5 mL MeOH) were added to give a pale yellow solution, and a pale yellow solid was isolated by vacuum filtration, washed with Et_2O, and dried under vacuo (0.587 g, 48% yield).

HRMS (ASAP) *m/z*: $[M+H]^+$ calc. for $C_{28}H_{37}O_{10}S_4^+$ 661.1270; found 661.1269.

Elemental Analysis calc. for $C_{28}H_{36}O_{10}S_4 \cdot ½CHCl_3$: C 47.50; H 5.12%; found: C 48.29; H 5.30%.

Melting Point decomposed above 140 °C

IR (cm^{-1}): $\tilde{\nu}$ = 2931(w), 2860(w), 1714(w), 1571(m), 1554(m), 1485(s), 1442(s), 1350(m), 1312(m), 1296(m), 1255(vs), 1209(vs), 1123(vs), 1082(vs), 1044(vs), 971(s), 931(s), 872(s), 823(m), 806(m), 722(w), 678(w), 609(w), 565(w), 546(w), 525(w), 472(w), 444(w), 416(w).

3.4.4 Preparation of [CpCo(dmobdt)]$_2$, (17).

Tetrathiocin **1** (0.200 g, 0.5 mmol) was placed in a microwave vial under inert atmosphere to which dry toluene (5 mL) was added. The vial was sealed and $CpCo(CO)_2$ (0.13 mL, 1 mmol) was added *via* syringe. The mixture was heated in the microwave at 150 °C for 30 minutes to afford a deep blue solution. After slowly releasing pressure from the vial, the solvent was evaporated by rotary evaporation, the resultant blue solid dissolved in $CHCl_3$, which was then filtered, evaporated and the dark blue-black solid washed with Et_2O and dried in air (0.262 g, 81% yield).

NMR (ppm) ($CDCl_3$)**: δ_H** (300 MHz) = 7.50 (2H, s, benzo C–H), 5.39 (5H, s, Cp C–H), 3.85 (6H, s, O–CH_3); **δ_C** (75 MHz)= 155.87 (s, aryl O–C), 147.13 (s, aryl S–C), 111.31 (s, benzo–C), 79.35 (s, Cp–C), 56.18 (s, O–CH_3).

HRMS (ASAP) *m/z*: $[M+H]^+$ calc. for $C_{26}H_{27}O_4S_4Co_2^+$ 648.9456; found 648.9449.

Elemental Analysis calc. for $C_{26}H_{26}O_4S_4Co_2$: C 48.15; H 4.04%; found: C 47.68; H 3.47%.

Melting Point greater than 300 °C

IR (cm^{-1}): $\tilde{\nu}$ = 2830(w), 1580(w), 1553(w), 1497(w), 1484(m), 1471(m), 1434(s), 1418(m), 1345(w), 1317(w), 1240(vs), 1202(s), 1179(s), 1153(w), 1105(w), 1059(w), 1037(vs), 1017(w), 1000(w), 942(w), 924(w), 852(m), 822(vs), 782(s), 682.13(m), 647(w), 583(w), 572.58(w), 445(m).

3.4.5 Preparation of CpCo(b-15-c-5-dt), (18).

Tetrathiocin **16** (0.330 g, 0.5 mmol) was placed in a microwave vial under inert atmosphere to which dry toluene (5 mL) was added. The vial was sealed and $CpCo(CO)_2$ (0.13 mL, 1 mmol) was added *via* syringe. The mixture was heated in the microwave at 150 °C for 30 minutes to afford a deep blue solution. After slowly releasing pressure from the vial, the solvent was evaporated by rotary evaporation, the resultant blue solid dissolved in $CHCl_3$, filtered, and the filtrate evaporated. A dark blue solid was collected by dissolving in a small amount of CH_2Cl_2 then precipitating with an excess of hexane, and filtering to get dark blue precipitate which was dried in air (0.320 g, 70.5% yield).

NMR (ppm) ($CDCl_3$)**: δ_H** (300 MHz) = 7.48 (2H, s, benzo C–H), 5.39 (5H, s, Cp C–H), 4.08 (4H, 4.08-4.07, d, crown C–H, J = 4.2 Hz), 3.92 (4H, 3.93-3.91, d, crown C–H, J = 4.2 Hz), 3.75 (8H, s, crown C–H); **δ_C** (75 MHz) = 156.06 (s, aryl O–C), 146.93 (s, aryl S–C), 113.16 (s, benzo–C), 79.33 (s, Cp–C), 71.34 (s, crown–C), 70.46 (s, crown–C), 69.44 (s, crown–C), 68.81 (s, crown–C).

HRMS (ASAP) *m/z*: $[M+H]^+$ calc. for $C_{19}H_{24}O_5S_2Co^+$ 455.0397; found 455.0396.

Elemental Analysis calc. for $C_{19}H_{23}O_5S_2Co \cdot CH_2Cl_2$: C 44.54; H 4.67%; found: C 46.43; H 4.15%.

IR (cm^{-1}): $\tilde{\nu}$ = 2924(w), 2864 (w), 1590 (w), 1516(m), 1485(m), 1475(m), 1446(s), 1411(w), 1357(m), 1334(w), 1306(vw),1246(vs), 1199(s), 1128(s), 1089(m), 1077(s), 1050(s), 1033(s), 999(m), 987(m), 928(m), 882(m), 847(m), 833(s), 825(s), 805(w), 732(vw), 692(w), 580(vw), 557(w), 530(w), 484(w), 425(w), 411(w), 406(w).

3.4.6 Preparation of [Na{CpCo(b-15-c-5-dt)}$_2$][BPh$_4$], (19).

Protocol #1: Complex **18** (0.0099 g, 0.0218 mmol) and Na[BPh_4] (0.010 g, 0.0292 mmol) were combined in a small 20 mL vial with a 1:1 mixture of CH_2Cl_2 and MeOH (6 mL total) and left to stir for 1 hour under ambient conditions. Layering hexane onto the solution afforded blue crystals suitable for X-ray diffraction (0.0054 g, 40% yield).

Protocol #2: Complex **18** (0.0099 g, 0.0218 mmol) and Na[BPh_4] (0.005 g, 0.0146 mmol) were combined in a small 20 mL vial with a 1:1 mixture of CH_2Cl_2 and MeOH (6 mL total) and left to stir for 1 hour under ambient conditions. Layering hexane onto the solution afforded blue crystals suitable for X-ray diffraction (0.0092 g, 50% yield).

HRMS (ESI-TOF) *m/z*: calc. for $C_{38}H_{46}O_{10}S_4Co_2Na^+$ 931.0535; found 931.0548

Elemental Analysis calc. for $C_{62}H_{66}O_{10}S_4BCo_2Na\cdot\frac{1}{2}CH_2Cl_2$: C 58.03; H 5.22%; found: C 58.04; H 5.24%.

IR (cm^{-1}): $\tilde{\nu}$ = 3099(w), 3051(w), 2863(w), 1594(w), 1579(w), 1525(w), 1476(m), 1447(m), 1423(w), 1411(m), 1360(m), 1336(w), 1299(w), 1246(vs), 1199(s), 1150(w),1124(m), 1096(s), 1079(s), 1046(vs), 1000(m), 929(s), 884(m), 859(s), 831(s), 750(m), 735(vs), 706(vs), 610(s), 570(m), 516(m), 470(m), 422(m), 411(m).

3.4.7 Preparation of [K{CpCo(b-15-c-5-dt)}$_2$][BPh$_4$], (20).

Protocol #1: Complex **18** (0.0099 g, 0.0218 mmol) was dissolved in CH_2Cl_2 (2 mL) and was layered with an acetone (2 mL) solution of K[BPh_4] (0.0078 g, 0.0218 mmol). After 1 day, blue plates suitable for X-ray diffraction were observed. More crystals could be afforded by layering hexane onto the solution (0.0055 g, 40% yield).

Protocol #2: Complex **18** (0.0099 g, 0.0218 mmol) was dissolved in CH_2Cl_2 (2 mL) and was layered with an acetone (2 mL) solution of K[BPh_4] (0.0039 g, 0.0109 mmol). After 1 day, hexane was layered onto the solution, affording blue crystals suitable for X-ray diffraction (0.0089 g, 64% yield).

HRMS (ESI-TOF) *m/z*: calc. for $C_{38}H_{46}O_{10}S_4Co_2K^+$ 947.0275; found 947.0275.

Elemental Analysis calc. for $C_{62}H_{66}O_{10}S_4BCo_2K$: C 58.76; H 5.25%; found: C 57.86; H 5.22%.

IR (cm^{-1}): $\tilde{\nu}$ = 3097(w), 3052(m), 2934(w), 2893(m), 2859(m), 1706(w), 1594(w), 1579(w), 1523(w), 1475(m), 1447(s), 1412(m), 1360(m), 1335(m), 1300(w), 1244(vs), 1198(s), 1149(w), 1124(s), 1105(m), 1093(s), 1078(s), 1043(s), 1002(m), 932(s), 883(m), 856(s), 833(s), 750(m), 736(vs), 708(vs), 611(m), 568(m), 526(m), 512(m), 471(m), 424(m), 411(m).

3.4.8 Preparation of [Rb{CpCo(b-15-c-5-dt)}$_2$][BPh_4], (21).

Protocol #1: Complex **18** (0.0099 g, 0.0218 mmol) was dissolved in CH_2Cl_2 (2 mL) and was layered with an acetone (2 mL) solution of Rb[BPh_4] (0.0088 g, 0.0218 mmol). After several days, the solution was layered with hexane, affording blue crystals suitable for X-ray diffraction (0.0119 g, 83% yield).

Protocol #2: Complex **18** (0.0099 g, 0.0218 mmol) was dissolved in CH_2Cl_2 (2 mL) and was layered with an acetone (2 mL) solution of Rb[BPh_4] (0.0044 g, 0.0109 mmol). After several days, the solution was layered with hexane, affording blue crystals suitable for X-ray diffraction (0.012 g, 84% yield).

Elemental Analysis calc. for $C_{62}H_{66}O_{10}S_4BCo_2Rb\cdot½hex$: C 57.54; H 5.42%; found: C 57.54; H 4.95%.

IR (cm^{-1}): $\tilde{\nu}$ = 3094(w), 3053(w), 2859(w), 1706(w), 1592(w), 1579(w), 1521(w), 1475(m), 1447(m), 1413(w), 1359(m), 1334(w), 1299(w), 1244(vs), 1197(m), 1149(w), 1124(m), 1105(m), 1091(m), 1075(m), 1041(s), 1002(m), 930(s), 882(m), 854(m), 832(s), 749(m), 735(vs), 707(s), 602(m), 565(m), 524(m), 510(m), 470(m), 439(w), 423(m), 408(m).

3.4.9 Preparation of [Cs{CpCo(b-15-c-5-dt)}$_2$][BPh$_4$], (22).

Protocol #1: Complex **18** (0.0099 g, 0.0218 mmol) and Cs[BPh_4] (0.0099 g, 0.0218 mmol) were combined in a small 20 mL vial with a 1:1 mixture of CH_2Cl_2 and MeOH (4 mL total) and left to stir for 1 hour under ambient conditions. Layering hexane onto the solution afforded blue crystals suitable for X-ray diffraction (0.0026 g, 18% yield).

Protocol #2: Complex **18** (0.0099 g, 0.0218 mmol) and Cs[BPh_4] (0.0050 g, 0.0109 mmol) were combined in a small 20 mL vial with a 1:1 mixture of CH_2Cl_2 and MeOH (4 mL total) and stirred for 1 hour under ambient conditions. Layering hexane onto the solution afforded blue crystals suitable for X-ray diffraction (0.0026 g, 18% yield).

Elemental Analysis calc. for $C_{62}H_{66}O_{10}S_4BCo_2Cs$: C 54.71; H 4.89%; found: C 54.92; H 4.64%.

3.4.10 Preparation of (b-15-c-5-dt)Pd(dppe), (14).

Tetrathiocin **16** (0.073 g 0.109 mmol), Pd_2dba_3 (0.100 g, 0.109 mmol), and dppe (0.087 g, 0.218 mmol) were added to an oven-dried 5 mL microwave vial in the glove box. Dry toluene (5 mL) was added and the suspension was heated in the microwave for 20 min at 150 °C. The solution was filtered, and the pink precipitate washed with hexane and dried in air (0.172 g, 94 % yield). Pink needles could be recrystallized from the slow diffusion of Et_2O into a saturated MeCN solution.

NMR (ppm) (MeCN-d_3)**:** δ_H (300 MHz) = 7.80 (8H, 7.83-7.77, m, *m*-H), 7.51 (12H, 7.53-7.50, m, *o,p*-H), 6.71 (2H, s, benzo C–H), 3.93 (4H, 3.94-3.92, m, crown C–H), 3.72 (4H, 3.74-3.71, m, crown C–H), 3.60 (8H, s, crown C–H), 2.63 (4H, 2.66-2.59, d, $^2J_{PH}$ = 21 Hz, PCH_2); $\delta_P\{^1H\}$ (121 MHz) = 52.89.

HRMS (ESI-TOF) ***m/z*****:** calc. for $C_{40}H_{42}O_5P_2S_2Pd^+$ 835.1076; found 835.1097.

Elemental Analysis calc. for $C_{40}H_{42}O_5P_2S_2Pd \cdot ½CH_2Cl_2$: C 55.42; H 4.95%; found: C 55.36; H 5.14%.

IR (cm^{-1}): $\tilde{\nu}$ = 2923(m), 2862(m), 1474(s), 1450(s), 1435(vs), 1244(s), 1134(m), 1102(vs), 1064(m), 876(w), 713(m), 703(s), 691(vs), 528(s), 481(m).

3.4.11 Preparation of [Na{(b-15-c-5-dt)Pd(dppe)}][BPh$_4$].

Protocol #1: Complex **14** (0.0018 g, 0.0218 mmol) and Na[BPh_4] (0.010 g, 0.0218 mmol) were combined in a small 20 mL vial with a 1:1 mixture of CH_2Cl_2 and MeOH (4 mL total) and left to stir for 1 hour under ambient conditions. Layering hexane onto the solution afforded orange crystals suitable for X-ray diffraction (0.0054 g, 40% yield).

Protocol #2: Complex **14** (0.0018 g, 0.0218 mmol) and Na[BPh_4] (0.005 g, 0.0109 mmol) were combined in a small 20 mL vial with a 1:1 mixture of CH_2Cl_2 and MeOH (4 mL total) and stirred for 1 hour under ambient conditions. Layering hexane onto the solution afforded orange crystals suitable for X-ray diffraction.

NMR (ppm) (MeCN-d_3)**:** δ_H (300 MHz) = 7.76 (8H, 7.77-7.75, m, *m*-H), 7.53 (12H, 7.56-7.50, m, *o,p*-H), 7.26 (8H, s, B-aryl C–H), 6.99 (8H, 7.01-6.96, t, J = 7.2 Hz, B-aryl C–H), 6.84 (4H, 6.85-6.83, d, J = 3.3 Hz, B-aryl C–H), 5.446 (2H, s, benzo CH), 4.03 (4H, s, crown C–H), 3.764 (4H, s, crown C–H), 3.66 (8H, s, crown C–H), 2.62 (4H, 2.66-2.59, d, $^2J_{PH}$ = 21.3 Hz, PCH_2); $\delta_P\{^1H\}$ (121 MHz) = 54.12.

HRMS (MALDI) ***m/z*****:** calc. for $C_{40}H_{42}O_5P_2S_2PdNa^+$ 857.0895; found 857.0896.

Elemental Analysis calc. for $C_{64}H_{62}O_5P_2S_2BPdNa \cdot MeOH$: C 64.55; H 5.50%; found: C 64.78; H 5.21%.

IR (cm^{-1}): $\tilde{\nu}$ = 3053(w), 2911(w), 2876(w), 1585(w), 1480(m), 1455(m), 1433(m), 1383(w), 1357(w), 1348(w), 1307(w), 1244(s), 1184(m), 1118(m), 1101(s), 1093(s), 1051(m), 1030(m), 998(w), 972(w), 927(m), 876(m), 858(w), 849(w), 840(m), 821(m), 747(s), 733(s), 704(vs), 690(vs), 623(w), 610(s), 530(s), 523(s), 482(s), 430(w).

3.4.12 Reaction of 18 and Li[ClO_4].

Complex **18** (0.0099 g, 0.0218 mmol) and Li[ClO_4] (0.0020 g, 0.0218 mmol) were combined in a small 20 mL vial with a 1:1 mixture of CH_2Cl_2 and MeOH (6 mL total) and stirred for 1 hour under ambient conditions. All attempts to recrystallize afforded no crystals.

3.4.13 Reaction of 18 and $Fe(BF_4)_2 \cdot 6H_2O$.

Protocol #1: Complex **18** (0.0099 g, 0.0218 mmol) and $Fe(BF_4)_2 \cdot 6H_2O$ (0.0074 g, 0.0218 mmol) were combined in a small 20 mL vial with a 1:1 mixture of CH_2Cl_2 and MeOH (4 mL total) and left to stir for 1.5 hours under ambient conditions. All attempts to recrystallize afforded no crystals.

Protocol #2: Complex **18** (0.0099 g, 0.0218 mmol) was dissolved in CH_2Cl_2 (2 mL) and was layered with a MeOH (2 mL) solution of $Fe(BF_4)_2 \cdot 6H_2O$ (0.0074 g, 0.0218 mmol). All attempts to recrystallize afforded no crystals.

3.4.14 Reaction of 18 and $Cu(ClO_4)_2 \cdot 6H_2O$.

Protocol #1: Complex **18** (0.0099 g, 0.0218 mmol) and $Cu(ClO_4)_2 \cdot 6H_2O$ (0.0081 g, 0.0218 mmol) were combined in a small 20 mL vial with a 1:1 mixture of CH_2Cl_2 and MeOH (4 mL total) and stirred for 1.5 hours under ambient conditions. All attempts to recrystallize afforded no crystals.

Protocol #2: Complex **18** (0.0099 g, 0.0218 mmol) was dissolved in CH_2Cl_2 (2 mL) and was layered with a MeOH (2 mL) solution of $Cu(ClO_4)_2 \cdot 6H_2O$ (0.0081 g, 0.0218 mmol). All attempts to recrystallize afforded no crystals.

3.4.15 Preparation of [CpCo(b-15-c-5-dt)]$_2$, (23).

Complex **18** (0.0099 g, 0.0218 mmol) and $Co(BF_4)_2 \cdot 6H_2O$ (0.0074 g, 0.0218 mmol) were combined in a small 20 mL vial with a 1:1 mixture of CH_2Cl_2 and MeOH (4 mL total) and stirred for 1.5 hours under ambient conditions. Slow diffusion of pentane into the reaction mixture afforded a small amount of blue crystals suitable for X-ray diffraction.

3.4.16 Preparation of [CpCo(b-15-c-5-dt]$_2$[CF_3SO_3]$_2$, (24).

Complex **18** (0.0099 g, 0.0218 mmol) and $Cu(CF_3SO_3)_2$ (0.0079 g, 0.0218 mmol) were combined in a small 20 mL vial with a 1:1 mixture of CH_2Cl_2 and MeOH (4 mL total) and stirred for 1.5 hour under ambient conditions. Slow diffusion of pentane into the reaction mixture afforded a small amount of blue crystals suitable for X-ray diffraction.

3.4.17 Reaction of 17 and $Cu(CF_3SO_3)_2$.

Protocol #1: Complex **17** (0.0141 g, 0.0218 mmol) and $Cu(CF_3SO_3)_2$ (0.0079 g, 0.0218 mmol) were combined in a small 20 mL vial with a 1:1 mixture of CH_2Cl_2 and MeOH (4 mL total) and stirred for 2 hours under ambient conditions. All attempts to recrystallize afforded no crystals.

Protocol #2: Complex **17** (0.0141 g, 0.0218 mmol) and $Cu(CF_3SO_3)_2$ (0.0158 g, 0.0436 mmol) were combined in a small 20 mL vial with a 1:1 mixture of CH_2Cl_2 and MeOH (4 mL total) and stirred for 2 hours under ambient conditions. All attempts to recrystallize afforded no crystals.

3.4.18 Reaction of 18 and $Sm(NO_3)_3 \cdot 6H_2O$.

Protocol #1: Complex **18** (0.0099 g, 0.0218 mmol) and $Sm(NO_3)_3 \cdot 6H_2O$ (0.0097 g, 0.0218 mmol) were combined in a small 20 mL vial with a 1:1 mixture of CH_2Cl_2 and MeOH (4 mL total) and stirred for 2 hours under ambient conditions. Slow diffusion of pentane into the reaction mixture yielded a small amount of crystals of **18**.

Protocol #2: Complex **18** (0.0099 g, 0.0218 mmol) and $Sm(NO_3)_3 \cdot 6H_2O$ (0.0097 g, 0.0218 mmol) were combined in a small 20 mL vial with a 1:3 mixture of MeOH and MeCN (4 mL total) and stirred for 4 hours at 55 °C, then filtered through cotton wool. All attempts to recrystallize afforded no crystals.

3.4.19 Reaction of 18 and $Yb(CF_3SO_3)_2 \cdot xH_2O$.

Protocol #1: Complex **18** (0.0099 g, 0.0218 mmol) and $Yb(CF_3SO_3)_2 \cdot xH_2O$ (0.0139 g, 0.0218 mmol) were combined in a small 20 mL vial with a 1:1 mixture of CH_2Cl_2 and MeOH (4 mL total) and stirred for 2 hours under ambient conditions. All attempts to recrystallize afforded no crystals.

Protocol #2: Complex **18** (0.0099 g, 0.0218 mmol) and $Yb(CF_3SO_3)_2 \cdot xH_2O$ (0.0139 g, 0.0218 mmol) were combined in a small 20 mL vial with a 1:3 mixture of MeOH and MeCN (4 mL total) and stirred for 4 hours at 55 °C, then filtered through cotton wool. All attempts to recrystallize afforded no crystals.

3.4.20 Reaction of 18 and $Dy(ClO_4)_3 \cdot 6H_2O$.

Protocol #1: Complex **18** (0.0099 g, 0.0218 mmol) and $Dy(ClO_4)_3 \cdot 6H_2O$ (0.02 mL, 0.0218 mmol) were combined in a small 20 mL vial with a 1:3 mixture of MeOH and MeCN (4 mL total) and stirred for 3 hours at 55 °C, then filtered through cotton wool. Layering Et_2O onto the solution yielded thin, branched crystals which were unsuitable for X-ray diffraction.

Protocol #2: Complex **18** (0.0099 g, 0.0218 mmol) and $Dy(ClO_4)_3 \cdot 6H_2O$ (0.02 mL, 0.0218 mmol) were combined in 4 mL CH_2Cl_2 in a small 20 mL vial and stirred for 4 hours at 55 °C, then filtered through cotton wool. Layering Et_2O onto the solution yielded thin, branched crystals which were unsuitable for X-ray diffraction.

Protocol #3: Complex **18** (0.0099 g, 0.0218 mmol) and $Dy(ClO_4)_3 \cdot 6H_2O$ (0.02 mL, 0.0218 mmol) were combined in 4 mL $CHCl_3$ in a small 20 mL vial and stirred for 4 hours at 55 °C, then filtered through cotton wool. All attempts to recrystallize afforded no crystals.

3.4.21 Reaction of 14 and $Dy(ClO_4)_3 \cdot 6H_2O$.

Protocol #1: Complex **14** (0.018 g, 0.0218 mmol) and $Dy(ClO_4)_3 \cdot 6H_2O$ (0.02 mL, 0.0218 mmol) were combined in a small 20 mL vial with a 1:3 mixture of MeOH and MeCN (4 mL total) and stirred for 3 hours at 55 °C, undergoing a change in colour from pink to blue. All attempts to recrystallize led to a pink-brown oil depositing at the bottom of the vial.

Protocol #2: Complex **14** (0.018 g, 0.0218 mmol) and $Dy(ClO_4)_3 \cdot 6H_2O$ (0.02 mL, 0.0218 mmol) were combined in 4 mL CH_2Cl_2 in a small 20 mL vial and stirred for 3.5 hours at 55 °C, undergoing a change in colour from pink to blue. The solution was filtered through cotton wool. All attempts to recrystallize led to a pink-brown oil depositing at the bottom of the vial.

3.5. References

1. *Dithiolene chemistry: Synthesis, properties, and applications*, ed. E. I. Stiefel, Interscience: Hoboken, New Jersey, 2003.

2. R. B. King, *J. Am. Chem. Soc.*, 1963, **85**, 1587–1590.

3. H. W. Baird and B. M. White, *J. Am. Chem. Soc.*, 1966, **88**, 4744–4745.

4. E. J. Miller, T. B. Brill, A. L. Rheingold and W. C. Fultz, *J. Am. Chem. Soc.*, 1983, **105**, 7580–7584.

5. C. J. Pedersen, *Angew. Chem. Int. Ed. Engl.*, 1988, **27**, 1021–1027.

6. G. W. Gokel, W. M. Leevy and M. E. Weber, *Chem. Rev.*, 2004, **104**, 2723−2750.

7. **(a)** R. G. Pearson, *J. Chem. Ed.*, 1968, **45**, 581–587; **(b)** R. G. Pearson, *J. Chem. Ed.*, 1968, **45**, 643–648.

8. A. E. Visser, R. P. Swatloski, W. M. Reichert, S. T. Griffin and R. D. Rogers, *Ind. Eng. Chem. Res.*, 2000, **39**, 3596–3604.

9. **(a)** T. Kaneda, K. Sugihara, H. Kamiya and S. Misumi, *Tetrahedron Lett.*, 1981, **22**, 4407–4408; **(b)** K. Nakashima, S. Nakatsuji, S. Akiyama, T. Kaneda and S. Misumi, *Chem. Lett.*, 1982, **11**, 1781–1782.

10. J. Bourson, J. Pouget and B. Valeur, *J. Phys. Chem.*, 1993, **97**, 4552–4557.

11. E. L. Gavey, M. Al Hareri, J. Regier, L. D. Carlos, R. A. S. Ferreira, F. S. Razavi, J. M. Rawson and M. Pilkington, *J. Mater. Chem. C*, 2015, **3**, 7738 – 7747.

12. M. Al Hareri, E. L. Gavey, J. Regier, Z. Ras Ali, L. D. Carlos, R. A. S. Ferreira and M. Pilkington, *Chem. Commun.*, 2016, **52**, 11335–11338.

13. Y. S. Ding, T. Han, Y. Q. Hu, M. Xu, S. Yang and Y. Z. Zheng, *Inorg. Chem. Front.*, 2016, **3**, 798–807.

14. S. Shinkai, T. Nakaji, Y. Nishida, T. Ogawa and O. Manabe, *J. Am. Chem. Soc*., 1980, **102**, 5860–5865.

15. A. Kaifer, L. Echegoyen, D. A. Gustowski, D. M. Goli and G. W. Gokel, *J. Am. Chem. Soc*., 1983, **105**, 7168–7169.

16. **(a)** R. R. Julian, J. L. Beauchamp, *Int. J. Mass Spectrom.*, 2001, **210/211**, 613–623; **(b)** R. R. Julian, M. Akin, J. A. May, B. M. Stoltz and J. L. Beauchamp, *Int. J. Mass Spectrom.*, 2002, **220**, 87–96; **(c)** R. R. Julian, J. A. May, B. M. Stoltz and J. L. Beauchamp, *Int. J. Mass Spectrom.*, 2003, **228**, 851–864; **(d)** R. R. Julian, J. A. May, B. M. Stoltz and J. L. Beauchamp, *Angew. Chem. Int. Ed.*, 2003, **42**, 1012–1015.

17. **(a)** N. Voyer and M. Robitaille, J. Am. Chem. Soc. 1995,117, 6599-6600; **(b)** E. Biron, N. Voyer, J. C. Meillon, M. E. Cormier, M. Auger, Peptide Science, 2000, 55, 364–372; **(c)** J. C. Meillon and N. Voyer, *Angew. Chem. Int. Ed. Engl.*, 1997, **36**, 967–969; **(d)** A. C. Hall, C. Suarez, A. Hom-Choudhury, A. N. A. Manu, C. D. Hall, G. J. Kirkovits and I. Ghiriviga, *Org. Biomol. Chem.*, 2003, **1**, 2973–2982.

18. **(a)** D. J. van Unen, J. F. J. Engbersen and D. N. Reinhoudt, *Biotechnol. Bioeng.*, 2002, **77**, 248–255; **(b)** T. Itoh, Y. Takagi, T. Murakami, Y. Hiyama and H. Tsukube, *J. Org. Chem.*, 1996, **61**, 2158–2163.

19. S. Vogel, K. Rohr, O. Dahl and J. Wengel, *Chem. Commun.*, 2003, 1006–1007.

20. A. Basak and H. Dugas, *Tetrahedron Let*., 1986, **27**, 3–6.

21. W. M. Leevy, G. M. Donato, R. Ferdani, W. E. Goldman, P. H. Schlesinger and G. W. Gokel, *J. Am. Chem. Soc.*, 2002, **124**, 9022–9023.

22. N. D. Lowe and C. D. Garner, *J. Chem. Soc. Dalton Trans.*, 1993, 2197–2207.

23. N. D. Lowe and C. D. Garner, *J. Chem. Soc. Dalton Trans.*, 1993, 3333–3340.

24. K. W. Stender, N. Wolki and G. Klar, *Phos, Sulf., Sil and Rel. Elts*, 1989, **42**, 111–114.

25. J. D. Wrixon, *Reactivity of 1,2,5,6-Tetrathiocines*, University of Windsor, 2015.

26. F. H. Allen, O. Kennard, D. G. Watson, L. Brammer, A. G. Orpen and R. Taylor, *J. Chem. Soc., Perkin Trans. II*, 1987, S1.

27. APEX-II, Bruker AXS Inc., Madison, Wisconsin, USA.

28. Sadabs, Bruker AXS Inc., Madison, Wisconsin, USA.

29. SHELXTL package for crystal structure solution and refinement, Bruker AXS Inc., Madison, Wisconsin, USA.

CHAPTER 4. Conclusions and Future Work

4.1. Conclusions

Previous work on the oxidative addition of 1,2,5,6-tetrathiocins to zero-valent group 10 metals showed that these reactions can be conducted under microwave conditions to yield metal dithiolene complexes in good yields. A variety of mono-, di-, and hexanuclear complexes were reported in which the metal centre, phosphine co-ligand, or tetrathiocin starting material (and therefore dithiolene) was varied, and some preliminary studies into the effects of these changes on redox potentials and/or structure of the complexes were conducted.[1]

In this thesis, Chapter 2 describes more detailed systematic studies of the effect of the phosphine co-ligand on the nuclearity of the complexes $Pd_xL_y(PR_3)_z$ formed. A series of homo-dimetallic Pd complexes were isolated showing a strong preference for dimer formation and no additional larger nuclearity complexes were isolated. The slower kinetics associated with platinum(II) chemistry allowed both mononuclear and dinuclear complexes of the form (dmobdt)Pt$(PPh_3)_2$ and [(dmobdt)Pt$(PPh_3)]_2$ to be prepared. Detailed studies revealed that conversion of the monometallic complrxes to the dimetallic platinum complexes appeared to require the presence of oxygen, with the phosphine oxide being formed as a by-product during these reactions. Reaction of $Pt_{1.9}dba_3$ with tetrathiocin **1** and P^tBu_3 generated a mixture of monometallic, dimetallic complexes as well as the first hexanuclear platinum dithiolene complex, $[Pt(dmobdt)]_6$. Notably the major dimetallic species isolated, [(dmobdt)Pt$(PH^tBu_2)]_2$, revealed non-innocent behavior of the phosphine. The combined observation of PH^tBu_2 complexes along with formation of OPR_3 during these oxidative addition reactions indicate that the phosphine may exhibit more than just the role of auxiliary ligand during these reactions.

Chapter 3 extended the oxidative addition route to group 9 through the synthesis of two cobalt dithiolate complexes from $CpCo(CO)_2$. Structural and solution studies reveal monomer-dimer equilibria are present for complexes of the type CpCo(dt). The

generation of benzo-crown-5 derivatives permited a series of hetero-trimetallic complexes to be prepared in which alkali metals (Na, K, Rb, Cs) adopted decacoordinate geometries, sandwiched between two crown-5 macrocycles.

4.2. Future Work

Chapter 2 developed the reactivity of dithiolate complexes of platinum and revealed the non-innocent nature of the phosphine in promoting formation of larger aggregates. In particular, further studies are required to probe the role of P^tBu_3 in this reaction chemistry and its conversion to the secondary phosphine PH^tBu_2 during the oxidative addition process. In this way, the aggregation process which leads to formation of the hexamer $[Pt(dmobdt)]_6$ may be clarified. Extension of the crown ether work developed in Chapter 3 in this area could lead to more complex multimetallic systems such as $[M(b\text{-}15\text{-}c\text{-}5\text{-}dt)]_6$ (M = Pd, Pt) in which the hexanuclear core could be decorated with a range of *s* or potentially oxophilic *d*- or *f*-block metals. The redox chemistry of the core and periphery might lead to interesting electronic or optical behavior. To date, the crowns have been implemented for *s*-block metal binding but could be extended to ammonium salts which are well-known to form hydrogen-bonded structures with crown ethers or to develop larger crowns which could be used to develop rotaxanes in which the benzo-crown 'wheel' could be tagged with a metal ion *via* the dithiolate group. To date, studies on group 10 dithiolates have examined factors which increase aggregation. Future studies might pursue taking higher nuclearity species such as dimers and adding additional coligands (L) to form mononuclear complexes of the form $M(dmobdt)(PR_3)L$ or (from the hexamer) $M(dmobdt)L_2$. This would provide access to a more diverse range of co-ligands (L = X^-, CO, CN^-, alkene, etc.) with potential to develop a more extensive organometallic chemistry. Preliminary research into metal dithiolene complexes of formula (dt)M(NN') (dt = dithiolate; M = Ni, Pd, Pt; NN' = NN' chelate ligand) has been investigated using oxidative addition chemistry as possible building blocks for non-linear optical materials.[2] Changing the substituents on the dithiolene ligand or the diimine or bypyridine co-ligand on nickel dithiolates showed that the HOMO-LUMO gap could be lowered by using dithiolenes bearing electron donating groups and N-based ligands bearing electron withdrawing groups, leading to a red shift of λ_{max} to higher wavelength,

which is important for solar cell applications where efficient absorbers in the NIR are desirable. Future experiments exploring crown ether functionalized dithiolene ligands with the N-based co-ligands could produce novel ion sensors in which the crown-bound cation tunes the HOMO-LUMO gap. Additionally, if lanthanides are incorporated into these crowns, the combination of lanthanide magnetic properties and nickel dithiolate optical properties could lead to the development of photo-switchable magnetic materials.

Continuation of the crown ether complexation reactions of Chapter 3 may allow us to discover a recrystallization technique which would yield crystals from the reaction of (dmobdt)Pd(dppe) and $Dy(ClO_3)_4 \cdot 6H_2O$, opening these complexes to possible magnetic applications. Although several *d*- and *f*-block metal salts were also examined, no crystals were isolated from these reactions. However, this does not preclude their complexation but may just reflect good solubility. Solution studies of the effects of cation binding such as shift in redox potential, UV/vis absorption maxima, or fluorescence, could be used to probe metal binding in solution. By synthesizing tetrathiocins bearing larger crown ether groups, such as benzo-18-crown-6, it may be possible to incorporate cations into the cavities in different ratios than those reported in Chapter 3, as well as even larger cations, including alkaline earth metals and lanthanides, into these complexes.

Studies have very recently begun in the Rawson group to extend the oxidative addition route to other transition metals including the first row metals vanadium, chromium, manganese, and iron, as well as the Cp-containing $[CpNi(CO)]_2$. Future experiments may include second row transition metals, such as Wilkinson's catalyst, $RhCl(PPh_3)_3$. These reactions have also recently been extended beyond the *d*-block metals to the *p*-block. A collaboration with the Macdonald group[3] found that the oxidative addition of tetrathiocins to the P(I) compound [P(dppe)][Br] produced new bis(trithio)phosphines which pass through a diphosphine intermediate. These results present promising new opportunities in the oxidative chemistry of low oxidation state main group elements, with the possibility to extend this chemistry to other low valent *d*-block metals, such as B(I), Ga(I), and In(I).

While the chemistry of metal dithiolene complexes have been examined extensively since the 1960s, their selenium analogues have not been as widely studied. In this respect, we

began looking at the synthesis of tetraselenocins from alkoxy-benzenes and Se_2Cl_2, from which metal diselenolene complexes could be produced.[4] The purification process of these tetraselenocins is more complex than that of the tetrathiocins, with the original reactions producing several selenium-rich byproducts, although somewhat pure samples were obtained by treatment of the crude bis(dimethoxybenzo)tetraselenocin product with PPh_3. From there, a series of mono-, di-, and hexanuclear diselenolate complexes were produced using similar techniques as those used for the dithiolates. This is an ongoing project, with the opportunity to open this family of compounds to include other functional groups on the diselenolene, other metal centres, and other auxiliary ligands. Due to selenium's lower electronegativity compared to sulfur and the resultant lowering of the HOMO-LUMO gap, these complexes are of particular interest for light harvesting devices.

4.3. References

1. **(a)** J. D. Wrixon, J. J. Hayward, O. Raza and J. M. Rawson, *Dalton Trans.*, 2014, **43**, 2134–2139; **(b)** J. D. Wrixon, J. J. Hayward and J. M. Rawson, *Inorg.Chem.*, 2015, **54**, 9384–9386; **(c)** J. D. Wrixon, Z. S. Ahmed, M. U. Anwar, Y. Beldjoudi, N. Hamidouche, J. J. Hayward and J. M. Rawson, *Polyhedron*, 2016, **108**, 115–121; **(d)** J. D. Wrixon, *Reactivity of 1,2,5,6-Tetrathiocines*, University of Windsor, 2015.

2. N. Fendi, *Synthesis, structural and physical studies "Push-Pull" nickel complexes of dithiolene based ligand*, University of Windsor, 2015, unpublished results.

3. S. C. Kosnik, M. C. Nascimento, J. M. Rawson and C. L. B. Macdonald, *Dalton Trans.*, 2017, **46**, 9769–9776.

4. **(a)** S. Zeine, *Replacement of Sulfur atom by Selenium atom in DTDA and tetrathiocin compounds*, University of Windsor, 2016, unpublished results; **(b)** I. Taarit, *Tetraselenocins: New precursors to diselenolate complexes*, University of Windsor, 2017, unpublished results.

APPENDIX

Crystallographic Information

** Note that any hydrogen atoms within each diagram have been removed for clarity. Where more than one molecule exists in the asymmetric unit, just one molecule is illustrated.*

Structure: ZA46

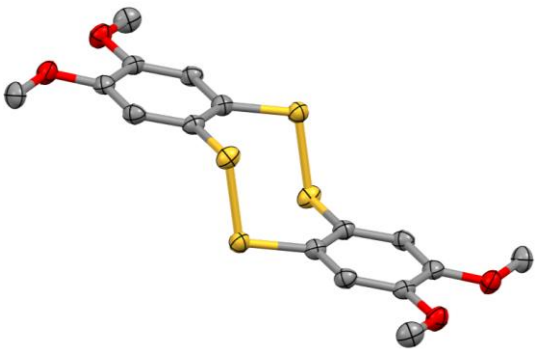

Table A-1. Crystal data and structure refinement for ZA46

Identification code	ZA46	
Empirical formula	C32 H32 O8 S8	
Formula weight	801.05	
Temperature	173(2) K	
Crystal system	monoclinic	
Space group	$P2_1/c$	
Unit cell dimensions	a = 8.4804(5) Å	α = 90°
	b = 8.3417(5) Å	β = 104.763(3)°
	c = 12.3427(9) Å	γ = 90°
Volume	844.31(9) $Å^3$	
Z	1	
Density (calculated)	1.575 g/cm^3	
Absorption coefficient	0.581 mm^{-1}	
F(000)	416.0	
Crystal size	0.210 × 0.100 × 0.050 mm^3	
Radiation	MoKα (λ = 0.71073)	
Theta range for data collection	5.958 to 52.798°	
Index ranges	$-10 \le h \le 10$, $-10 \le k \le 9$, $-15 \le l \le 15$	
Reflections collected	9752	
Independent reflections	1733 [R_{int} = 0.0472]	
Data / restraints / parameters	1733 / 0 / 111	
Goodness-of-fit on F^2	1.209	
Final R indices [$I \ge 2\sigma$ (I)]	R_1 = 0.0600, wR_2 = 0.1193	
R indices (all data)	R_1 = 0.0685, wR_2 = 0.1224	
Largest diff. peak and hole	0.54 and -0.51 $e.Å^{-3}$	

Structure: mo_za83_2_a_sq

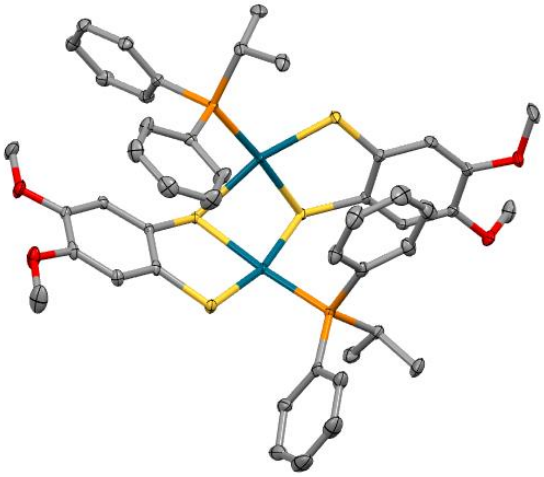

Table A-2. Crystal data and structure refinement for mo_za83_2_a_sq

Identification code	mo_za83_2_a_sq	
Empirical formula	C46 H50 O4 P2 Pd2 S4	
Formula weight	1069.84	
Temperature	130(2) K	
Crystal system	monoclinic	
Space group	$P2_1/n$	
Unit cell dimensions	a = 9.389(5) Å	α = 90°
	b = 32.961(15) Å	β = 101.001(17)°
	c = 15.592(7) Å	γ = 90°
Volume	4737(4) $Å^3$	
Z	4	
Density (calculated)	1.500 g/cm^3	
Absorption coefficient	1.044 mm^{-1}	
F(000)	2176.0	
Crystal size	0.310 × 0.300 × 0.050 mm^3	
Radiation	MoKα (λ = 0.71073)	
Theta range for data collection	5.614 to 55.178°	
Index ranges	$-12 \le h \le 12$, $-42 \le k \le 42$, $-20 \le l \le 20$	
Reflections collected	73383	
Independent reflections	10921 [R_{int} = 0.0534]	
Data / restraints / parameters	10921 / 0 / 531	
Goodness-of-fit on F^2	1.023	
Final R indices [$I \ge 2\sigma$ (I)]	R_1 = 0.0290, wR_2 = 0.0538	
R indices (all data)	R_1 = 0.0425, wR_2 = 0.0578	
Largest diff. peak and hole	0.39 and -0.65 $e.Å^{-3}$	

Structure: HEZA109

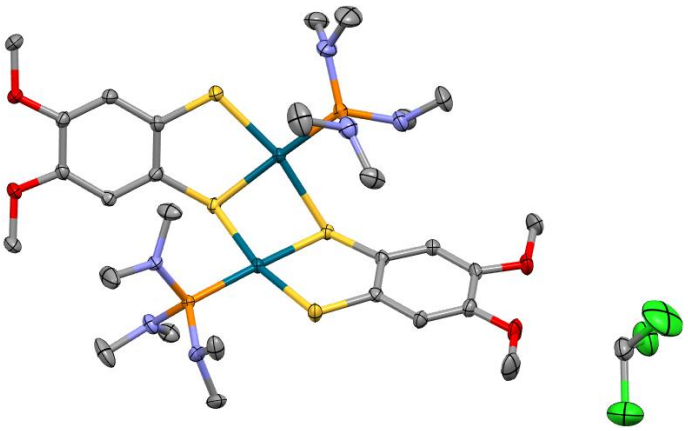

Table A-3. Crystal data and structure refinement for HEZA109

Identification code	HEZA109	
Empirical formula	C29 H53 Cl3 N6 O4 P2 Pd2 S4	
Formula weight	1059.10	
Temperature	170(2) K	
Crystal system	monoclinic	
Space group	$P2_1/c$	
Unit cell dimensions	a = 17.495(3) Å	α = 90.00(0)°
	b = 13.363(3) Å	β = 94.87(3)°
	c = 18.465(4) Å	γ = 90.00(0)°
Volume	4301.4(15) $Å^3$	
Z	4	
Density (calculated)	1.635 g/cm^3	
Absorption coefficient	1.331 mm^{-1}	
F(000)	2152.0	
Crystal size	0.402 × 0.196 × 0.028 mm^3	
Radiation	MoKα (λ = 0.71073)	
Theta range for data collection	5.376 to 58.45°	
Index ranges	$-24 \leq h \leq 23$, $-17 \leq k \leq 17$, $-22 \leq l \leq 22$	
Reflections collected	94375	
Independent reflections	9931 [R_{int} = 0.0721]	
Data / restraints / parameters	9931 / 0 / 467	
Goodness-of-fit on F^2	1.102	
Final R indices [$I \geq 2\sigma$ (I)]	R_1 = 0.0359, wR_2 = 0.0736	
R indices (all data)	R_1 = 0.0617, wR_2 = 0.0876	
Largest diff. peak and hole	1.17 and -0.90 e.$Å^{-3}$	

Structure: mo_heza110a_0m_a

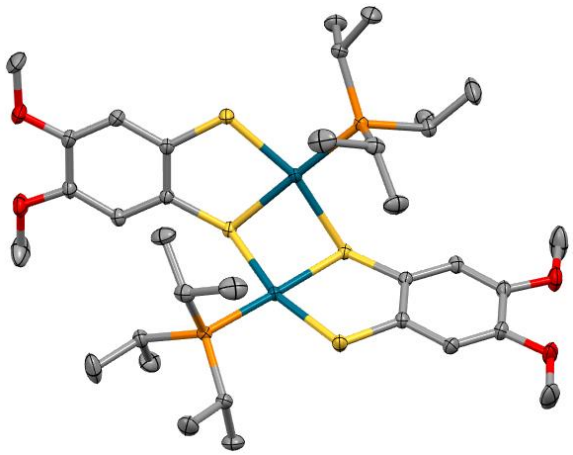

Table A-4. Crystal data and structure refinement for mo_heza110a_0m_a

Identification code	mo_heza110a_0m_a
Empirical formula	C34 H58 O4 P2 Pd2 S4
Formula weight	933.78
Temperature	170(2) K
Crystal system	monoclinic
Space group	C2/c
Unit cell dimensions	a = 21.2837(10) Å α = 90°
	b = 13.2445(7) Å β = 95.881(2)°
	c = 14.4928(7) Å γ = 90°
Volume	4063.9(3) $Å^3$
Z	4
Density (calculated)	1.526 g/cm^3
Absorption coefficient	1.203 mm^{-1}
F(000)	1920.0
Crystal size	0.576 × 0.176 × 0.088 mm^3
Radiation	MoKα (λ = 0.71073)
Theta range for data collection	5.652 to 66.436°
Index ranges	$-32 \leq h \leq 32$, $-20 \leq k \leq 20$, $-22 \leq l \leq 21$
Reflections collected	58981
Independent reflections	7793 [R_{int} = 0.0255]
Data / restraints / parameters	7793 / 0 / 216
Goodness-of-fit on F^2	1.094
Final R indices [$I \geq 2\sigma$ (I)]	R_1 = 0.0206, wR_2 = 0.0467
R indices (all data)	R_1 = 0.0270, wR_2 = 0.0492
Largest diff. peak and hole	0.45 and -0.84 $e.Å^{-3}$

Structure: za88c2_a_sq

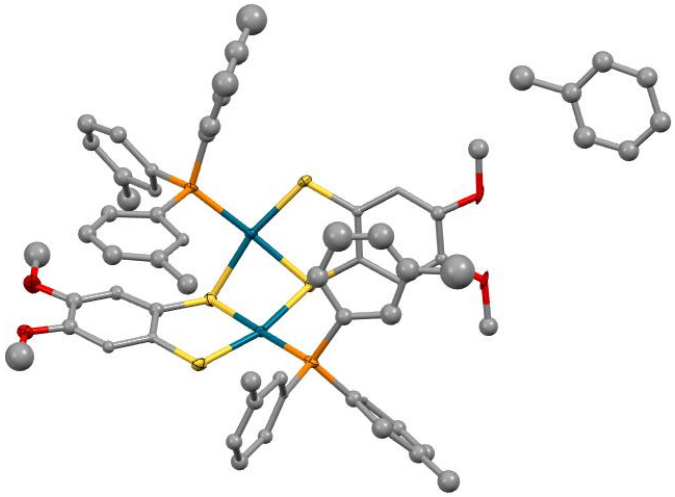

Table A-5. Crystal data and structure refinement for za88c2_a_sq

Identification code	za88c2_a_sq
Empirical formula	C58 H58 O4 P2 Pd2 S4, ½ (C7 H8)
Formula weight	1268.09
Temperature	143(2) K
Crystal system	triclinic
Space group	P-1
Unit cell dimensions	a = 8.2764(5) Å α = 76.727(4)°
	b = 24.6398(14) Å β = 88.353(4)°
	c = 30.0597(18) Å γ = 83.694(4)°
Volume	5930.2(6) $Å^3$
Z	4
Density (calculated)	1.420 g/cm^3
Absorption coefficient	7.071 mm^{-1}
F(000)	2196.0
Crystal size	0.16 × 0.11 × 0.07 mm^3
Radiation	CuKα (λ = 1.54178)
Theta range for data collection	3.02 to 109.992°
Index ranges	$-8 \le h \le 8$, $-26 \le k \le 26$, $-31 \le l \le 31$
Reflections collected	89785
Independent reflections	14548 [R_{int} = 0.3069]
Data / restraints / parameters	14548 / 60 / 718
Goodness-of-fit on F^2	1.102
Final R indices [$I \ge 2\sigma(I)$]	R_1 = 0.1697 wR_2 = 0.3147
R indices (all data)	R_1 = 0.2410, wR_2 = 0.3519
Largest diff. peak and hole	1.42 and -1.63 e.$Å^{-3}$

This was a very poor weakly diffracting thin plate. Although it was measured using a copper micro-source, the quality of the data for this structure was very poor with $I/\sigma < 2.0$ for data beyond 0.90 Å resolution and a correspondingly large R_{int}. Pd, S, P and O atoms were refined anisotropically but attempts to refine C atoms anisotropically persistently led to many non-positive definite atoms and so all C atoms were refined isotropically in this structure. Although the final R_1 is large (0.16) the structure was stable and clearly revealed the molecular connectivity.

Structure: ZA89b_a

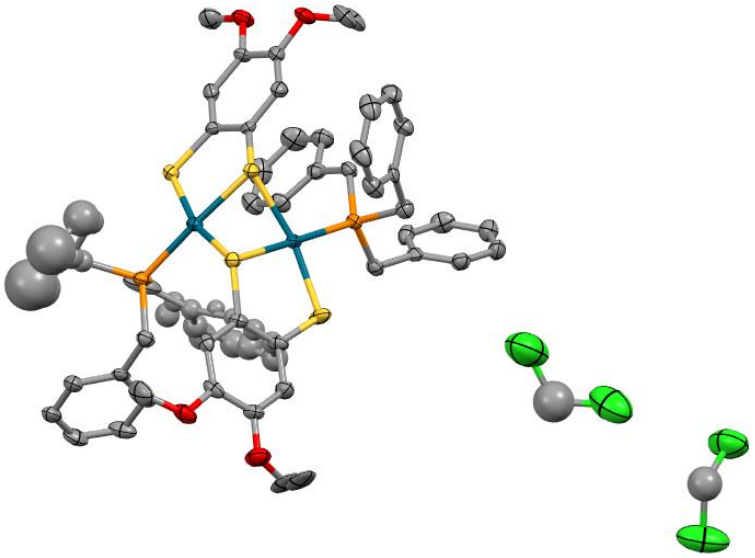

Table A-6. Crystal data and structure refinement for ZA89b_a

Identification code	ZA89b_a
Empirical formula	C60 H62 Cl4 O4 P2 Pd2 S4
Formula weight	1391.87
Temperature	170(2) K
Crystal system	orthorhombic
Space group	Pbca
Unit cell dimensions	a = 23.2070(6) Å α = 90°
	b = 19.6867(5) Å β = 90°
	c = 26.4150(6) Å γ = 90°
Volume	12068.2(5) $Å^3$
Z	8
Density (calculated)	1.532 g/cm^3
Absorption coefficient	8.595 mm^{-1}
F(000)	5664.0
Crystal size	0.170 × 0.090 × 0.090 mm^3
Radiation	CuKα (λ = 1.54178)
Theta range for data collection	6.692 to 122°
Index ranges	$-19 \le h \le 26$, $-22 \le k \le 22$, $-29 \le l \le 29$
Reflections collected	88230
Independent reflections	9226 [R_{int} = 0.1145]
Data / restraints / parameters	9226 / 18 / 634
Goodness-of-fit on F^2	1.085
Final R indices [$I \ge 2\sigma$ (I)]	R_1 = 0.0674, wR_2 = 0.1415
R indices (all data)	R_1 = 0.0915, wR_2 = 0.1527
Largest diff. peak and hole	1.24 and -1.13 e.$Å^{-3}$

Structure: ZA81cde_twin5

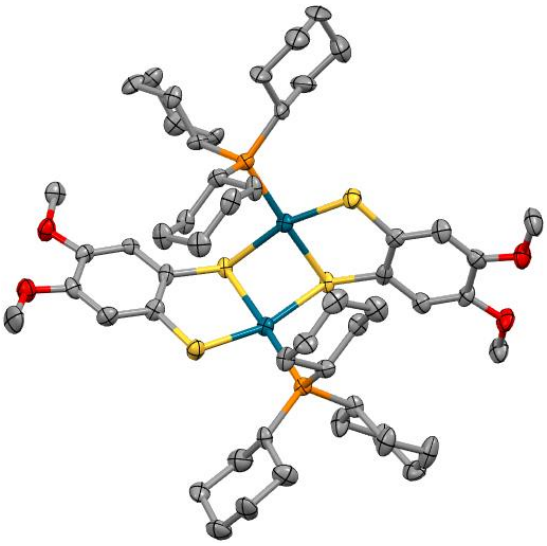

Table A-7. Crystal data and structure refinement for ZA81cde_twin5

Identification code	ZA81cde_twin5	
Empirical formula	C52 H82 O4 P2 Pd2 S4	
Formula weight	1174.15	
Temperature	170(2) K	
Crystal system	triclinic	
Space group	P-1	
Unit cell dimensions	a = 9.7965(5) Å	α = 96.541(11)°
	b = 15.236(3) Å	β = 104.277(7)°
	c = 19.179(4) Å	γ = 101.825(7)°
Volume	2674.3(7) $Å^3$	
Z	2	
Density (calculated)	1.458 g/cm^3	
Absorption coefficient	0.931 mm^{-1}	
F(000)	1224.0	
Crystal size	0.360 × 0.310 × 0.120 mm^3	
Radiation	MoKα (λ = 0.71073)	
Theta range for data collection	5.638 to 49.618°	
Index ranges	$-11 \le h \le 11$, $-17 \le k \le 17$, $0 \le l \le 22$	
Reflections collected	9157	
Independent reflections	9157	
Data / restraints / parameters	9157 / 0 / 582	
Goodness-of-fit on F^2	1.142	
Final R indices [$I \ge 2\sigma$ (I)]	R_1 = 0.0858, wR_2 = 0.2039	
R indices (all data)	R_1 = 0.1229, wR_2 = 0.2352	
Largest diff. peak and hole	2.19 and -1.94 $e.Å^{-3}$	

Refined as a 2-component non-merohedral twin.

Structure: zapt6_ortho_a_sq

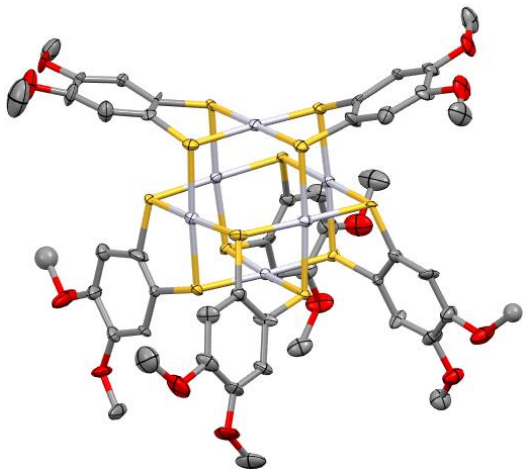

Table A-8. Crystal data and structure refinement for zapt6_ortho_a_sq

Identification code	zapt6_ortho_a_sq
Empirical formula	C48 H48 O12 Pt6 S12
Formula weight	2372.12
Temperature	150(2) K
Crystal system	orthorhombic
Space group	$P2_12_12$
Unit cell dimensions	a = 21.8577(8) Å α = 90°
	b = 22.4432(9) Å β = 90°
	c = 16.5753(5) Å γ = 90°
Volume	8131.1(5) $Å^3$
Z	4
Density (calculated)	1.938 g/cm^3
Absorption coefficient	10.634 mm^{-1}
F(000)	4368.0
Crystal size	0.120 × 0.050 × 0.030 mm^3
Radiation	MoKα (λ = 0.71073)
Theta range for data collection	5.754 to 49.458°
Index ranges	$-25 \le h \le 25$, $-26 \le k \le 26$, $-16 \le l \le 19$
Reflections collected	90153
Independent reflections	13870 [R_{int} = 0.1424]
Data / restraints / parameters	13870 / 272 / 703
Goodness-of-fit on F^2	1.005
Final R indices [$I \ge 2\sigma$ (I)]	R_1 = 0.0391, wR_2 = 0.0713
R indices (all data)	R_1 = 0.0694, wR_2 = 0.0807
Largest diff. peak and hole	1.75 and -1.22 $e.Å^{-3}$

Structure: mo_HEZA134b_0m_a

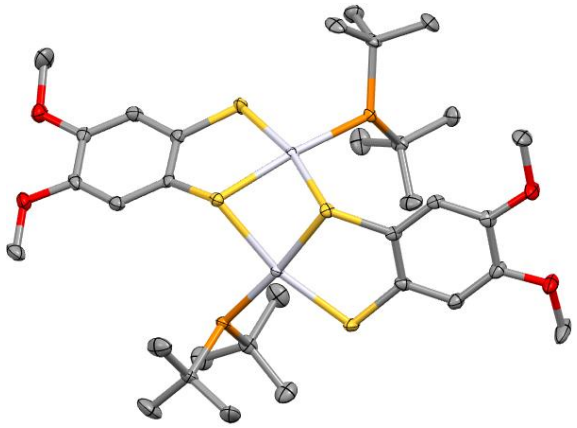

Table A-9. Crystal data and structure refinement for mo_HEZA134b_0m_a

Identification code	mo_HEZA134b_0m_a	
Empirical formula	C32 H54 O4 P2 Pt2 S4	
Formula weight	1083.11	
Temperature	150(2) K	
Crystal system	monoclinic	
Space group	$P2_1/n$	
Unit cell dimensions	a = 11.0046(4) Å	α = 90°
	b = 19.9995(8) Å	β = 90.7560(10)°
	c = 17.5906(7) Å	γ = 90°
Volume	3871.1(3) $Å^3$	
Z	4	
Density (calculated)	1.858 g/cm^3	
Absorption coefficient	7.551 mm^{-1}	
F(000)	2112.0	
Crystal size	0.50 × 0.32 × 0.15 mm^3	
Radiation	MoKα (λ = 0.71073)	
Theta range for data collection	5.504 to 56.686°	
Index ranges	$-14 \le h \le 13$, $-26 \le k \le 26$, $-23 \le l \le 23$	
Reflections collected	41234	
Independent reflections	9654 [R_{int} = 0.0426]	
Data / restraints / parameters	9654 / 0 / 413	
Goodness-of-fit on F^2	1.231	
Final R indices [$I \ge 2\sigma(I)$]	R_1 = 0.0271, wR_2 = 0.0612	
R indices (all data)	R_1 = 0.0333, wR_2 = 0.0646	
Largest diff. peak and hole	1.11 and -1.78 $e.Å^{-3}$	

Structure: mo_JJHCpCoS2_0m_a

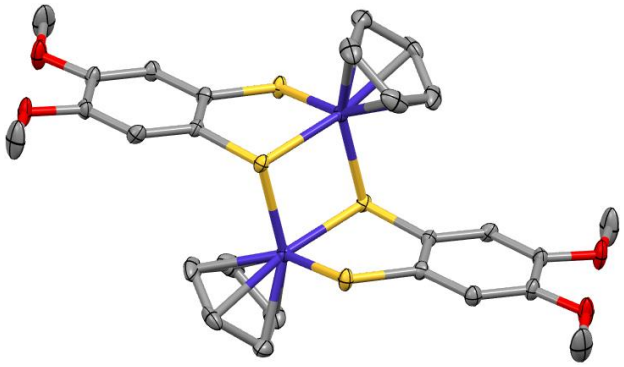

Table A-10. Crystal data and structure refinement for mo_JJHCpCoS2_0m_a

Identification code	mo_JJHCpCoS2_0m_a	
Empirical formula	C26 H26 Co2 O4 S4	
Formula weight	648.57	
Temperature	170(2) K	
Crystal system	monoclinic	
Space group	$P2_1/n$	
Unit cell dimensions	a = 8.3163(4) Å	α = 90°
	b = 7.7394(4) Å	β = 101.737(2)°
	c = 20.2842(10) Å	γ = 90°
Volume	1278.26(11) $Å^3$	
Z	2	
Density (calculated)	1.685 g/cm^3	
Absorption coefficient	1.657 mm^{-1}	
F(000)	664.0	
Crystal size	0.290 × 0.280 × 0.250 mm^3	
Radiation	MoKα (λ = 0.71073)	
Theta range for data collection	5.65 to 54.984°	
Index ranges	$-10 \le h \le 10$, $-9 \le k \le 10$, $-23 \le l \le 26$	
Reflections collected	6380	
Independent reflections	1686 [R_{int} = 0.0298]	
Data / restraints / parameters	1686 / 0 / 165	
Goodness-of-fit on F^2	1.101	
Final R indices [$I \ge 2\sigma$ (I)]	R_1 = 0.0283, wR_2 = 0.0597	
R indices (all data)	R_1 = 0.0373, wR_2 = 0.0616	
Largest diff. peak and hole	0.25 and -0.24 $e.Å^{-3}$	

Structure: HEZA126av

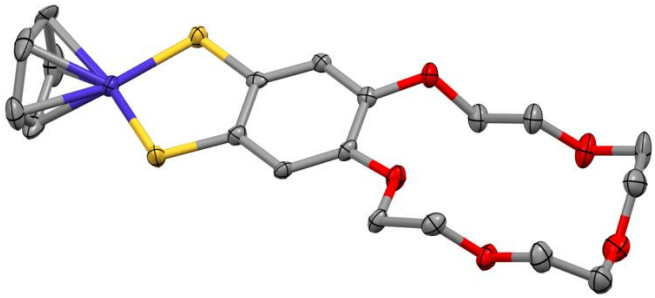

Table A-11. Crystal data and structure refinement for HEZA126av

Identification code	HEZA126av	
Empirical formula	C19 H23 Co O5 S2	
Formula weight	454.42	
Temperature	170(2) K	
Crystal system	monoclinic	
Space group	Cc	
Unit cell dimensions	a = 25.617(8) Å	α = 90°
	b = 9.222(2) Å	β = 95.649(14)°
	c = 8.2524(16) Å	γ = 90°
Volume	1940.1(8) $Å^3$	
Z	4	
Density (calculated)	1.556 g/cm^3	
Absorption coefficient	1.128 mm^{-1}	
F(000)	944.0	
Crystal size	0.560 × 0.273 × 0.195 mm^3	
Radiation	MoKα (λ = 0.71073)	
Theta range for data collection	6.392 to 54.274°	
Index ranges	$-32 \leq h \leq 32$, $-11 \leq k \leq 11$, $-10 \leq l \leq 10$	
Reflections collected	20446	
Independent reflections	4246 [R_{int} = 0.0545]	
Data / restraints / parameters	4246 / 2 / 245	
Goodness-of-fit on F^2	1.017	
Final R indices [$I \geq 2\sigma(I)$]	R_1 = 0.0334, wR_2 = 0.0775	
R indices (all data)	R_1 = 0.0412, wR_2 = 0.0831	
Largest diff. peak and hole	0.36 and -0.46 $e.Å^{-3}$	

Structure: mo_HEZA116_0m

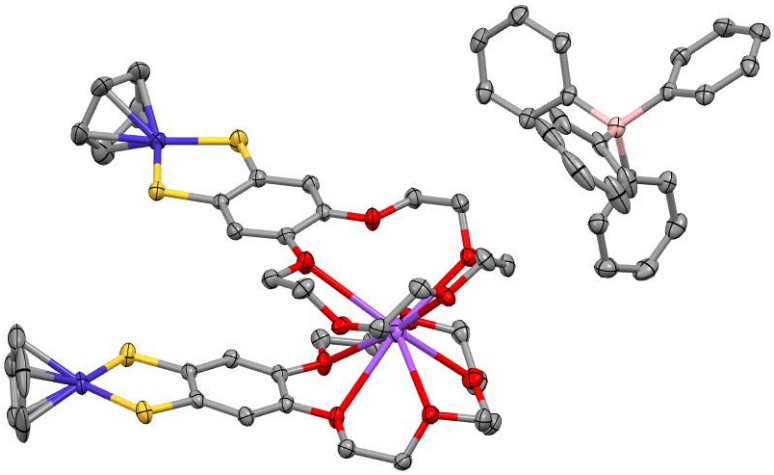

Table A-12. Crystal data and structure refinement for mo_HEZA116_0m

Identification code	mo_HEZA116_0m
Empirical formula	C62 H66 B Co2 Na O10 S4
Formula weight	1251.15
Temperature	170.0 K
Crystal system	monoclinic
Space group	C2/c
Unit cell dimensions	a = 23.666(6) Å α = 90°
	b = 15.585(4) Å β = 100.904(8)°
	c = 34.260(9) Å γ = 90°
Volume	12408(6) $Å^3$
Z	8
Density (calculated)	1.3394 g/cm^3
Absorption coefficient	0.732 mm^{-1}
F(000)	5227.9
Crystal size	0.591 × 0.219 × 0.188 mm^3
Radiation	MoKα (λ = 0.71073)
Theta range for data collection	5.76 to 56.78°
Index ranges	$-26 \le h \le 31$, $-20 \le k \le 20$, $-45 \le l \le 45$
Reflections collected	126678
Independent reflections	15482 [R_{int} = 0.0408]
Data / restraints / parameters	15482 / 0 / 721
Goodness-of-fit on F^2	1.060
Final R indices [$I \ge 2\sigma$ (I)]	R_1 = 0.0386, wR_2 = 0.0875
R indices (all data)	R_1 = 0.0495, wR_2 = 0.0926
Largest diff. peak and hole	0.83 and -0.75 $e.Å^{-3}$

Structure: mo_HEZA117g_2_0m

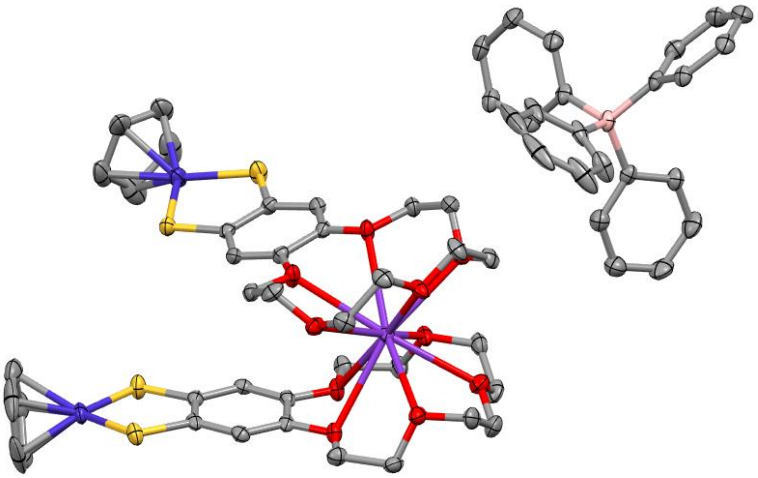

Table A-13. Crystal data and structure refinement for mo_HEZA117g_2_0m

Identification code	mo_HEZA117g_2_0m
Empirical formula	C62 H66 B Co2 K O10 S4
Formula weight	1267.15
Temperature	170.0 K
Crystal system	monoclinic
Space group	C2/c
Unit cell dimensions	a = 23.5978(17) Å α = 90°
	b = 15.8163(10) Å β = 101.095(2)°
	c = 34.229(2) Å γ = 90°
Volume	12536.4(15) $Å^3$
Z	8
Density (calculated)	1.343 g/cm^3
Absorption coefficient	0.784 mm^{-1}
F(000)	5280.0
Crystal size	0.525 × 0.257 × 0.103 mm^3
Radiation	MoKα (λ = 0.71073)
Theta range for data collection	5.694 to 47.706°
Index ranges	$-26 \le h \le 26$, $-17 \le k \le 17$, $-38 \le l \le 38$
Reflections collected	64397
Independent reflections	9633 [R_{int} = 0.0394]
Data / restraints / parameters	9633 / 0 / 746
Goodness-of-fit on F^2	1.024
Final R indices [$I \ge 2\sigma$ (I)]	R_1 = 0.0719, wR_2 = 0.2290
R indices (all data)	R_1 = 0.0824, wR_2 = 0.2400
Largest diff. peak and hole	5.08 and -0.54 $e.Å^{-3}$

Structure: heza132_2_sq

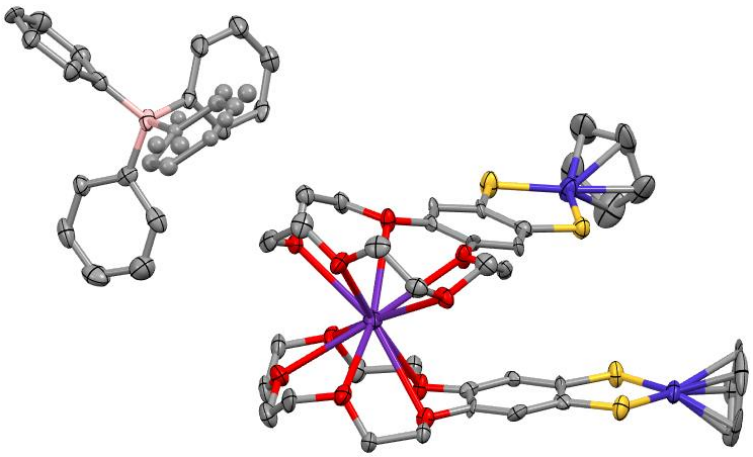

Table A-14. Crystal data and structure refinement for heza132_2_sq

Identification code	heza132_2_sq
Empirical formula	C62 H66 B Co2 O10 Rb S4
Formula weight	1313.52
Temperature	170(2) K
Crystal system	monoclinic
Space group	C2/c
Unit cell dimensions	a = 23.4199(9) Å α = 90°
	b = 16.0367(9) Å β = 100.935(3)°
	c = 34.0682(14) Å γ = 90°
Volume	12562.5(10) $Å^3$
Z	8
Density (calculated)	1.389 g/cm^3
Absorption coefficient	6.762 mm^{-1}
F(000)	5424.0
Crystal size	0.370 × 0.147 × 0.060 mm^3
Radiation	CuKα (λ = 1.54178)
Theta range for data collection	5.284 to 89.3°
Index ranges	$-21 \leq h \leq 21$, $-14 \leq k \leq 14$, $-30 \leq l \leq 30$
Reflections collected	69405
Independent reflections	4973 [R_{int} = 0.1133]
Data / restraints / parameters	4973 / 0 / 685
Goodness-of-fit on F^2	1.044
Final R indices [$I \geq 2\sigma$ (I)]	R_1 = 0.0509, wR_2 = 0.1018
R indices (all data)	R_1 = 0.0711, wR_2 = 0.1094
Largest diff. peak and hole	0.40 and -0.43 e.$Å^{-3}$

Structure: heza017_a_pl_sq

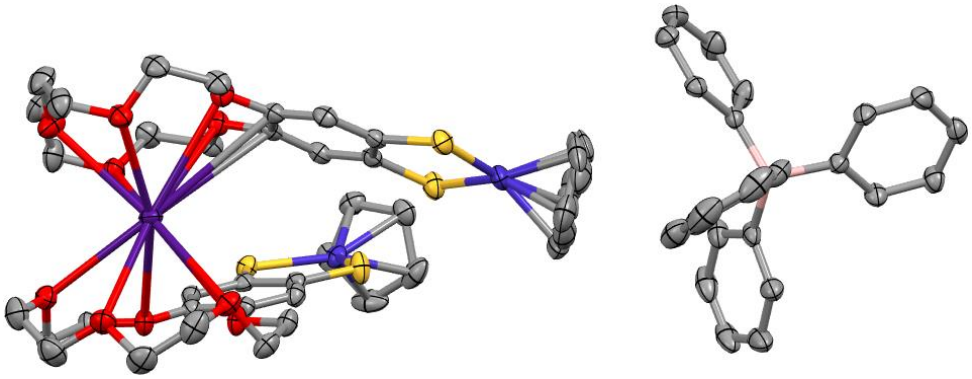

Table A-15. Crystal data and structure refinement for heza017_a_pl_sq

Identification code	heza017_a_pl_sq	
Empirical formula	C62 H66 B Co2 Cs O10 S4	
Formula weight	1360.96	
Temperature	170(2) K	
Crystal system	monoclinic	
Space group	C2/c	
Unit cell dimensions	a = 17.591(6) Å	α = 90°
	b = 22.017(7) Å	β = 92.088(16)°
	c = 32.559(15) Å	γ = 90°
Volume	12602(8) $Å^3$	
Z	8	
Density (calculated)	1.435 g/cm^3	
Absorption coefficient	1.283 mm^{-1}	
F(000)	5568.0	
Crystal size	0.500 × 0.120 × 0.070 mm^3	
Radiation	MoKα (λ = 0.71073)	
Theta range for data collection	5.748 to 54.194°	
Index ranges	$-22 \leq h \leq 22$, $-27 \leq k \leq 27$, $-41 \leq l \leq 40$	
Reflections collected	239187	
Independent reflections	13110 [R_{int} = 0.0498]	
Data / restraints / parameters	13110 / 176 / 752	
Goodness-of-fit on F^2	1.058	
Final R indices [$I \geq 2\sigma$ (I)]	R_1 = 0.0269, wR_2 = 0.0560	
R indices (all data)	R_1 = 0.0381, wR_2 = 0.0591	
Largest diff. peak and hole	0.55 and -0.78 $e.Å^{-3}$	

Structure: mo_za87_a_sq

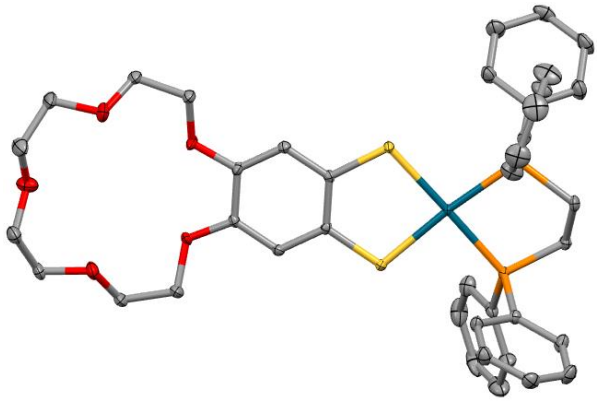

Table A-16. Crystal data and structure refinement for mo_za87_a_sq

Identification code	mo_za87_a_sq	
Empirical formula	C40 H42 O5 P2 Pd S2	
Formula weight	835.19	
Temperature	130(2) K	
Crystal system	monoclinic	
Space group	$P2_1/c$	
Unit cell dimensions	a = 11.820(2) Å	α = 90°
	b = 13.589(3) Å	β = 101.800(9)°
	c = 24.595(6) Å	γ = 90°
Volume	3867.0(14) $Å^3$	
Z	4	
Density (calculated)	1.435 g/cm^3	
Absorption coefficient	0.713 mm^{-1}	
F(000)	1720.0	
Crystal size	0.460 × 0.380 × 0.320 mm^3	
Radiation	MoKα (λ = 0.71073)	
Theta range for data collection	5.896 to 54.412°	
Index ranges	$-15 \le h \le 15$, $-17 \le k \le 17$, $-31 \le l \le 31$	
Reflections collected	52168	
Independent reflections	8537 [R_{int} = 0.0231]	
Data / restraints / parameters	8537 / 0 / 451	
Goodness-of-fit on F^2	1.162	
Final R indices [$I \ge 2\sigma$ (I)]	R_1 = 0.0260, wR_2 = 0.0562	
R indices (all data)	R_1 = 0.0310, wR_2 = 0.0593	
\Largest diff. peak and hole	0.48 and -0.56 e.$Å^{-3}$	

Structure: ZA121cv_a

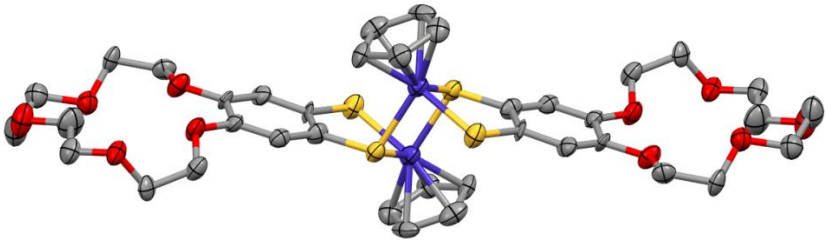

Table A-17. Crystal data and structure refinement for ZA121cv_a

Identification code	ZA121cv_a	
Empirical formula	C38 H46 Co2 O10 S4	
Formula weight	908.85	
Temperature	170(2) K	
Crystal system	monoclinic	
Space group	C2/c	
Unit cell dimensions	a = 27.749(12) Å	α = 90°
	b = 7.699(3) Å	β = 107.45(3)°
	c = 18.434(7) Å	γ = 90°
Volume	3757(3) $Å^3$	
Z	4	
Density (calculated)	1.607 g/cm^3	
Absorption coefficient	9.493 mm^{-1}	
F(000)	1888.0	
Crystal size	0.017 × 0.017 × 0.001 mm^3	
Radiation	CuKα (λ = 1.54178)	
Theta range for data collection	6.678 to 109.994°	
Index ranges	$-29 \leq h \leq 29$, $-8 \leq k \leq 8$, $-19 \leq l \leq 19$	
Reflections collected	36622	
Independent reflections	2361 [R_{int} = 0.3568]	
Data / restraints / parameters	2361 / 0 / 245	
Goodness-of-fit on F^2	0.961	
Final R indices [$I \geq 2\sigma(I)$]	R_1 = 0.0732, wR_2 = 0.1382	
R indices (all data)	R_1 = 0.1532, wR_2 = 0.1689	
Largest diff. peak and hole	0.52 and -0.41 e.$Å^{-3}$	

Very thin plate (0.017 × 0.017 × <0.003 mm) which led to very weak diffraction and large R_{int} with reflections greater than 1.08 Å resolution having $I/\sigma < 2$. In other respects, refinement stable.

Structure: mo_za121av_0m_a_sq

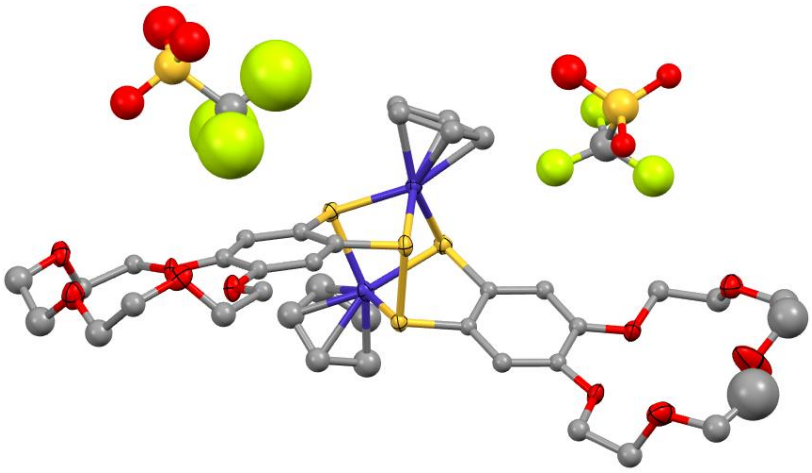

Table A-18. Crystal data and structure refinement for mo_za121av_0m_a_sq

Identification code	mo_za121av_0m_a_sq	
Empirical formula	C40 H46 Co2 F6 O16 S6	
Formula weight	1206.99	
Temperature	170(2) K	
Crystal system	monoclinic	
Space group	$P2_1/n$	
Unit cell dimensions	a = 16.862(7) Å	α = 90°
	b = 33.052(14) Å	β = 90.713(10)°
	c = 19.155(7) Å	γ = 90°
Volume	10674(8) $Å^3$	
Z	8	
Density (calculated)	1.502 g/cm^3	
Absorption coefficient	0.939 mm^{-1}	
F(000)	4944.0	
Radiation	MoKα (λ = 0.71073)	
Theta range for data collection	5.636 to 49.6°	
Index ranges	$-19 \leq h \leq 19$, $-38 \leq k \leq 38$, $-22 \leq l \leq 22$	
Reflections collected	260750	
Independent reflections	18114 [R_{int} = 0.2509]	
Data / restraints / parameters	18114 / 52 / 718	
Goodness-of-fit on F^2	1.010	
Final R indices [$I \geq 2\sigma$ (I)]	R_1 = 0.1280, wR_2 = 0.3103	
R indices (all data)	R_1 = 0.1941, wR_2 = 0.3647	
Largest diff. peak and hole	6.71 and -2.75 $e.Å^{-3}$	

This was a problematic crystal where the scattering dropped off rapidly to high angle and showed some evidence for non-merohedral twinning with only ~50% of observed reflections were used in indexing and Fo > Fc for most disagreeable reflections in subsequent refinement. Nevertheless, the data were adequate for the molecular connectivity to be determined. Attempts to resolve the (non-merohedral) TWIN law are ongoing.

VITA AUCTORIS

Name: Zeinab Sadiq Ahmed

Education: Vincent Massey Secondary School, Windsor, ON, 2010.

University of Windsor, Windsor, ON, 2014, B.Sc.[H] Chemistry.

University of Windsor, Windsor, ON, 2017, M.Sc. Chemistry.

Publications: J. D. Wrixon, Z. S. Ahmed, M. U. Anwar, Y. Beldjoudi, N. Hamidouche, J. J. Hayward and J. M. Rawson, *Polyhedron*, 2016, **108**, 115–121.

Conferences: 3rd Crystal Engineering and Emerging Materials Workshop of Ontario and Quebec, Windsor, ON, May 13 – 15, 2016. (***Poster Presentation***)

99th Canadian Society for Chemistry Conference and Exhibition, Halifax, NS, June 5 – 9, 2016. (***Poster Presentation***)

49th Inorganic Discussion Weekend, Hamilton, ON, November 11 – 13, 2016. (***Oral Presentation***)

100th Canadian Society for Chemistry Conference and Exhibition, Toronto, ON, May 28 – June 1, 2017. (***Oral Presentation***)